Spring 5-15-2020

Cognitive Recovery in the Post-Infectious CNS

Charise Joy Garber
Washington University in St. Louis

WASHINGTON UNIVERSITY IN ST. LOUIS

Division of Biology and Biomedical Sciences
Neurosciences

Dissertation Examination Committee:
Robyn Klein, Chair
Michael Diamond
Keiko Hirose
Jonathan Kipnis
Haina Shin

Cognitive Recovery in the Post-Infectious CNS

by
Charise Garber

A dissertation presented to
The Graduate School
of Washington University in
partial fulfillment of the
requirements for the degree
of Doctor of Philosophy

May 2020
St. Louis, Missouri

Table of Contents

List of Figures iv
Acknowledgments vi
Abstract viii
Chapter 1: Introduction to neuroimmunity and cognitive function 1
1.1 Overview of neuroimmunology and CNS function 1
1.2 Microglia 1
1.2.1 Neurodevelopment 1
1.2.2 Homeostatic function 2
1.2.3 Role in disease 3
1.2.4 Role in disease 4
1.3 Astrocytes 4
1.3.1 Neurodevelopment 4
1.3.2 Homeostatic function 5
1.3.3 Role in disease 6
1.3.4 Enhanced innate immune responses of hindbrain neurons and astrocytes 7
1.4 T cells 8
1.4.1 Meningeal Immunity 8
1.4.2 Response to RNA virus infection 9
1.5 Hippocampal function in learning and memory 11
1.5.1 Hippocampal circuitry 11
1.5.2 Hippocampal circuitry 11
1.5.3 Synaptic plasticity 12
1.6 Inflammation-induced CNS dysfunction in parenchyma infection 13
1.6.1 Viruses 13
1.6.2 Neurotropic parasites 16
1.7 West Nile virus 18
1.7.1 Virology 18
1.7.2 Epidemiology and clinical presentation 19
1.8 Zika virus 19
1.8.1 Epidemiology and clinical presentation 19

1.8.2 Neurotropism 20
1.9 References 21
Chapter 2: Astrocytes decrease adult neurogenesis during memory dysfunction via Il-1 33
2.1 Abstract 33
2.2 Introduction 34
2.3 Results 37
2.4 Discussion 43
2.5 Methods 48
2.6 Acknowledgements 53
2.7 References 54
2.8 Figures 58
Chapter 3: T cells promote microglia-mediated synaptic elimination and cognitive dysfunction during recovery from neuropathogenic flaviviruses 71
3.1 Abstract 71
3.2 Introduction 72
3.3 Results 75
3.4 Discussion 84
3.5 Methods 89
3.7 References 95
3.8 Figures 100
Chapter 4: Conclusions and future directions 127
4.1 Astrocytes, neurogenesis and synapse recovery 127
4.2 References 130

List of Figures

Figure 2.1: Gene transcripts that impact neurogenesis and markers of proinflammatory astrocytes are altered in WNV-recovered mice …….. ……..…….....……58

Figure 2.2: Fewer new neurons are born within the dentate gyrus during WNV-NS5-E218A recovery ……...…….. ……...……60

Figure 2.3: Deficits in adult neurogenesis during WNV infection ……...…61

Figure 2.4: Greater numbers of astrocytes are born within the hippocampus uring acute WNV encephalitis which adopt a proinflammatory phenotype and express IL-1b. ……...……62

Figure 2.5: IL-1R1$^{-/-}$ mice resist WNV-mediated alterations in neuroblast proliferation and recover synapses earlier than wildtype controls. ……..…63

Figure 2.6: IL-1R1$^{-/-}$ WNV-NS5-E218A-infected mice are protected from virus-induced spatial learning deficits on the Barnes Maze behavior task ……...…….. ……...……64

Figure 2.7: WNV-NS5-E218A infected mice treated with Anakinra are protected from virus-induced spatial learning deficits on the Barnes Maze behavior task……..……...……65

Figure 2.8: Flow cytometry gating strategy ……..…...……..…66

Figure 2.9: WNV permissivity of DCX+ neuroblasts *in vivo* ……...……67

Figure 2.10: Determination of astrocyte and microglia purity …….……68

Figure 2.11: Lack of IL-1 signaling does not affect viral control of immune cell infiltrates to the CNS…… ……...……69

Figure 2.12: Blood brain barrier opening peaks at 6 dpi, and closes by 12 dpi…….....……70

Figure 3.1: ZIKV targets the hippocampus…….……..…100

Figure 3.2: ZIKV induces neuroinflammation and neuronal loss in the hippocampus……...102

Figure 3.3: T cells express IFN-γ in the post-infected hippocampus…….……... ……..…104

Figure 3.4: Loss of IFN-γ signaling protects animals against spatial-learning deficits ……..…106

Figure 3.5: IFN-γ promotes neuronal apoptosis in ZIKV-infected animals post recovery …..…107

Figure 3.6: IFNgR is required for repair of presynaptic and postsynaptic termini in flavivirus-infected animals post recovery…….109

Figure 3.7: IFN-γ potentiates microglial engulfment of postsynaptic termini and neurons in ZIKV-infected animals post recovery……...……...……111

Figure 3.8: Loss of IFN-γ signaling in microglia during recovery protects animals against spatial learning deficits……...……...……..…113

Figure 3.9: ZIKV targets the hippocampus……..……..…..115

Figure 3.10: Kinetics of immune cell infiltration to the hippocampus……...…….116

Figure 3.11: IFN-γ^+ T cells persist in the hippocampus…….……..…117

Figure 3.12: *Ifngr1*$^{-/-}$ mice display similar clinical course and viral burden as WT mice …...…118

Figure 3.13: *Ifngr1*$^{-/-}$ mice have slight decrease in CD103$^+$CD8$^+$ T cells, which express high levels of CCR2**.**……....119

Figure 3.14: Decreases in post-synaptic terminals and increase in apoptotic neurons are observed during ZIKV acute infection and long-term recovery…...……. ……120

Figure 3.15: Significant differences in numbers of microglia in the hippocampus of WT and *Ifngr1*$^{-/-}$ WNV and ZIKV-recovered mice……...122

Figure 3.16: Conditional deletion of IFNGR in Cx3CR1$^+$ microglia……..124

Figure 3.17: T cell-derived IFNγ targets microglia to mediate neurocognitive dysfunction during recovery from WNV and ZIKV infection……126

Acknowledgments

Simply put, this work would not have been possible without the support and encouragement of many people. I would like to begin by thanking John Russel and the BioMedRAP staff for giving me the opportunity to try my hand at biomedical research through an incredible summer program. You opened my eyes to the amazing opportunity to pursue basic biomedical research questions as a career, and I would not be where I am today without that first introduction.

I would like to thank Robyn Klein, for being the best mentor I could have asked for. Thank you for recognizing both my gifts and my needs, and tailoring your advice so the former could flourish and the latter could be met. Thank you for creating such a wonderful atmosphere to work in, and for taking time to celebrate life in and out of lab. Thank you for being a strong and supportive role model and mentor. I would also like to thank the members of my thesis committee: Keiko Hirose, Michael Diamond, Haina Shin and Jonathan Kipnis. Thank you for investing time in my scientific training, providing valuable insight into the project and critical feedback of my work. I would also like to thank the members of the Klein lab (past and present) for making lab a fun place to work, for helping me with experiments, and for always giving me the biggest piece of cake. Funding for this work was provided by the MSTP training grant, the ID training grant, and NIH grants to Robyn Klein.

Finally, I would like to thank my family for their constant and consistent support and encouragement over the years. You have helped me along this journey in more ways than I can say and I am so very thankful. I love you!

Charise Garber

Washington University in St. Louis

May 2020

Dedicated to my parents.

ABSTRACT OF THE DISSERTATION

Cognitive Recovery in the Post Infectious CNS

by

Charise Garber

Doctor of Philosophy in Biology and Biomedical Sciences

Neurosciences

Washington University in St. Louis, 2020

Professor Robyn Klein, Chair

Neuroinflammation plays a pivotal role in a variety of diseases of the CNS associated with cognitive impairment, including Alzheimer's Disease, Parkinson's Disease with dementia, Multiple Sclerosis, anti-NMDA receptor encephalitis, and West Nile Virus Neuroinvasive disease (WNND). Despite strong evidence that infiltration of peripheral immune cells and activation of resident microglia and astrocytes occurs in these various diseases, very little is known about how this altered immune environment may influence normal cognitive function. Given that communication between the nervous and immune system is essential for normal cognitive function, the central motivation of my thesis work is to understand the mechanisms by which immune activation, which is vital for pathogen control, may influence cognitive recovery in the setting of viral infection of the CNS.

First, using a recovery model of WNND in which intracranial infection of adult mice with an attenuated strain of West Nile Virus leads to spatial learning deficits on the Barnes Maze

behavioral task, we demonstrate that following viral clearance activated astrocytes express the cytokine interleukin-1 (IL-1) which decreases neurogenesis and increases the generation of astrocytes. Animals deficient in the receptor for IL-1 (IL1R1-/-) are protected from this decrease in neurogenesis and display early recovery of synaptic terminals and protection from virus-induced spatial learning deficits. In addition, treatment of mice with Anakinra, an FDA-approved IL-1R antagonist, during acute disease similarly led to protection from spatial learning deficits.

Next, using the same recovery model of WNND, we demonstrate that T cells persist in the hippocampus for weeks following viral clearance and continue to express the cytokine interferon-gamma (IFNg) leading to persistent activation of microglia. Animals deficient in the receptor for IFNg (IFNgR-/-) are protected from microglial activation and spatial learning deficits, despite delayed viral clearance and increased persistence of viral RNA in the hippocampus compared to wildtype controls. Conditional deletion of IFNgR from microglia upon tamoxifen administration to Cx3CR1-Cre^{ER} x IFNgR-fl/fl mice was sufficient to protect animals from spatial learning deficits. These results were confirmed in animals infected with Zika-virus (ZIKV), a related flavivirus with different neural tropism, suggesting a common mechanism by which altered immune activation in the CNS leads to long term cognitive deficits. These studies provide valuable insights into the neuroimmune processes that influence tissue repair and cognitive recovery in the hippocampus following viral encephalitis, and identify IFNg signaling in microglia as a critical signal underlying diverse recovery mechanisms.

Chapter 1: Introduction to neuroimmunity and cognitive function

1.1 Overview of neuroimmunology and CNS function

Neuroinflammation is a hallmark of many diseases associated with cognitive impairment including Alzheimer's disease, Parkinson's disease with dementia, multiple sclerosis, anti-NMDA receptor encephalitis and viral encephalitis. However, even under homeostatic, disease-free conditions, communication between the nervous and immune systems is essential for proper brain function. This includes a role for microglia, the resident immune cells of the CNS, which actively extend and retract their processes to remodel their local environment by engulfment of synapses[1–3] or newborn neurons[4–6], and for T cells, non-resident adaptive immune cells, which continuously patrol the CNS and influence cognitive processing through the secretion of cytokines[7–10]. Thus, the neuroprotective or pathological effect of inflammation may depend on specific cytokine expression induced in regionally distinct ways.

1.2 Microglia

1.2.1 Neurodevelopment

The Microglia arise from erythromyeloid progenitors (EMP) of the fetal yolk sac during primitive hematopoiesis and begin seeding the CNS around E9.5 in mice[11,12]. In addition to microglia, other myeloid cells of the CNS including perivascular, meningeal, and choroid plexus macrophages also derive from EMPs of the fetal yolk sac and seed the CNS between E9.5-12.5[13]. The kinetics of microglial seeding into the CNS, coincident with angiogenesis and neurogenesis,

and prior to astrocyte and oligodendrocyte genesis, provides a unique opportunity for microglia to influence neurodevelopment[14]. Indeed, ingenuity pathway analysis (IPA) of microglial gene expression identified many functions associated with nervous system development[15].

Several signaling pathways have been described which are important for microglial development and maintenance in the adult brain including transforming growth factor (TGF)-beta, the transcription factor Pu.1, interferon regulatory factor (IRF)-8 and colony stimulating factor 1 receptor (CSF1R)[11,15–18]. CSF1R signaling is required for proliferation of yolk sac macrophages, as such CSF1R-/- mice do not have microglia although microglia are present in the CNS of animals lacking the ligand CSF1, which suggested an alternate CSF1R ligand is important for maintenance of microglia in the CNS. IL-34 can also signal through CSF1R, and is expressed by neurons in the cortex and hippocampus, but not the cerebellum of adult mice. Accordingly, animals deficient in IL-34 show decreased numbers of microglia in the cortex and hippocampus, with no changes observed in the cerebellum[17,18].

Pioneering *in vivo* imaging studies revealed that microglia in the adult brain are highly dynamic, constantly extending and retracting processes to sample the surrounding environment, contacting neuronal cell bodies, astrocytes, blood vessels and synapses[1,19,20]. Transcriptome analysis revealed that microglia in the adult brain express many genes involved in sensing the environment, and the majority of these recognize intrinsic CNS antigens while a much smaller percentage recognized bacterial or other pathogen associated products[21], suggesting that surveillance of the local environment represents an important microglial function.

1.2.2 Homeostatic function

During development, microglia play a crucial role in refining circuits by pruning excess synapses[2,3], or promoting the formation of new ones[22,23]. In the lateral geniculate nucleus of the

thalamus, visual circuits are modified through activity dependent synaptic pruning via complement[3]. A recent report has also suggested a role for astrocyte derived IL-33, an IL-1 family member, in signaling to microglia to promote synapse pruning in the thalamus and spinal cord during postnatal synapse maturation[24]. During adulthood, microglia contribute to learning-dependent spine formation[23].

As the specialized tissue-resident macrophage in the CNS, microglia have multiple functions during development and adulthood related to phagocytosis of debris. In addition to the pruning of synapses mentioned above, microglia also remove apoptotic purkinje cell neurons in the developing cerebellum[4], apoptotic newborn cells in the neurogenic niche of the hippocampus[5], and non-apoptotic tbr2+ neural progenitors in the developing cerebral cortex[6].

1.2.3 Role in disease

Under homeostatic conditions, microglia, and other myeloid cells of the CNS derived from EMPs of the yolk sac are long lived and are not replaced by circulating monocytes, with the exception of choroid plexus macrophages which have more frequent turnover[13]. However, during blood brain barrier disruption in the setting of disease, peripheral monocytes can be recruited into the CNS parenchyma and contribute to the pathogenesis or resolution of disease. There continues to be a strong debate over the relative contributions of peripheral-derived macrophages and resident microglia in CNS diseases; in particular the ability of the former to enter and engraft in the CNS and the ability of the latter to proliferate and expand in response to disease. Following facial nerve axotomy, in which microgliosis is observed in the absence of blood brain barrier breakdown, microglia seem to proliferate locally in response to the injury[25]. Single-cell tracking by in vivo imaging confirmed the long-lived nature of microglial cells in the cortex, and suggested that in the setting of Alzheimer's disease the increased density of microglia around

plaques is most likely due to proliferation of neighboring microglia whose daughter cells migrate towards the plaque[26]. These studies suggest that microglia can proliferate in response to disease.

1.2.4 Role in disease

Microglia isolated from different regions of the brain express unique genetic signatures[27]. Cortical and striatal microglia cluster distinctly from cerebellar microglia, with hippocampal microglial demonstrating an intermediate expression profile. Some of the most regionally distinct pathways include those involved in immune function and energy metabolism, which are increased in hippocampal and cerebellar microglia. Interestingly, hippocampal microglia show particular variability in aging, acquiring a profile that more closely resembles cortical microglia. In contrast, cerebellar microglia show increased expression of immune-related genes, consistent with the immune vigilant status of the hindbrain (see section 1.4.4)[27]. Baseline differences in the transcriptional profile of microglia suggest that microglia from distinct brain regions may respond differently to infection or injury, providing an exciting new area of research to be explored.

1.3 Astrocytes

1.3.1 Neurodevelopment

In the developing CNS, neurogenesis precedes astrogenesis. Astrocytes develop from the neural stem cells, although the precise transcriptional cues regulating this "gliogenic switch" remain unknown. Activation of the Janus kinase-signal transducer and activator of transcription (JAK-STAT) signaling pathway promotes astrocyte differentiation[28,29]. Fate-mapping revealed that astrocytes proliferate in the ventricular zone and early astrocyte-restricted precursors migrate to specific regions of the CNS according to their initial site of origin in the ventricular zone[30,31]. *In* vivo imaging studies demonstrated that differentiated astrocytes in the cortex then divide

postnatally to expand and functionally integrate with other CNS cell types[32]. Thus both asymmetric division occurring in germinal centers in late embryogenesis and symmetric division occurring in the final brain region where they will reside accounts for the 6-8 fold increase in astrocyte numbers observed in the first thee postnatal weeks[33]t.

1.3.2 Homeostatic function

Astrocytes perform a diverse array of functions in the developing and adult CNS. Astrocyte end-feet surround cerebrovascular endothelial cells to form the blood brain barrier which regulates entry of molecules and cells into the CNS parenchyma[34]. Astrocytes also send processes toward synaptic connections between neurons to regulate synapse formation and neurotransmitter recycling[35]. Neighboring astrocytes are coupled electrically by gap junctions and buffer extracellular ions, in particular potassium, through expression of the potassium channel Kir4.1[36]. Recent studies have identified unique roles for astrocytes in more complex behaviors. Astrocytes located in the chemoreceptor areas of the brainstem, respond rapidly to changes in pH and release ATP which triggered breathing in mice[37]. Astrocytes from other brain regions were not sensitive to changes in pH, suggesting that astrocytes may acquire regionally distinct functions as they integrate into CNS circuits[37]. Indeed, an early study found that astrocytes from the hippocampus promote neurogenesis when cultured with neural stem cells, but astrocytes from the spinal cord do not[38]. More recent studies have shown that astrocytes in the ventral (motor) and dorsal (sensory) regions of the spinal cord display unique genetic signatures, which influence axon orientation and synapse formation during development[39] and astrocytes in the trigeminal nucleus induce bursting in rhythmogenic neurons by secretion of the calcium binding protein S100β[40]. Collectively, these studies demonstrate that astrocytes perform a wide range of functions, which may be unique to the region of the CNS where they are found.

1.3.3 Role in disease

Astrocytes have long been known to react to injury, however the extent to which this reaction is neuroprotective or pathological has become a recent focus in the field of glial biology. In a pioneering study, Zamanian et al purified astrocytes from the CNS following two different types of injury: ischemic injury by middle cerebral artery occlusion (MCAO) and neuroinflammation by a single i.p. injection of LPS[41]. Transcriptional profiling revealed a set of genes which showed increased expression after both MCAO and LPS, as well as genetic signatures that were unique to one injury or the other[41]. A follow up study further refined the expression profile to define a set of genes coined "pan-reactive" (upregulated in both MCAO and LPS), "A1" (upregulated after LPS) and "A2" (upregulated after MCAO)[42]. Although the nomenclature has sparked some criticism, in part due to controversy surrounding the M1/M2 designation for reactive microglia[43], these studies made important advances by identifying patterns of gene expression associated with neuroprotective or neurotoxic responses.

Astrocytes can serve neuroprotective roles after CNS injury. Recent work has provided evidence to challenge the prevailing the dogma that glial scar formation after spinal cord injury prevents axonal regrowth. In an elegant series of experiments, Anderson et al prevented or removed glial scars and did not see spontaneous regrowth of axons. However, delivery of growth factors via synthetic hydrogel depots in the lesion led to robust regrowth of axons, and this regrowth was significantly blunted in the absence of glial scar formation[44]. Another study identified a unique mechanism of astrocyte-derived mitochondria to neurons to promote survival following stroke[45]. Astrocytes can also serve neurotoxic roles after CNS injury or prevent recovery. LPS reactive astrocytes release a neurotoxic factor, the identity of which is currently

unknown, which kills alpha motor neurons *in vitro*[42]. In a mouse model of Alzheimer's disease, plaque associated astrocytes produced increased levels of the inhibitory neurotransmitter GABA which impaired synaptic plasticity and learning and memory[46]. These studies suggest a functional diversity in the reaction of astrocytes to various types of CNS damage which may promote or prevent recovery.

1.3.4 Enhanced innate immune responses of hindbrain neurons and astrocytes

**The following section is adapted from a box I wrote for our published review[47]*

Astrocytes from different brain regions display distinct immune signatures at baseline and in response to an inflammatory stimulus. Early *in vitro* experiments demonstrated that brain stem astrocytes had elevated MHC-II and ICAM-I expression compared to various forebrain structures[48]. Cerebellar and spinal cord astrocytes additionally released higher basal levels of many chemokines/cytokines *in vitro* compared to cortical astrocytes including IL-1B, CCL2, IL-6, and IL-9, and brain region had specific effects on chemokine/cytokine levels following exposure to HIV proteins[49].

Neurons also display regional heterogeneity of innate immune response at baseline and in response to infection. *In situ* hybridization studies demonstrate that ISG-49 (IFIT-3) is highly expressed in the Purkinje cell layer of the cerebellum, corpus callosum, and choroid plexus following LCMV infection. In contrast, ISG-56 (IFIT-1) is most highly expressed in the olfactory bulb and olfactory neurons. Striking differences in ISG expression occurs even in neuronal subpopulations within a given region. For example, while ISG-49 was resent at high levels in Purkinje cell, molecular, and granule neurons of the cerebellum, ISG-56 was primarily restricted to granule neuron layer while ISG-54 (IFIT-2) was found in the Purkinje cell layer.

Granule cell neurons also expressed high levels of ISG-49 and ISG-56 following WNV infection[50]. In fact, differences in expression of innate immune genes can be seen at baseline. Microarray analysis comparing granule cell neurons of the cerebellum to cortical neurons of the cerebral cortex revealed that IFN related genes including *Ifit1, Irf7, Stat1 and OasI* were higher in cerebellar granule cell neurons. Granule cell neurons displayed increased resistance to viral infection at baseline and in response to IFN-b treatment. Indeed, even the kinetics response to IFN-b treatment was increased in cerebellar granule cell neurons peak expression levels of several genes including *Ifit1, Rsad2, and Oas* reached peak expression levels at an earlier time point compared to cortical neurons[51].

1.4 T cells

1.4.1 Meningeal Immunity

A growing body of literature has demonstrated the important role of meningeal T cells in influencing spatial learning in mice[52]. Early experiments demonstrated that SCID mice, which lack functional B and T cells, have impaired performance on the Morris Water Maze[53]. This impairment in spatial learning was not due to differences in motor function or baseline psychomotor abnormalities, and could be reversed with CD3 T cell replenishment[54]. Mice undergoing a spatial learning task demonstrated an increase in CD4+ T cells in the meninges relative to naïve mice which did not undergo cognitive testing[8], and further studies demonstrated a critical role for CD4+ T cells in spatial learning[7,9]. Importantly, surgical resection of deep cervical lymph nodes led to an increase of CD4+ T cells in the meninges and was correlated with deficits in spatial learning relative to sham operated controls[55], suggesting that spatial learning depends in part on maintenance of particular T cell subsets in the meninges[9,55,56]. The discovery of meningeal lymphatics, which demonstrated a structural route for recirculation of meningeal

lymphocytes and drainage of cerebral spinal fluid (CSF), provides an important advance in understanding the interchange between peripheral immune compartments and the CNS[10,57].

1.4.2 Response to RNA virus infection

T cells play a critical role in viral clearance from the CNS, although the response must be carefully controlled to limit immunopathology in an organ with limited capacity for repair. T cell recruitment to the CNS occurs primarily via chemokine signaling pathways. During WNV infection, neuronal production of CXCL10 leads to the recruitment of CXCR3+ T cells to the CNS to control viral infection and promote survival[58]. Reactivation of recruited T cells occurs via interaction with CD11c+ dendritic cells in an IL1R1 dependent manner[59], and release of T cells from the perivascular space into the parenchyma is in part mediated via alterations in polarity of CXCL12 expression at the endothelium[60]. Recent work in a model of neurotropic coronavirus infection highlights the importance of CD8+ T cell reactivation in perivascular spaces of the CNS for viral control and survival. In this work, expression of CCL19 and 21 by stromal endothelial and fibroblast reticular like cells in the perivascular spaces of the CNS was shown to be important for coordinating recruitment and reactivation of antiviral CD8+ T cells to the CNS via CCR7 signaling[61]. The specific chemokine milieu in the infected CNS appears to also influence T cell activity and antiviral response. During acute infection with LCMV, cytotoxic T lymphocytes express chemokines which leads to peripheral myeloid cell recruitment, severe immunopathology and death[62]. However, during chronic LCMV infection, therapeutic administration of virus specific T cells can lead to non-cytopathic clearance of virus[63].

T cells can persist in the CNS for months to years following neurotropic infection with dengue[64], VSV[65], WNV[66,67] and influenza[68], however the functional implications of this persistence are relatively unknown. Tissue resident memory T cells (T_{RM} cells) are a recently

described class of long lived memory T cells which reside in non-lymphoid tissues at sites of prior antigen exposure and coordinate a rapid recall response to re-challenge[69,70]. T_{RM} cells are classically defined by the expression of the integrin αE (CD103) and the early activation marker CD69, however expression of these two markers is not uniform across all circulation-independent T_{RM} cells in non-lymphoid tissues. CD69 is rapidly upregulated upon activation through TCR signaling and exposure to type I interferons, and interferes with signaling through the sphingosine 1 phosphate 1 receptor S1P1, preventing T cell egress from the tissue[71,72]. In the CNS, generation of T_{RM} cells appears to be antigen dependent[65,73]. However, persistent antigen exposure was not required for T_{RM} persistence in the CNS[65,68]. CD69+ brain T_{RM} cells also express high levels of the pro-survival molecule Bcl-2[74], which may explain their long term survival despite lack of continuous antigen exposure.

Consistent with studies of T_{RM} cells in other tissues, brain T_{RM} cells are poised to provide enhanced protection against returning pathogens. An early study identified CD69+ CD8+ T cells persisting in the CNS to 320 days post infection (the latest time point analyzed) which retained killing function when exposed to peptide or virus loaded cells *ex vivo*[68]. More recent studies have demonstrated that brain T_{RM} cells can provide enhanced protection and survival in mice upon re-challenge[74,75]. This protection could occur despite depletion of peripheral CD4 and CD8 cells, and was dependent on interferon-gamma and perforin production by the brain T_{RM} cells[74]. While these studies demonstrate the existence of brain T_{RM} cells, and the capacity to provide functional pathogen control upon re-exposure, very little is known about how the presence and activity of persistent T cells may influence activity of resident CNS cells including microglia, astrocytes, and neurons in the absence of overt infection.

1.5 Hippocampal function in learning and memory

1.5.1 Hippocampal circuitry

The hippocampus plays a critical role in the processing, storage and retrieval of different types of memory, in particular spatial memory. Memory is encoded through a feedforward circuit loop that centers around the CA3 region of the hippocampus[76]. The CA3 receives input from the entorhinal cortex either directly through the perforant path, or indirectly through the dentate gyrus (DG). There are excitatory connections between CA3 pyramidal cells, as well as inhibitory input from CA3 interneurons. The primary output of the CA3 is through axons which synapse on CA1 pyramidal cells and interneurons[76]. Different sub-regions of the hippocampus have distinct functions in computational memory processing. In particular, the dentate gyrus, which receives numerous connections from the entorhinal cortex but sends sparse input to the CA3, is responsible for pattern separation[77]. The excitatory connections between CA3 pyramidal cells allow for pattern completion to integrate new spatial memory information into the pattern of what was previously experienced[77]. Elegant studies using a multi-electrode approach to simultaneously record neurons in the DG and CA3 during a spatial processing task in which local and global cues were spatially rotated at distinct angles provided experimental and computational evidence for this long-standing, anatomically-based, hypothesis[78].

1.5.2 Hippocampal circuitry

Neurogenesis occurs in two distinct brain regions in adult animals: the subgranular zone (SGZ) of the dentate gyrus (DG), and the subventricular zone (SVZ) of the lateral ventricles[79]. Genetic labeling studies demonstrated that SVZ neurogenesis contributes to the replacement of olfactory bulb neurons without a change in overall number[80]. In contrast, neurogenesis in the SGZ appears to account for the increase in the number of DG neurons observed as animals age[80]. Blockade of

neurogenesis by radiation or anti-mitotic drugs has led to mixed results over the requirement of adult neurogenesis for spatial learning in adult mice[81]. However, specific targeting of neural precursor cells by genetic ablation in C57BL/6 mice demonstrated that adult neurogenesis is important for spatial learning and memory recall on the Barnes Maze behavioral task[80]. More specifically, hippocampal neurogenesis appears to be important for pattern separation, or the ability to encode and recall small changes between similar inputs, in the dentate gyrus. Ablation of neurogenesis in the SGZ prevented animals from correctly distinguishing between spatially similar reward arms during a modified radial arm maze designed to test pattern separation. Performance of depleted animals was similar to sham-operated controls if the arms were separated by a greater distance[82]. Exercise induced increases in neurogenesis was recently shown to improve spatial pattern separation in adult mice, and aged animals which were exposed to exercise but resistant to increases in neurogenesis were subsequently resistant to exercise-induced benefits in spatial memory[83]. These studies suggest that neurogenesis in the adult rodent hippocampus contributes to spatial memory encoding.

1.5.3 Synaptic plasticity

Long-term potentiation, the ability of repeated afferent stimulation to produce a long-term enhancement of synaptic transmission, has long been the leading hypothesis to explain how synaptic plasticity influences hippocampal encoding of spatial memory[84]. This phenomenon was first observed in the dentate gyrus anesthetized rabbits[85] and has since been validated in other model systems including mice[84]. One of the first studies using the cre-lox system for conditional gene expression, specifically deleted N-methyl-D-aspartate receptors (NMDARs), which are important mediators of LTP, in CA1 neurons to demonstrate that loss of LTP in the CA1 impaired spatial learning on the morris water maze[86]. A seminal study using an inhibitory

avoidance paradigm, which creates a stable memory in rats after one trial, provided experimental evidence that learning induces LTP in the hippocampus[87].

1.6 Inflammation-induced CNS dysfunction in parenchyma infection

*The following sections are adapted from material I wrote for our published review[47]

1.6.1 Viruses

Both DNA and RNA viruses of different families can infect the CNS, leading to the clinical syndromes of meningitis, encephalitis, or meningoencephalitis. Many DNA viruses and few RNA viruses replicate in the nucleus, establishing latency by integrating into the cellular DNA, while most RNA viruses primarily replicate in the cytosol, and generally do not establish latency[88]. Herpes simplex encephalitis (HSE), caused by the DNA virus herpes simplex virus (HSV)-1, is the most common acute, sporadic encephalitis in the US and worldwide[89]. Arthropod-born viruses, or arboviruses, are another important cause of encephalitis (Reviewed in[90]). West Nile virus (WNV), a positive sense RNA flavivirus, is the most widely distributed arbovirus worldwide, with cases reported on every continent but Antarctica[91]. The pathophysiology, diagnosis, and management of acute HSE and WNV have been recently reviewed[92]. Patients with viral encephalitis of any etiology typically present with fever, headache, confusion and altered mental status but may also present with seizures or focal neurological signs. Animal and human studies have demonstrated that both innate immune responses and lymphocyte trafficking to the CNS are important mechanisms of virologic control[93,94]. Neurological and neuropsychiatric sequelae can persist or develop following encephalitis due to a variety of neurotropic pathogens, which has become a prioritized area of research[95]. Patients surviving HSE or WNV encephalitis experience high rates of neurological sequelae including memory impairment (60%), speech disorders (35%) and cognitive

impairment (29%)[96]. Of the 90% of patients who survive WNV, about 50% experience cognitive sequelae deficits including depression, fatigue, memory impairment or changes in executive function that may persist for years[97,98]. Here, we will focus on mechanisms underlying neurological sequelae in HSE and WNV encephalitis in individuals with intact immunity.

Increasing evidence suggests that developmental pathways regulating synaptic plasticity by microglia and astrocytes can be reactivated during disease states. Alterations in synapse homeostasis resulting from aberrant activation of glia may contribute to the cognitive dysfunction seen in many neurocognitive disorders, including Autism Spectrum Disorders and a variety of dementias including Alzheimer's Disease (AD)[99,100]. The complement system, part of innate immunity that initiates adaptive responses to clear virus peripherally[101], influences synapse homeostasis during development[20,102] and can promote synapse elimination during neurodegenerative and neuroinfectious diseases[103,104]. In a model of AD using J20 transgenic mice which harbor a familial AD-mutant of human amyloid precursor protein[105], C1q deposition preceded synapse elimination and plaque formation, and mice deficient in complement signaling had fewer phagocytic microglia and reduced synaptic elimination[104]. Loss of C1q also protected animals from synaptic elimination and downstream behavioral phenotypes in a model of dementia caused by deficiency of progranulin, a pleotropic protein that plays a major role in genetic causes of frontotemporal dementia[106]. Progranulin-deficient microglia exhibit increased lysosomal activity and complement production, leading to preferential elimination of inhibitory neurons[107]. In a model of WNV-induced memory impairment, phagocytic microglia persisted for weeks after viral clearance, and gene signatures associated with complement-mediated synapse remodeling were elevated in the hippocampus, a CNS region responsible for memory[103]. Delayed recovery from acute synapse loss correlated with poor spatial learning, and mice with fewer

microglia (*Il34*$^{-/-}$) or complement deficiency (*C3*$^{-/-}$ or *C3ar*$^{-/-}$) were protected from virus-induced synaptic elimination[103], suggesting aberrant microglial activation and complement-mediated deletion of neuronal communication following viral encephalitis may result in neurological sequelae seen in neurotropic virus-infected survivors.

While instituting intravenous acyclovir as the standard of care for HSE has greatly improved survival rates[108], patients surviving acute infection are at risk for clinical neurologic relapse and the development of new neuropsychiatric symptoms including memory loss and epilepsy[109]. PCR analysis of the CSF during relapse at times reveal an absence of CNS viral replication, leading to the hypothesis that these relapses are in fact immune-mediated[110]. In recent years, numerous studies and case reports have linked clinical relapses to the development of autoimmune encephalitis, and in particular to anti-N-methyl-D-aspartate receptor (NMDAR) encephalitis (Reviewed in[111]). Administration of patient, but not control, CSF to hippocampal cultures leads to a titer-dependent but reversible decrease in NMDAR density without altering the number of synapses or the density of other synaptic proteins like PSD-95, GluR1, GluR2 receptor clusters or GABA receptor[112]. Intracerebral infusion of patient CSF or purified IgG similarly increases NMDAR internalization *in vivo* and alteration in glutamate homeostasis and signaling[112,113]. Furthermore, these autoantibodies inhibited the development of long-term synaptic plasticity *in vitro*[114]. The recent development of a rodent model for anti-NMDAR encephalitis demonstrates that continuous infusion of patient autoantibodies can lead to behavioral deficits, providing a platform for preclinical testing[113]. Whether autoantibodies develop due to molecular mimicry, secondary to release of antigens following neuronal lysis, or as a primary mechanism of neuroprotection by the immune system requires further study.

1.6.2 Neurotropic parasites

CNS infections with certain neurotropic parasites are also known to cause alterations in host behavior. Among the most well-known is *Toxoplasma gondii*, a common zoonotic parasite with a worldwide seroprevalance between 30-70%. *T. gondii*, causes chronic CNS infection and neuroinflammation after ingestion of oocysts in contaminated food or water[115]. Ingested oocysts develop into fast-dividing tachyzoites that invade the gut epithelium and lamina propria, replicate asexually through a process called endodyogeny, and then exit and infect myeloid cells, which allow dissemination to multiple tissue sites in the body (including the eye, heart, liver, lung, lymph nodes, muscles and CNS (Reviewed in[116]). The life cycle of *T. gondii* requires infection of feline prey intermediate hosts whose ingestion leads to infection of feline definitive hosts (Reviewed in[117]). Infection of intermediate host CNS appears to be a critical stage of the *T. gondii* life cycle, ensuring successful predation via modifications in prey's olfactory preferences that reduce predator avoidance[118,119]. Epidemiologic studies of *T. gondii* infection in humans, which may have evolved when human ancestors were still under feline predation[120], similarly link parasite seropositivity with alterations in olfactory preference and behavioral abnormalities in immunocompetent individuals, the latter of which include those associated with neurodegenerative and psychiatric diseases.

CNS invasion by *T. gondii* (Reviewed in[121]), leads to infection of all neural cell types, most of which are promptly cleared of parasite via astrocyte and microglial expression of T cell chemoattractants CCL5, CXCL9 and CXCL10, that recruit IFN-γ-expressing $CD4^+$ and $CD8^+$ T cells directed at *T. gondii* antigens[122]. Neurons remain latently infected with slowly replicating bradyzoites for the life of the host. In murine studies, behavioral effects of *T. gondii* are associated with direct infection of cortical neurons and astrocytes with modification in their

functions, including those that impact innate immunity and dopaminergic and glutamate signaling[123,124]. Direct effects of *T. gondii* on neuronal function, including derailments of neurotransmitter expression, modulation of calcium signaling, and loss of myelinated fibers, MAP-2^{+} neurites and NeuN^{+} cells are all suggestive of parasite-mediated impairment or injury (Reviewed in[125]). These effects are proposed to underlie a variety of behavioral alterations, psychiatric diseases and certain neurodegenerative disorders observed in *T. gondii*–infected hosts. However, aversion to cat urine is also observed in rodents after clearance of cysts[126], and low total cyst burdens and lack of specific neuronal tropism observed in infected brain regions raise the important possibility that chronic *T. gondii* infection induces inflammatory-mediated dysfunction that does not require the persistence of parasite.

The *T. gondii*-infected CNS exhibits increased astrocyte expression of TNF, IL-1a, and IL-6[127], each of which have been implicated in the regulation of neural correlates of memory including adult neurogenesis, synaptic plasticity and modulation of long-term potentiation[128–130]. Molecular interactions between dopaminergic and inflammatory cascades within neurons may underlie behavioral alterations during chronic infection with *T. gondii*. NR4A transcription factors NR4A1, NR4A2, and NR4A3 (also known as Nur77, Nurr1, and Nor1, respectively) share similar DNA-binding properties and have been implicated in regulation of dopamine neurotransmission genes[131]. Nurr1, in particular, induces tyrosine hydroxylase (TH) expression during differentiation of dopaminergic neurons and plays a key role in the maintenance of the dopaminergic system of the adult brain. Consistent with this, *NR4A2* polymorphisms are associated with a variety of neurologic and psychiatric disorders including Parkinson's disease, Lewy body dementia, addiction and attention deficit disorder[132]. Nurr1 and its co-regulating factor, glycogen synthase kinase 3, recruits CoREST, a complex made of several proteins that

assembles chromatin-modifying enzymes, also interacts with the transcription factor complex NF-kB-p65, protecting dopaminergic neurons during LPS-induced inflammation by reducing expression of inflammatory genes, including *Tnf*, NO and *Il1b*, in microglia and astrocytes[133]. Nurr1-heterozygous mice show increased exploratory behavior and reduced anxiety that is exacerbated by chronic infection with *T. gondii* compared with similarly infected wild-type animals[134]. While there are no studies examining *NR4A2* polymorphisms in psychiatric patients chronically infected with *T. gondii,* cognitive deterioration among bipolar disorder patients infected by *T. gondii* has been reported[135]. Genome-wide analyses may be a useful approach to identify susceptibility genes that predispose individuals to development or worsening of affective disorders after infection with *T. gondii.*

1.7 West Nile virus

1.7.1 Virology

West Nile virus (WNV) is a neurotropic, mosquito-borne flavivirus that cycles primarily between birds and rodents. Humans and horses can incidentally serve as dead-end hosts when bitten by an infected mosquito, but due to low levels of viremia do not contribute to the transmission cycle for the virus. WNV is a member of the *Flaviviridae* family which includes other viruses that cause a significant burden of disease worldwide including Dengue virus (DENV)[136], Japanese Encephalitis virus (JEV), Tick-borne encephalitis virus (TBEV) and Zika virus (ZIKV, see section 1.9). Like other flaviviruses, WNV is a single-stranded positive-sense RNA virus containing a single open reading frame. The translated polyprotein is cleaved by viral and host proteases to generate three structural proteins (C, prM, and E) and seven non-structural proteins (NS1, NS2A, NS2B, NS3, NS4a, NS4b)[137].

1.7.2 Epidemiology and clinical presentation

WNV was first isolated from a febrile patient in Uganda in 1947[138] and was introduced to the US in New York in 1999[139]. Since then the virus has spread across the US and is the leading cause of domestically acquired arboviral disease with about 2,000 cases reported to the CDC every year[140]. Most patients who become infected with WNV are asymptomatic or experience non-specific flu-like symptoms that cause significant morbidity but remain undiagnosed[141]. A subset of patients may experience severe and potentially fatal neuroinvasive disease including encephalitis, meningitis, and/or flaccid paralysis[142]. Patients surviving West nile virus experience significant morbidity due to the presence of persistent neurological sequelae which can last for years[98,143–150]. A systematic review of the clinical literature revealed that muscle weakness, fatigue, memory loss and depression are among the most commonly reported symptoms[150]. Fatigue was present in 48-75% of patients after neuroinvasive disease and 48% of patients with WNV fever[150]. Memory loss was present in up to 59% of patients for up to 8 years following infection with WNV[150].

1.8 Zika virus

1.8.1 Epidemiology and clinical presentation

Zika virus was first isolated in 1947 from a rhesus monkey in the Zika forest of Uganda[151]. In 2007 there was an outbreak in the Yap Island of Micronesia primarily characterized by rash, fever, arthralgia and conjunctivitis which represented the first occasion of spread outside of Africa and Asia[152]. In 2013 and 2014 another major outbreak of Zika virus occurred, this time associated with Guillain-Barre syndrome, an autoimmune flaccid paralysis[153]. In 2016 the Zika virus epidemic was named a Public Health Emergency of International Concern (PHEIC) due to the clustered reports of microcephaly and GBS cases in Brazil and other countries[154].

The recent epidemic has revealed multiple outcomes of Zika virus infection causing human disease. Congenital ZIKV exposure can cause multiple abnormalities, now clinically defined as Congenital Zika Syndrome, including severe microcephaly, cortical malformation, subcortical or basal ganglia calcifications, and hypertonia[155]. In addition to Guillain-Barre Syndrome (GBS), which was associated with Zika virus infection in French Polynesia[153], a range of other neurological complications in adults infected with Zika virus have been reported, and the long-term outcomes for patients surviving this emerging neurotropic virus remain unknown[156–162]. Animal studies have demonstrated increased neurotropism and neurovirulence of African lineage strains, particularly in the CNS. Some have suggested that outbreaks may have occurred, but went unnoticed due to the low capacity for detecting and reporting emerging threats in much of the continent[163]. Indeed, a retrospective cohort study in Nigeria in 2012 identified 340 cases of microcephaly among 3196 infants enrolled (10.6%), which at the time was attributed to suspected CMV[164].

1.8.2 Neurotropism

Zika virus can infect human neural progenitor cells derived from human induced pleuripotent stem cells (hiPSCs), leading to increased cell death and cell cycle disturbance[165] which prevents neurosphere proliferation and brain organoid growth *in vitro*[166]. In triple knock out mice deficient in *Irf3, Irf5,* and *Irf7*, retro-orbital injection of a Cambodian isolate of ZIKV led to infection of adult neural progenitor cells in neurogenic zones leading to caspase-3 activation and apoptosis[167]. Another study found early infection of GFAP+ astrocytes and mature neurons in the CNS after intraperitoneal (ip) injection of wildtype pups with a Cambodian isolate on the day of birth (P0), with sparse infection of neural progenitor cells at this developmental stage[168]. Another group infected WT mice at P7 or P21 by intracranial injection with ZIKV MR766 and found

immunoreactivity for the apoptotic marker cleaved caspase 3 (CC3) to colocalize with NeuN, a marker of mature neurons[169]. Finally, a recent study of congenital Zika virus infection in pigtail macaques found decreased numbers of neural progenitors in the neurogenic SGZ and SVZ as well as increases in astrocytes in virus-exposed fetal tissue harvested by caesarean section within one month of their due date[170].

High levels of ZIKV RNA and infectious virus were detected in the spinal cord and brains of 4-6 week old *Ifnar1-/-* mice infected with a ZIKV isolate from French Polynesia[171]. ZIKV non-structural protein 5 (NS5) targets human STAT2 for proteasome-dependent degradation, which allows it to evade the Type I interferon response and cause disease[172,173]. NS5 does not bind mouse STAT2, which could explain the lack of disease in wild-type mice[173]. Indeed, in *Stat2-/-* mice, subcutaneous infection with African lineage strains (Uganda MR766 and Dakar 41519) led to high levels of virus in the brain, robust induction of chemokines and cytokines, and lethality by 7 days post infection. WT animals infected with the same strains did not lose weight or succumb to the infection[174].

1.9 References

1. Davalos D, Grutzendler J, Yang G, et al. ATP mediates rapid microglial response to local brain injury in vivo. *Nat Neurosci*. 2005;8(6):752-758. doi:10.1038/nn1472.
2. Paolicelli RC, Bolasco G, Pagani F, et al. Synaptic pruning by microglia is necessary for normal brain development. *Science*. 2011;333(6048):1456-1458. doi:10.1126/science.1202529.
3. Schafer DP, Lehrman EK, Kautzman AG, et al. Microglia Sculpt Postnatal Neural Circuits in an Activity and Complement-Dependent Manner. *Neuron*. 2012;74(4):691-705. doi:10.1016/j.neuron.2012.03.026.
4. Marín-Teva JL, Dusart I, Colin C, Gervais A, van Rooijen N, Mallat M. Microglia Promote the Death of Developing Purkinje Cells. *Neuron*. 2004;41(4):535-547. doi:10.1016/S0896-6273(04)00069-8.
5. Sierra A, Encinas JM, Deudero JJP, et al. Microglia Shape Adult Hippocampal Neurogenesis through Apoptosis-Coupled Phagocytosis. *Cell Stem Cell*. 2010;7(4):483-495. doi:10.1016/J.STEM.2010.08.014.
6. Cunningham CL, Martínez-Cerdeño V, Noctor SC. Microglia regulate the number of

neural precursor cells in the developing cerebral cortex. *J Neurosci*. 2013;33(10):4216-4233. doi:10.1523/JNEUROSCI.3441-12.2013.
7. Wolf SA, Steiner B, Akpinarli A, et al. CD4-positive T lymphocytes provide a neuroimmunological link in the control of adult hippocampal neurogenesis. *J Immunol*. 2009;182(7):3979-3984. doi:10.4049/jimmunol.0801218.
8. Derecki NC, Cardani AN, Yang CH, et al. Regulation of learning and memory by meningeal immunity: a key role for IL-4. *J Exp Med*. 2010;207(5):1067-1080. doi:10.1084/jem.20091419.
9. Radjavi A, Smirnov I, Kipnis J. Brain antigen-reactive CD4+ T cells are sufficient to support learning behavior in mice with limited T cell repertoire. *Brain Behav Immun*. 2014;35:58-63. doi:10.1016/J.BBI.2013.08.013.
10. Louveau A, Smirnov I, Keyes TJ, et al. Structural and functional features of central nervous system lymphatic vessels. *Nature*. 2015;523(7560):337-341. doi:10.1038/nature14432.
11. Ginhoux F, Greter M, Leboeuf M, et al. Fate mapping analysis reveals that adult microglia derive from primitive macrophages. *Science*. 2010;330(6005):841-845. doi:10.1126/science.1194637.
12. Gomez Perdiguero E, Klapproth K, Schulz C, et al. Tissue-resident macrophages originate from yolk-sac-derived erythro-myeloid progenitors. *Nature*. 2015;518(7540):547-551. doi:10.1038/nature13989.
13. Goldmann T, Wieghofer P, Jordão MJC, et al. Origin, fate and dynamics of macrophages at central nervous system interfaces. *Nat Immunol*. 2016;17(7):797-805. doi:10.1038/ni.3423.
14. Li Q, Barres BA. Microglia and macrophages in brain homeostasis and disease. *Nat Rev Immunol*. 2017;18(4):225-242. doi:10.1038/nri.2017.125.
15. Butovsky O, Jedrychowski MP, Moore CS, et al. Identification of a unique TGF-β–dependent molecular and functional signature in microglia. *Nat Neurosci*. 2014;17(1):131-143. doi:10.1038/nn.3599.
16. Goldmann T, Wieghofer P, Jordão MJC, et al. Origin, fate and dynamics of macrophages at central nervous system interfaces. *Nat Immunol*. 2016;17(7):797-805. doi:10.1038/ni.3423.
17. Greter M, Lelios I, Pelczar P, et al. Stroma-derived interleukin-34 controls the development and maintenance of langerhans cells and the maintenance of microglia. *Immunity*. 2012;37(6):1050-1060. doi:10.1016/j.immuni.2012.11.001.
18. Wang Y, Szretter KJ, Vermi W, et al. IL-34 is a tissue-restricted ligand of CSF1R required for the development of Langerhans cells and microglia. *Nat Immunol*. 2012;13(8):753-760. doi:10.1038/ni.2360.
19. Nimmerjahn A, Kirchhoff F, Helmchen F. Resting microglial cells are highly dynamic surveillants of brain parenchyma in vivo. *Science*. 2005;308(5726):1314-1318. doi:10.1126/science.1110647.
20. Tremblay M-È, Lowery RL, Majewska AK. Microglial Interactions with Synapses Are Modulated by Visual Experience. Dalva M, ed. *PLoS Biol*. 2010;8(11):e1000527. doi:10.1371/journal.pbio.1000527.
21. Hickman SE, Kingery ND, Ohsumi TK, et al. The microglial sensome revealed by direct RNA sequencing. *Nat Neurosci*. 2013;16(12):1896-1905. doi:10.1038/nn.3554.
22. Miyamoto A, Wake H, Ishikawa AW, et al. Microglia contact induces synapse formation

in developing somatosensory cortex. *Nat Commun*. 2016;7:12540. doi:10.1038/ncomms12540.
23. Parkhurst CN, Yang G, Ninan I, et al. Microglia promote learning-dependent synapse formation through brain-derived neurotrophic factor. *Cell*. 2013;155(7):1596-1609. doi:10.1016/j.cell.2013.11.030.
24. Vainchtein ID, Chin G, Cho FS, et al. Astrocyte-derived interleukin-33 promotes microglial synapse engulfment and neural circuit development. *Science*. 2018;359(6381):1269-1273. doi:10.1126/science.aal3589.
25. Tay TL, Mai D, Dautzenberg J, et al. A new fate mapping system reveals context-dependent random or clonal expansion of microglia. *Nat Neurosci*. 2017;20(6):793-803. doi:10.1038/nn.4547.
26. Füger P, Hefendehl JK, Veeraraghavalu K, et al. Microglia turnover with aging and in an Alzheimer's model via long-term in vivo single-cell imaging. *Nat Neurosci*. 2017;20(10):1371-1376. doi:10.1038/nn.4631.
27. Grabert K, Michoel T, Karavolos MH, et al. Microglial brain region−dependent diversity and selective regional sensitivities to aging. *Nat Neurosci*. 2016;19(3):504-516. doi:10.1038/nn.4222.
28. Bonni A, Sun Y, Nadal-Vicens M, et al. Regulation of gilogenesis in the central nervous system by the jak-stat signaling pathway. *Science (80-)*. 1997;278(October):477-483.
29. He F, Ge W, Martinowich K, et al. A positive autoregulatory loop of Jak-STAT signaling controls the onset of astrogliogenesis. *Nat Neurosci*. 2005;8(5):616-625. doi:10.1038/nn1440.
30. Tien A-C, Tsai H-H, Molofsky A V., et al. Regulated temporal-spatial astrocyte precursor cell proliferation involves BRAF signalling in mammalian spinal cord. *Development*. 2012;139(14):2477-2487. doi:10.1242/dev.077214.
31. Tsai HH, Li H, Fuentealba LC, et al. Regional astrocyte allocation regulates CNS synaptogenesis and repair. *Science (80-)*. 2012;337(6092):358-362. doi:10.1126/science.1222381.
32. Ge W-P, Miyawaki A, Gage FH, Jan YN, Jan LY. Local generation of glia is a major astrocyte source in postnatal cortex. *Nature*. 2012;484(7394):376-380. doi:10.1038/nature10959.
33. Bandeira F, Lent R, Herculano-Houzel S. Changing numbers of neuronal and non-neuronal cells underlie postnatal brain growth in the rat. *Proc Natl Acad Sci U S A*. 2009;106(33):14108-14113. doi:10.1073/pnas.0804650106.
34. Abbott NJ, Rönnbäck L, Hansson E. Astrocyte–endothelial interactions at the blood–brain barrier. *Nat Rev Neurosci*. 2006;7(1):41-53. doi:10.1038/nrn1824.
35. Clarke LE, Barres BA. Emerging roles of astrocytes in neural circuit development. *Nat Rev Neurosci*. 2013;14(5):311-321. doi:10.1038/nrn3484.
36. Seifert G, Huttmann K, Binder DK, et al. Analysis of Astroglial K+ Channel Expression in the Developing Hippocampus Reveals a Predominant Role of the Kir4.1 Subunit. *J Neurosci*. 2009;29(23):7474-7488. doi:10.1523/JNEUROSCI.3790-08.2009.
37. Gourine A V, Kasymov V, Marina N, et al. Astrocytes control breathing through pH-dependent release of ATP. *Science*. 2010;329(5991):571-575. doi:10.1126/science.1190721.
38. Song H, Stevens CF, Gage FH. Astroglia induce neurogenesis from adult neural stem cells. *Nature*. 2002;417(6884):39-44. doi:10.1038/417039a.

39. Molofsky A V., Kelley KW, Tsai H-H, et al. Astrocyte-encoded positional cues maintain sensorimotor circuit integrity. *Nature*. 2014;509(7499):189-194. doi:10.1038/nature13161.
40. Morquette P, Verdier D, Kadala A, et al. An astrocyte-dependent mechanism for neuronal rhythmogenesis. *Nat Neurosci*. 2015;18(6):844-854. doi:10.1038/nn.4013.
41. Zamanian JL, Xu L, Foo LC, et al. Genomic analysis of reactive astrogliosis. *J Neurosci*. 2012;32(18):6391-6410. doi:10.1523/JNEUROSCI.6221-11.2012.
42. Liddelow SA, Guttenplan KA, Clarke LE, et al. Neurotoxic reactive astrocytes are induced by activated microglia. *Nature*. 2017;541(7638):481-487. doi:10.1038/nature21029.
43. Ransohoff RM. A polarizing question: do M1 and M2 microglia exist? *Nat Neurosci*. 2016;19(8):987-991. doi:10.1038/nn.4338.
44. Anderson MA, Burda JE, Ren Y, et al. Astrocyte scar formation aids central nervous system axon regeneration. *Nature*. 2016;532(7598):195-200. doi:10.1038/nature17623.
45. Hayakawa K, Esposito E, Wang X, et al. Transfer of mitochondria from astrocytes to neurons after stroke. *Nature*. 2016;535(7613):551-555. doi:10.1038/nature18928.
46. Jo S, Yarishkin O, Hwang YJ, et al. GABA from reactive astrocytes impairs memory in mouse models of Alzheimer's disease. *Nat Med*. 2014;20(8):886-896. doi:10.1038/nm.3639.
47. Klein RS, Garber C, Howard N. Infectious immunity in the central nervous system and brain function. *Nat Immunol 2017 182*. 2017;18(2):132. doi:10.1038/ni.3656.
48. Morga E, Faber C, Heuschling P. Cultured astrocytes express regional heterogeneity of the immunoreactive phenotype under basal conditions and after γ-IFN induction. *J Neuroimmunol*. 1998;87(1):179-184. doi:10.1016/S0165-5728(98)00099-X.
49. Fitting S, Zou S, Chen W, Vo P, Hauser KF, Knapp PE. Regional Heterogeneity and Diversity in Cytokine and Chemokine Production by Astroglia: Differential Responses to HIV-1 Tat, gp120 and Morphine Revealed by Multiplex Analysis. *J Proteome Res J Proteome Res April*. 2010;5(94):1795-1804. doi:10.1021/pr900926n.
50. Wacher C, Müller M, Hofer MJ, et al. Coordinated regulation and widespread cellular expression of interferon-stimulated genes (ISG) ISG-49, ISG-54, and ISG-56 in the central nervous system after infection with distinct viruses. *J Virol*. 2007;81(2):860-871. doi:10.1128/JVI.01167-06.
51. Cho H, Proll SC, Szretter KJ, Katze MG, Gale M, Diamond MS. Differential innate immune response programs in neuronal subtypes determine susceptibility to infection in the brain by positive-stranded RNA viruses. *Nat Med*. 2013;19(4):458-464. doi:10.1038/nm.3108.
52. Kipnis J. Multifaceted interactions between adaptive immunity and the central nervous system. *Science*. 2016;353(6301):766-771. doi:10.1126/science.aag2638.
53. Kipnis J, Cohen H, Cardon M, Ziv Y, Schwartz M. T cell deficiency leads to cognitive dysfunction: Implications for therapeutic vaccination for schizophrenia and other psychiatric conditions. 2004;101(21):8180-8185.
54. Brynskikh A, Warren T, Zhu J, Kipnis J. Adaptive immunity affects learning behavior in mice. *Brain Behav Immun*. 2008;22(6):861-869. doi:10.1016/J.BBI.2007.12.008.
55. Radjavi A, Smirnov I, Derecki N, Kipnis J. Dynamics of the meningeal CD4+ T-cell repertoire are defined by the cervical lymph nodes and facilitate cognitive task performance in mice. *Mol Psychiatry*. 2014;19(5):531-532. doi:10.1038/mp.2013.79.
56. Ziv Y, Ron N, Butovsky O, et al. Immune cells contribute to the maintenance of

neurogenesis and spatial learning abilities in adulthood. *Nat Neurosci*. 2006;9(2):268-275. doi:10.1038/nn1629.
57. Aspelund A, Antila S, Proulx ST, et al. A dural lymphatic vascular system that drains brain interstitial fluid and macromolecules. *J Exp Med*. 2015;212(7):991-999. doi:10.1084/jem.20142290.
58. Klein RS, Lin E, Zhang B, et al. Neuronal CXCL10 directs CD8+ T-cell recruitment and control of West Nile virus encephalitis. *J Virol*. 2005;79(17):11457-11466. doi:10.1128/JVI.79.17.11457-11466.2005.
59. Durrant DM, Robinette ML, Klein RS. IL-1R1 is required for dendritic cell-mediated T cell reactivation within the CNS during West Nile virus encephalitis. *J Exp Med*. 2013;210(3):503-516. doi:10.1084/jem.20121897.
60. McCandless EE, Zhang B, Diamond MS, Klein RS. CXCR4 antagonism increases T cell trafficking in the central nervous system and improves survival from West Nile virus encephalitis. *Proc Natl Acad Sci U S A*. 2008;105(32):11270-11275. doi:10.1073/pnas.0800898105.
61. Cupovic J, Onder L, Gil-Cruz C, et al. Central Nervous System Stromal Cells Control Local CD8(+) T Cell Responses during Virus-Induced Neuroinflammation. *Immunity*. 2016;44(3):622-633. doi:10.1016/j.immuni.2015.12.022.
62. Kim J V., Kang SS, Dustin ML, McGavern DB. Myelomonocytic cell recruitment causes fatal CNS vascular injury during acute viral meningitis. *Nature*. 2009;457(7226):191-195. doi:10.1038/nature07591.
63. Herz J, Johnson KR, McGavern DB. Therapeutic antiviral T cells noncytopathically clear persistently infected microglia after conversion into antigen-presenting cells. *J Exp Med*. 2015;212(8):1153-1169. doi:10.1084/jem.20142047.
64. Most RG v. d. Prolonged presence of effector-memory CD8 T cells in the central nervous system after dengue virus encephalitis. *Int Immunol*. 2003;15(1):119-125. doi:10.1093/intimm/dxg009.
65. Wakim LM, Woodward-davis A, Bevan MJ. Memory T cells persisting within the brain after local infection show functional adaptations to their tissue of residence. 2010. doi:10.1073/pnas.1010201107/-/DCSupplemental.www.pnas.org/cgi/doi/10.1073/pnas.1010201107.
66. Graham JB, Da Costa A, Lund JM. Regulatory T cells shape the resident memory T cell response to virus infection in the tissues. *J Immunol*. 2014;192(2):683-690. doi:10.4049/jimmunol.1202153.
67. Stewart BS, Demarest VL, Wong SJ, Green S, Bernard KA. Persistence of virus-specific immune responses in the central nervous system of mice after West Nile virus infection. *BMC Immunol*. 2011;12(1):6. doi:10.1186/1471-2172-12-6.
68. Hawke S, Stevenson PG, Freeman S, Bangham CR. Long-term persistence of activated cytotoxic T lymphocytes after viral infection of the central nervous system. *J Exp Med*. 1998;187(10):1575-1582. doi:10.1084/JEM.187.10.1575.
69. Mueller SN, Mackay LK. Tissue-resident memory T cells: local specialists in immune defence. *Nat Rev Immunol*. 2016;16(2):79-89. doi:10.1038/nri.2015.3.
70. Schenkel JM, Fraser K a, Beura LK, Pauken KE, Vezys V, Masopust D. Resident memory CD8 T cells trigger protective innate and adaptive immune responses. *Science (80-)*. 2014;346(6205):98-101. doi:10.1126/science.1254536.
71. Shiow LR, Rosen DB, Brdičková N, et al. CD69 acts downstream of interferon-α/β to

inhibit S1P1 and lymphocyte egress from lymphoid organs. *Nature*. 2006;440(7083):540-544. doi:10.1038/nature04606.
72. Mackay LK, Braun A, Macleod BL, et al. Cutting edge: CD69 interference with sphingosine-1-phosphate receptor function regulates peripheral T cell retention. *J Immunol*. 2015;194(5):2059-2063. doi:10.4049/jimmunol.1402256.
73. Casey KA, Fraser KA, Schenkel JM, et al. Antigen-independent differentiation and maintenance of effector-like resident memory T cells in tissues. *J Immunol*. 2012;188(10):4866-4875. doi:10.4049/jimmunol.1200402.
74. Steinbach K, Vincenti I, Kreutzfeldt M, et al. Brain-resident memory T cells represent an autonomous cytotoxic barrier to viral infection. *J Exp Med*. 2016;213(8):1571-1587. doi:10.1084/jem.20151916.
75. Wakim LM, Woodward-Davis A, Liu R, et al. The molecular signature of tissue resident memory CD8 T cells isolated from the brain. *J Immunol*. 2012;189(7):3462-3471. doi:10.4049/jimmunol.1201305.
76. Rebola N, Carta M, Mulle C. Operation and plasticity of hippocampal CA3 circuits: implications for memory encoding. *Nat Rev Neurosci*. 2017;18(4):208-220. doi:10.1038/nrn.2017.10.
77. Newman EL, Hasselmo ME. CA3 Sees the Big Picture while Dentate Gyrus Splits Hairs. *Neuron*. 2014;81(2):226-228. doi:10.1016/J.NEURON.2014.01.004.
78. Neunuebel JP, Knierim JJ. CA3 Retrieves Coherent Representations from Degraded Input: Direct Evidence for CA3 Pattern Completion and Dentate Gyrus Pattern Separation. *Neuron*. 2014;81(2):416-427. doi:10.1016/J.NEURON.2013.11.017.
79. Deng W, Aimone JB, Gage FH. New neurons and new memories: how does adult hippocampal neurogenesis affect learning and memory? *Nat Rev Neurosci*. 2010;11(5):339-350. doi:10.1038/nrn2822.
80. Imayoshi I, Sakamoto M, Ohtsuka T, et al. Roles of continuous neurogenesis in the structural and functional integrity of the adult forebrain. *Nat Neurosci*. 2008;11(10):1153-1161. doi:10.1038/nn.2185.
81. Yau S, Li A, So K-F. Involvement of Adult Hippocampal Neurogenesis in Learning and Forgetting. *Neural Plast*. 2015;2015:717958. doi:10.1155/2015/717958.
82. Clelland CD, Choi M, Romberg C, et al. A functional role for adult hippocampal neurogenesis in spatial pattern separation. *Science*. 2009;325(5937):210-213. doi:10.1126/science.1173215.
83. Creer DJ, Romberg C, Saksida LM, van Praag H, Bussey TJ. Running enhances spatial pattern separation in mice. *Proc Natl Acad Sci U S A*. 2010;107(5):2367-2372. doi:10.1073/pnas.0911725107.
84. Neves G, Cooke SF, Bliss TVP. Synaptic plasticity, memory and the hippocampus: a neural network approach to causality. *Nat Rev Neurosci*. 2008;9(1):65-75. doi:10.1038/nrn2303.
85. Bliss TVP, Lømo T. Long-lasting potentiation of synaptic transmission in the dentate area of the anaesthetized rabbit following stimulation of the perforant path. *J Physiol*. 1973;232(2):331-356. doi:10.1113/jphysiol.1973.sp010273.
86. Tsien JZ, Huerta PT, Tonegawa S. The Essential Role of Hippocampal CA1 NMDA Receptor–Dependent Synaptic Plasticity in Spatial Memory. *Cell*. 1996;87(7):1327-1338. doi:10.1016/S0092-8674(00)81827-9.
87. Whitlock JR, Heynen AJ, Shuler MG, Bear MF. Learning induces long-term potentiation

in the hippocampus. *Science*. 2006;313(5790):1093-1097. doi:10.1126/science.1128134.
88. Mettenleiter TC. Breaching the Barrier—The Nuclear Envelope in Virus Infection. *J Mol Biol*. 2016;428(10):1949-1961. doi:10.1016/J.JMB.2015.10.001.
89. Granerod J, Ambrose HE, Davies NW, et al. Causes of encephalitis and differences in their clinical presentations in England: a multicentre, population-based prospective study. *Lancet Infect Dis*. 2010;10(12):835-844. doi:10.1016/S1473-3099(10)70222-X.
90. Salimi H, Cain MD, Klein RS. Encephalitic Arboviruses: Emergence, Clinical Presentation, and Neuropathogenesis. *Neurotherapeutics*. 2016;13(3):514-534. doi:10.1007/s13311-016-0443-5.
91. Kramer LD, Styer LM, Ebel GD. A Global Perspective on the Epidemiology of West Nile Virus. *Annu Rev Entomol*. 2008;53(1):61-81. doi:10.1146/annurev.ento.53.103106.093258.
92. Bradshaw MJ, Venkatesan A. Herpes Simplex Virus-1 Encephalitis in Adults: Pathophysiology, Diagnosis, and Management. *Neurotherapeutics*. 2016;13(3):493-508. doi:10.1007/s13311-016-0433-7.
93. Altfeld M, Gale Jr M. Innate immunity against HIV-1 infection. *Nat Immunol*. 2015;16(6):554-562. doi:10.1038/ni.3157.
94. Armangue T, Moris G, Cantarín-Extremera V, et al. Autoimmune post-herpes simplex encephalitis of adults and teenagers. *Neurology*. 2015;85(20):1736-1743. doi:10.1212/WNL.0000000000002125.
95. John CC, Carabin H, Montano SM, Bangirana P, Zunt JR, Peterson PK. Global research priorities for infections that affect the nervous system. *Nature*. 2015;527(7578):S178-S186. doi:10.1038/nature16033.
96. STAHL JP, MAILLES A, De BROUCKER T, Group the SC and I. Herpes simplex encephalitis and management of acyclovir in encephalitis patients in France. *Epidemiol Infect*. 2012;140(2):372-381. doi:10.1017/S0950268811000483.
97. Garcia MN, Hause AM, Walker CM, Orange JS, Hasbun R, Murray KO. Evaluation of Prolonged Fatigue Post–West Nile Virus Infection and Association of Fatigue with Elevated Antiviral and Proinflammatory Cytokines. *Viral Immunol*. 2014;27(7):327-333. doi:10.1089/vim.2014.0035.
98. Sadek JR, Pergam S a, Harrington J a, et al. Persistent neuropsychological impairment associated with West Nile virus infection. *J Clin Exp Neuropsychol*. 2010;32(1):81-87. doi:10.1080/13803390902881918.
99. Guerreiro R, Wojtas A, Bras J, et al. *TREM2* Variants in Alzheimer's Disease. *N Engl J Med*. 2013;368(2):117-127. doi:10.1056/NEJMoa1211851.
100. Chung W-S, Welsh CA, Barres BA, Stevens B. Do glia drive synaptic and cognitive impairment in disease? *Nat Neurosci*. 2015;18(11):1539-1545. doi:10.1038/nn.4142.
101. Mehlhop E, Diamond MS. Protective immune responses against West Nile virus are primed by distinct complement activation pathways. *J Exp Med*. 2006;203(5):1371-1381. doi:10.1084/jem.20052388.
102. Schafer DP, Lehrman EK, Kautzman AG, et al. Microglia Sculpt Postnatal Neural Circuits in an Activity and Complement-Dependent Manner. *Neuron*. 2012;74(4):691-705. doi:10.1016/J.NEURON.2012.03.026.
103. Vasek MJ, Garber C, Dorsey D, et al. A complement–microglial axis drives synapse loss during virus-induced memory impairment. *Nature*. 2016;534(7608):538-543. doi:10.1038/nature18283.

104. Hong S, Beja-Glasser VF, Nfonoyim BM, et al. Complement and microglia mediate early synapse loss in Alzheimer mouse models. *Science*. 2016;352(6286):712-716. doi:10.1126/science.aad8373.
105. Mucke L, Masliah E, Yu GQ, et al. High-level neuronal expression of abeta 1-42 in wild-type human amyloid protein precursor transgenic mice: synaptotoxicity without plaque formation. *J Neurosci*. 2000;20(11):4050-4058. doi:10.1523/JNEUROSCI.20-11-04050.2000.
106. Woollacott IOC, Rohrer JD. The clinical spectrum of sporadic and familial forms of frontotemporal dementia. *J Neurochem*. 2016;138:6-31. doi:10.1111/jnc.13654.
107. Lui H, Zhang J, Makinson SR, et al. Progranulin Deficiency Promotes Circuit-Specific Synaptic Pruning by Microglia via Complement Activation. *Cell*. 2016;165(4):921-935. doi:10.1016/j.cell.2016.04.001.
108. Sköldenberg B, Alestig K, Burman L, et al. ACYCLOVIR VERSUS VIDARABINE IN HERPES SIMPLEX ENCEPHALITIS. *Lancet*. 1984;324(8405):707-711. doi:10.1016/S0140-6736(84)92623-0.
109. Sili U, Kaya A, Mert A, et al. Herpes simplex virus encephalitis: clinical manifestations, diagnosis and outcome in 106 adult patients. *J Clin Virol*. 2014;60(2):112-118. doi:10.1016/j.jcv.2014.03.010.
110. De Tiege X, Rozenberg F, Des Portes V, et al. Herpes simplex encephalitis relapses in children: Differentiation of two neurologic entities. *Neurology*. 2003;61(2):241-243. doi:10.1212/01.WNL.0000073985.71759.7C.
111. Leypoldt F, Armangue T, Dalmau J. Autoimmune encephalopathies. *Ann N Y Acad Sci*. 2015;1338(1):94-114. doi:10.1111/nyas.12553.
112. Hughes EG, Peng X, Gleichman AJ, et al. Cellular and synaptic mechanisms of anti-NMDA receptor encephalitis. *J Neurosci*. 2010;30(17):5866-5875. doi:10.1523/JNEUROSCI.0167-10.2010.
113. Planagumà J, Leypoldt F, Mannara F, et al. Human N-methyl D-aspartate receptor antibodies alter memory and behaviour in mice. *Brain*. 2015;138(Pt 1):94-109. doi:10.1093/brain/awu310.
114. Mikasova L, De Rossi P, Bouchet D, et al. Disrupted surface cross-talk between NMDA and Ephrin-B2 receptors in anti-NMDA encephalitis. *Brain*. 2012;135(Pt 5):1606-1621. doi:10.1093/brain/aws092.
115. Guo M, Mishra A, Buchanan RL, et al. A Systematic Meta-Analysis of *Toxoplasma gondii* Prevalence in Food Animals in the United States. *Foodborne Pathog Dis*. 2016;13(3):109-118. doi:10.1089/fpd.2015.2070.
116. Ueno N, Lodoen MB. From the blood to the brain: avenues of eukaryotic pathogen dissemination to the central nervous system. *Curr Opin Microbiol*. 2015;26:53-59. doi:10.1016/J.MIB.2015.05.006.
117. White MW, Radke JR, Radke JB. *T oxoplasma* development - turn the switch on or off? *Cell Microbiol*. 2014;16(4):466-472. doi:10.1111/cmi.12267.
118. Flegr J, Lenochová P, Hodný Z, Vondrová M. Fatal Attraction Phenomenon in Humans – Cat Odour Attractiveness Increased for Toxoplasma-Infected Men While Decreased for Infected Women. Webster JP, ed. *PLoS Negl Trop Dis*. 2011;5(11):e1389. doi:10.1371/journal.pntd.0001389.
119. Vyas A, Kim S-K, Giacomini N, Boothroyd JC, Sapolsky RM. Behavioral changes induced by Toxoplasma infection of rodents are highly specific to aversion of cat odors.

Proc Natl Acad Sci U S A. 2007;104(15):6442-6447. doi:10.1073/pnas.0608310104.
120. Poirotte C, Kappeler PM, Ngoubangoye B, Bourgeois S, Moussodji M, Charpentier MJE. Morbid attraction to leopard urine in Toxoplasma-infected chimpanzees. *Curr Biol*. 2016;26(3):R98-R99. doi:10.1016/J.CUB.2015.12.020.
121. Blanchard N, Dunay IR, Schlüter D. Persistence of *Toxoplasma gondii* in the central nervous system: a fine-tuned balance between the parasite, the brain and the immune system. *Parasite Immunol*. 2015;37(3):150-158. doi:10.1111/pim.12173.
122. Landrith TA, Harris TH, Wilson EH. Characteristics and critical function of CD8+ T cells in the Toxoplasma-infected brain. *Semin Immunopathol*. 2015;37(3):261-270. doi:10.1007/s00281-015-0487-3.
123. Cabral CM, Tuladhar S, Dietrich HK, et al. Neurons are the Primary Target Cell for the Brain-Tropic Intracellular Parasite Toxoplasma gondii. Denkers EY, ed. *PLOS Pathog*. 2016;12(2):e1005447. doi:10.1371/journal.ppat.1005447.
124. David CN, Frias ES, Szu JI, et al. GLT-1-Dependent Disruption of CNS Glutamate Homeostasis and Neuronal Function by the Protozoan Parasite Toxoplasma gondii. Pletnikov M, ed. *PLOS Pathog*. 2016;12(6):e1005643. doi:10.1371/journal.ppat.1005643.
125. Parlog A, Schlüter D, Dunay IR. *Toxoplasma gondii* -induced neuronal alterations. *Parasite Immunol*. 2015;37(3):159-170. doi:10.1111/pim.12157.
126. Ingram WM, Goodrich LM, Robey EA, Eisen MB. Mice Infected with Low-Virulence Strains of Toxoplasma gondii Lose Their Innate Aversion to Cat Urine, Even after Extensive Parasite Clearance. Wilson EH, ed. *PLoS One*. 2013;8(9):e75246. doi:10.1371/journal.pone.0075246.
127. Mahmoudvand H, Ziaali N, Ghazvini H, et al. Toxoplasma gondii Infection Promotes Neuroinflammation Through Cytokine Networks and Induced Hyperalgesia in BALB/c Mice. *Inflammation*. 2016;39(1):405-412. doi:10.1007/s10753-015-0262-6.
128. Riazi K, Galic MA, Kentner AC, Reid AY, Sharkey KA, Pittman QJ. Microglia-dependent alteration of glutamatergic synaptic transmission and plasticity in the hippocampus during peripheral inflammation. *J Neurosci*. 2015;35(12):4942-4952. doi:10.1523/JNEUROSCI.4485-14.2015.
129. Wu MD, Montgomery SL, Rivera-Escalera F, Olschowka JA, O'Banion MK. Sustained IL-1β expression impairs adult hippocampal neurogenesis independent of IL-1 signaling in nestin+ neural precursor cells. *Brain Behav Immun*. 2013;32:9-18. doi:10.1016/J.BBI.2013.03.003.
130. del Rey A, Balschun D, Wetzel W, Randolf A, Besedovsky HO. A cytokine network involving brain-borne IL-1β, IL-1ra, IL-18, IL-6, and TNFα operates during long-term potentiation and learning. *Brain Behav Immun*. 2013;33:15-23. doi:10.1016/J.BBI.2013.05.011.
131. Eells JB, Wilcots J, Sisk S, Guo-Ross SX. NR4A Gene Expression Is Dynamically Regulated in the Ventral Tegmental Area Dopamine Neurons and Is Related to Expression of Dopamine Neurotransmission Genes. *J Mol Neurosci*. 2012;46(3):545-553. doi:10.1007/s12031-011-9642-z.
132. Grimes DA, Han F, Panisset M, et al. Translated mutation in the Nurr1 gene as a cause for Parkinson's disease. *Mov Disord*. 2006;21(7):906-909. doi:10.1002/mds.20820.
133. Lallier SW, Graf AE, Waidyarante GR, Rogers LK. Nurr1 expression is modified by inflammation in microglia. *Neuroreport*. 2016;27(15):1120-1127. doi:10.1097/WNR.0000000000000665.

134. Eells JB, Varela-Stokes A, Guo-Ross SX, et al. Chronic Toxoplasma gondii in Nurr1-Null Heterozygous Mice Exacerbates Elevated Open Field Activity. Wilson EH, ed. *PLoS One*. 2015;10(4):e0119280. doi:10.1371/journal.pone.0119280.
135. Hamdani N, Daban-Huard C, Lajnef M, et al. Cognitive deterioration among bipolar disorder patients infected by Toxoplasma gondii is correlated to interleukin 6 levels. *J Affect Disord*. 2015;179:161-166. doi:10.1016/J.JAD.2015.03.038.
136. Stanaway JD, Shepard DS, Undurraga EA, et al. The global burden of dengue: an analysis from the Global Burden of Disease Study 2013. *Lancet Infect Dis*. 2016;16(6):712-723. doi:10.1016/S1473-3099(16)00026-8.
137. Brinton MA. The Molecular Biology of West Nile Virus: A New Invader of the Western Hemisphere. *Annu Rev Microbiol*. 2002;56(1):371-402. doi:10.1146/annurev.micro.56.012302.160654.
138. Hughes TP, Paul JH, Smithburn KC, Burke AW. A Neurotropic Virus Isolated from the Blood of a Native of Uganda 1. *Am J Trop Med Hyg*. 1940;s1-20(4):471-492. doi:10.4269/ajtmh.1940.s1-20.471.
139. Nash D, Mostashari F, Fine A, et al. The Outbreak of West Nile Virus Infection in the New York City Area in 1999. *N Engl J Med*. 2001;344(24):1807-1814. doi:10.1056/NEJM200106143442401.
140. Burakoff A, Lehman J, Fischer M, Staples JE, Lindsey NP. West Nile Virus and Other Nationally Notifiable Arboviral Diseases — United States, 2016. *MMWR Morb Mortal Wkly Rep*. 2018;67(1):13-17. doi:10.15585/mmwr.mm6701a3.
141. Zou S, Foster GA, Dodd RY, Petersen LR, Stramer SL. West Nile Fever Characteristics among Viremic Persons Identified through Blood Donor Screening. *J Infect Dis*. 2010;202(9):1354-1361. doi:10.1086/656602.
142. Davis LE, DeBiasi R, Goade DE, et al. West Nile virus neuroinvasive disease. *Ann Neurol*. 2006;60(3):286-300. doi:10.1002/ana.20959.
143. Carson PJ, Konewko P, Wold KS, et al. Long-term clinical and neuropsychological outcomes of West Nile virus infection. *Clin Infect Dis*. 2006;43(6):723-730. doi:10.1086/506939.
144. Loeb M. Prognosis after West Nile Virus Infection. *Ann Intern Med*. 2008;149(4):232. doi:10.7326/0003-4819-149-4-200808190-00004.
145. Sejvar JJ, Haddad MB, Tierney BC, et al. Neurologic manifestations and outcome of West Nile virus infection. *JAMA*. 2003;290(4):511-515. doi:10.1001/jama.290.4.511.
146. Klee AL, Maldin B, Edwin B, et al. Long-Term Prognosis for Clinical West Nile Virus Infection. 2004;10(8):8-14.
147. Patnaik JL, Harmon H, Vogt RL. Human West Nile Virus Infections ,. 2006;12(7):1129-1131.
148. Haaland KY, Sadek J, Pergam S, et al. Mental status after West Nile virus infection. *Emerg Infect Dis*. 2006;12(8):1260-1262. doi:10.3201/eid1208.060097.
149. Murray K, Walker C, Herrington E, et al. Persistent Infection with West Nile Virus Years after Initial Infection. *J Infect Dis*. 2010;201(1):2-4. doi:10.1086/648731.
150. Patel H, Sander B, Nelder MP. Long-term sequelae of West Nile virus-related illness: a systematic review. *Lancet Infect Dis*. 2015;15(8):951-959. doi:10.1016/S1473-3099(15)00134-6.
151. Dick GW., Kitchen S., Haddow A. Zika Virus (I). Isolations and serological specificity. *Trans R Soc Trop Med Hyg*. 1952;46(5):509-520. doi:10.1016/0035-9203(52)90042-4.

152. Duffy MR, Chen T-H, Hancock WT, et al. Zika Virus Outbreak on Yap Island, Federated States of Micronesia. *N Engl J Med*. 2009;360(24):2536-2543. doi:10.1056/NEJMoa0805715.
153. Cao-Lormeau V-M, Blake A, Mons S, et al. Guillain-Barré Syndrome outbreak associated with Zika virus infection in French Polynesia: a case-control study. *Lancet*. 2016;387(10027):1531-1539. doi:10.1016/S0140-6736(16)00562-6.
154. WHO | WHO statement on the first meeting of the International Health Regulations (2005) (IHR 2005) Emergency Committee on Zika virus and observed increase in neurological disorders and neonatal malformations. *WHO*. 2016. http://www.who.int/mediacentre/news/statements/2016/1st-emergency-committee-zika/en/. Accessed April 18, 2018.
155. Moore CA, Staples JE, Dobyns WB, et al. Characterizing the Pattern of Anomalies in Congenital Zika Syndrome for Pediatric Clinicians. *JAMA Pediatr*. 2017;171(3):288. doi:10.1001/jamapediatrics.2016.3982.
156. Roth W, Tyshkov C, Thakur K, Vargas W. Encephalomyelitis Following Definitive Zika Virus Infection. *Neurol Neuroimmunol neuroinflammation*. 2017;4(4):e349. doi:10.1212/NXI.0000000000000349.
157. Rozé B, Najioullah F, Signate A, et al. Zika virus detection in cerebrospinal fluid from two patients with encephalopathy, Martinique, February 2016. *Eurosurveillance*. 2016;21(16):30205. doi:10.2807/1560-7917.ES.2016.21.16.30205.
158. Carteaux G, Maquart M, Bedet A, et al. Zika Virus Associated with Meningoencephalitis. *N Engl J Med*. 2016;374(16):1595-1596. doi:10.1056/NEJMc1602964.
159. Soares CN, Brasil P, Carrera RM, et al. Fatal encephalitis associated with Zika virus infection in an adult. *J Clin Virol*. 2016;83:63-65. doi:10.1016/J.JCV.2016.08.297.
160. Mécharles S, Herrmann C, Poullain P, et al. Acute myelitis due to Zika virus infection. *Lancet*. 2016;387(10026):1481. doi:10.1016/S0140-6736(16)00644-9.
161. Muñoz LS, Parra B, Pardo CA. Neurological Implications of Zika Virus Infection in Adults. *J Infect Dis*. 2017;216(suppl_10):S897-S905. doi:10.1093/infdis/jix511.
162. Mehta R, Soares CN, Medialdea-Carrera R, et al. The spectrum of neurological disease associated with Zika and chikungunya viruses in adults in Rio de Janeiro, Brazil: A case series. Beasley DWC, ed. *PLoS Negl Trop Dis*. 2018;12(2):e0006212. doi:10.1371/journal.pntd.0006212.
163. Meda N, Salinas S, Kagoné T, Simonin Y, Van de Perre P. Zika virus epidemic: Africa should not be neglected. *Lancet*. 2016;388(10042):337-338. doi:10.1016/S0140-6736(16)31103-5.
164. Olusanya BO. Full-term newborns with congenital microcephaly and macrocephaly in Southwest Nigeria. *Int Health*. 2012;4(2):128-134. doi:10.1016/J.INHE.2011.12.006.
165. Tang H, Hammack C, Ogden SC, et al. Zika virus infects human cortical neural progenitors and attenuates their growth. *Cell Stem Cell*. 2016;18(5):587-590. doi:10.1016/j.stem.2016.02.016.
166. Garcez PP, Loiola EC, Madeiro da Costa R, et al. Zika virus impairs growth in human neurospheres and brain organoids. *Science*. 2016;352(6287):816-818. doi:10.1126/science.aaf6116.
167. Li H, Saucedo-Cuevas L, Regla-Nava JA, et al. Zika Virus Infects Neural Progenitors in the Adult Mouse Brain and Alters Proliferation. *Cell Stem Cell*. 2016;19(5):593-598. doi:10.1016/j.stem.2016.08.005.

168. van den Pol AN, Mao G, Yang Y, Ornaghi S, Davis JN. Zika Virus Targeting in the Developing Brain. *J Neurosci*. 2017;37(8):2161-2175. doi:10.1523/JNEUROSCI.3124-16.2017.
169. Huang W-C, Abraham R, Shim B-S, Choe H, Page DT. Zika virus infection during the period of maximal brain growth causes microcephaly and corticospinal neuron apoptosis in wild type mice. *Sci Rep*. 2016;6(1):34793. doi:10.1038/srep34793.
170. Adams Waldorf KM, Nelson BR, Stencel-Baerenwald JE, et al. Congenital Zika virus infection as a silent pathology with loss of neurogenic output in the fetal brain. *Nat Med*. 2018;24(3):368-374. doi:10.1038/nm.4485.
171. Lazear HM, Govero J, Smith AM, et al. A Mouse Model of Zika Virus Pathogenesis. *Cell Host Microbe*. 2016;19(5):720-730. doi:10.1016/j.chom.2016.03.010.
172. Kumar A, Hou S, Airo AM, et al. Zika virus inhibits type-I interferon production and downstream signaling. *EMBO Rep*. 2016;17(12):1766-1775. doi:10.15252/embr.201642627.
173. Grant A, Ponia SS, Tripathi S, et al. Zika Virus Targets Human STAT2 to Inhibit Type I Interferon Signaling. *Cell Host Microbe*. 2016;19(6):882-890. doi:10.1016/J.CHOM.2016.05.009.
174. Tripathi S, Balasubramaniam VRMT, Brown JA, et al. A novel Zika virus mouse model reveals strain specific differences in virus pathogenesis and host inflammatory immune responses. Pierson TC, ed. *PLOS Pathog*. 2017;13(3):e1006258. doi:10.1371/journal.ppat.1006258.

Chapter 2: Astrocytes decrease adult neurogenesis during memory dysfunction via Il-1

This chapter is adapted from a manuscript published in Nature Immunology:

Garber C, Vasek MJ, Vollmer LL, Sun T, Jiang X, Klein RS. Astrocytes decrease adult neurogenesis during virus-induced memory dysfunction via IL-1. *Nat Immunol*. 2018;19(2):151-161. doi:10.1038/s41590-017-0021-y.

C.G., M.J.V., and R.S.K. designed the experiments; C.G. and M.J.V. did most of the experiments, compiled and analyzed the data; C.G., M.J.V., and R.S.K. prepared the figures; L.L.V., T.S. and X.J. were involved in specific experiments; C.G., M.J.V., and R.S.K. analyzed the data and wrote the manuscript.

2.1 Abstract

Memory impairment following West Nile virus neuroinvasive disease (WNND) is associated with loss of hippocampal synapses with lack of recovery. Adult neurogenesis and synaptogenesis are fundamental features of hippocampal repair, suggesting viruses impact these processes. Here, using an established model of WNND-induced cognitive dysfunction, transcriptional profiling revealed alterations in gene expression that limit adult neurogenesis, including interleukin (IL)-1. WNND-recovered animals exhibit decreased neuroblasts and increased astrogenesis, without recovery of hippocampal neurogenesis at thirty days. Analysis of cytokine production in *ex vivo* isolated microglia and astrocytes revealed the latter to be the predominant source of IL-1. IL-1R1-deficient, WNND-recovered mice exhibit normal neurogenesis, recovery of presynaptic termini, and resistance to spatial learning defects, the latter of which likewise occurred after

treatment with IL-1R1 antagonist. Thus, preferential generation of proinflammatory astrocytes impairs neuronal progenitor cell homeostasis via expression of IL-1, which may underlie long-term cognitive consequences of WNND, but provides a therapeutic target.

2.2 Introduction

Members of the Flavivirus genus, which include West Nile (WNV), Japanese encephalitis (JEV), and Zika (ZIKV) viruses, are the most important arthropod-borne viruses causing encephalitis in humans[1]. Acutely, patients suffering from WNV neuroinvasive disease (WNND) can experience confusion, fatigue, loss of motor control, memory loss, coma, and a mortality rate of 5-10%[1]. WNV is a (+)-sense single-stranded RNA virus that targets fully differentiated neurons, but may be cleared by immune-mediated processes, even after infection of the central nervous system (CNS)[2]. However, approximately half of survivors experience debilitating, long-term cognitive sequelae, including defects in verbal and visuospatial learning, for months to years beyond the acute infectious event[3,4]. Animal studies have identified multiple cytokines that play critical roles in cell-mediated antiviral immunity, including tumor necrosis factor (TNF)[5], type I, II and III interferons (IFNs)[6-9], and interleukin (IL)-1[10,11], which improve survival. Prior studies have determined that human and murine neurons are the target of WNV *in vivo*[12-14]. Importantly, studies in which critical cytokines have been deleted via genetic approaches have not led to expanded tropism of WNV to nonneuronal cells within the CNS[10,15]. While neuronal death is associated with high mortality in human and murine cases of WNV encephalitis[16], survivors may exhibit limited neuronal loss[14,17], suggesting inflammatory processes triggered acutely contribute to long-term memory dysfunction. That many patients recovering from WNND experience memory impairments for months to years beyond viral clearance indeed suggests a chronic condition with either sustained damage or limited repair.

In a murine model of recovery from WNND, in which intracranial inoculation of a mutant WNV (WNV-NS5-E218A) leads to high survival rates with visuospatial learning defects, hippocampi exhibit up-regulation of genes involved in microglial-mediated synaptic remodeling, including drivers of phagocytosis and the classical complement pathway, and decreased expression of synaptic scaffolding proteins and glutamate receptors[14]. Complement-mediated synapse elimination has been reported to occur in numerous neuroinflammatory diseases, including multiple sclerosis[18], Alzheimer's disease[19], and schizophrenia[20], suggesting this may be a general mechanism underlying inflammation-associated disruption of neural circuitry. The hippocampus, essential for spatial and contextual memory formation, receives input from the entorhinal cortex, which relays through the dentate gyrus, CA3, and CA1[21]. WNV-NS5-E218A-recovered mice with poor spatial learning show persistence of phagocytic microglia engulfing presynaptic terminals within the hippocampal CA3 acutely, and during recovery[14]. While this provides molecular explanations for poor spatial learning in WNV-recovered animals, it does not explain why other hippocampal correlates of learning, such as adult neurogenesis, are not able to restore spatial learning.

Adult neurogenesis occurs within the hippocampal dentate gyrus (DG) and the subventricular zone (SVZ)[22]. Within the DG, adult neural stem cells (NSCs) give rise to astrocytes and intermediate neuronal progenitors, the latter of which proliferate and differentiate into neuroblasts that mature into granule cell neurons and integrate into the hippocampal circuit over the course of a few weeks[23]. This process is regulated by intrinsic and extrinsic factors, including local signaling molecules, exercise, aging and inflammation[24]. A variety of endogenous factors play critical roles in the generation and integration of newly generated neurons in the adult hippocampus. These include morphogens, such as neurogenic locus *notch* homolog (Notch)

proteins, sonic hedgehog (Shh), wingless integrated signals (Wnts), and bone morphogenic proteins (BMPs), and neurotrophic factors, such as brain-derived neurotrophic factor (BDNF), ciliary neurotrophic factor (CNTF), insulin-like growth factor-1 (IGF-1), and vascular endothelium growth factor (VEGF)[25]. Recently, proinflammatory pathways, including those triggered by systemic accumulations of TNF, interleukin (IL)-1β, and IL-6, and microglial activation have been implicated in the regulation of neural correlates of memory including adult neurogenesis, synaptic plasticity and modulation of long-term potentiation[14,26-29].

IL-1, in particular, has gained attention for its impact on cognitive function in the context of neuroinflammation. IL-1 signaling is mediated by a family of proteins comprised of IL-1α, IL-1β, and IL-1 receptor antagonist (IL-1ra) primarily through type I IL-1 receptor (IL-1R1). IL-1β is generated via proteolytic cleavage of pro-IL-1β by Caspase 1 during inflammasome activation[30]. IL-1 is highly expressed *in vivo* by infiltrating myeloid cells during WNV encephalitis, where it critically regulates antiviral effector T cell responses[10,11]. While IL-1 is a key player in orchestrating CNS immune responses, including onset of fever[27], it also plays a role in spatial learning and memory-related behavior[28]. Indeed, injection of IL-1β into the brain impairs spatial learning, contextual fear memory, and adult neurogenesis[29–31]. Although several studies have investigated impacts of IL-1 on hippocampal-based learning and behavior in neurologic diseases[31-35], none have done so in a setting of IL-1 induction during CNS viral infection.

Here, using an established model of post-infectious cognitive dysfunction from WNND in which animals display defects in spatial learning, we investigated the regulation of neurogenesis during repair and recovery. We identified a novel feed forward mechanism in which IL-1 contributes to spatial learning defects via derailment of hippocampal neurogenesis to generate proinflammatory astrocytes, which exhibit a previously unidentified role in IL-1-

mediated cognitive dysfunction, and that this pathway may be successfully targeted for the prevention of learning defects during recovery from viral encephalitis.

2.3 Results

WNND-recovered mice exhibit genetic signatures of derailed neurogenesis

Our previous microarray study of hippocampal gene expression in WNV-NS5-E218A-recovered mice identified several significantly altered pathways in mice with impaired spatial memory including axon guidance, Wnt signaling, and p53 signaling[14], which point to potential effects on adult neurogenesis. To further examine these pathways, we grouped the genes altered between Mock and WNV-NS5-E218A-recovered animals into those that promote or inhibit neurogenesis, here shown as gene expression heatmaps (**Fig. 2.1a, b**). Expression of genes associated with inflammation and/or prohibition of neurogenesis (*Casp1, Il1a, Tnf, Tnfrsf1a*) was higher in WNV-NS5-E218A-recovered (**Fig. 2.1a**) compared with mock-infected mice, which exhibited higher expression of genes that promote proliferation and differentiation of neuroblasts (*Epha5, Wnt2, Nrg3*) and axon guidance (*Robo2, Sema3*) (**Fig. 2.1b**). Markers for recently identified subgroups of reactive astrocytes[36] deemed A2 and A1, the latter of which are proposed to be induced by activated microglia and lose the ability to promote neuronal survival, outgrowth, were also significantly elevated (**Fig. 2.1c, d**). Alterations in genes that impact neurogenesis after infection with WNV-NS5-E218A and markers of reactive astrocytes, including additional panreactive astrocyte markers[36] were validated in an independent set of hippocampal samples by qPCR (**Fig. 2.1e-h**). These data suggest that WNND might limit adult neurogenesis in favor of astrogenesis.

WNND induces acute loss of adult neurogenesis in the hippocampus

Given that genetic signatures in the hippocampi of WNV-recovered mice are consistent with pathways that negatively impact adult neurogenesis, we evaluated the generation of new neurons during WNV encephalitis. We administered BrdU during the peak of WNV encephalitis for a period of 4 days (days 3-7), allowed mice to recover for 45 days and then evaluated numbers of newly generated neurons (**Fig. 2.2a-d**). WNV-recovered mice exhibited fewer BrdU-labeled neurons within the DG granule cell layer than mock-infected controls (**Fig. 2.2a, c, d**). To determine whether reduction in newly generated neurons in WNV-recovered mice is due to alteration in the rate of neuronal progenitor cell proliferation, mock-infected versus WNV-NY99-infected or WNV-NS5-E218A-infected mice were administered BrdU during the peak of encephalitis, followed by either immunohistochemical (**Fig. 2.3a, b**) or flow cytometric (**Fig. 2.8**) evaluation of neuronal progenitors, which express doublecortin (DCX^+), in the SVZ or hippocampi, as described previously[37]. Infections with wild-type WNV (NY-99) via either the peripheral footpad or intracranial route, or attenuated WNV-NS5-E218A all led to fewer BrdU-labeled neuroblasts at 6-8 days post-infection (**Fig. 2.3c**). This reduction in generation of neuroblasts was assessed over the course of recovery from WNND, at days 6, 15, and 30 post-infection (d.p.i.) as compared to age-matched mock-infected controls. This analysis revealed that significant deficits persist until day 30 in the hippocampus, with a trend towards recovery observed in the SVZ (**Fig. 2.3d**). Taken together, these data indicate that hippocampal neuronal repair is defective after WNND.

WNV does not target NSCs or neuronal progenitors

One possible explanation of fewer new neurons after the recovery period of WNV encephalitis is that neuroblasts are dying before reaching maturity. In agreement with previous studies, we

confirmed that neural stem cells and intermediate neuronal progenitors were not permissive to WNV infection[36], and observed that less than 1% of DCX^+ neuroblasts were infected *in vivo* in both the SVZ and DG (**Fig. 2.9a**). Furthermore, rates of neuroblast apoptosis during acute WNND were equivalent to mock-infected controls (data not shown). The few infected neuroblasts that were observed within the DG were located within the granule cell layer, suggesting that these may be late-stage DCX+ cells during their transition into immature neurons. Late-stage neuroblasts exhibit many of the same properties as neurons including, receptors, filament proteins, and cellular processes (e.g. axon and dendrite formation), thus potentially explaining the ability of WNV to infect them. Alterations in the proliferation rates of neural progenitors could result in changes to the overall pool of stem cells over time. Using mice expressing GFP under the *Nestin* promoter, we counted the numbers of Nestin and GFAP-double positive neural stem cells remaining within the hippocampal DG at 45 days post-infection, but found no differences in the numbers of these cells present in mock and WNV-NS5-E218A recovered mice (**Fig. 2.9b**). Thus, WNV does not target or alter the numbers of NSCs, nor does it infection neuroblasts.

Astrocytes are the primary source of IL-1β in the recovering CNS

To further investigate the potential for an alteration in cell fate of early stage progenitors, we determined whether fewer neuronal progenitors were produced in favor of more glial progenitors within the hippocampus of WNV-infected mice. To test this, mock- versus WNV-NY- or WNV-NS5-E218A-infected mice were administered BrdU during the peak of encephalitis followed by flow cytometric evaluation of hippocampal neuronal progenitors and astrocytes 48 hours later (**Fig. 2.4a, b**). Infections with either wild type WNV (NY-99) or WNV-NS5-E218A led to more BrdU-labeled GFAP-expressing astrocytes in the hippocampus at 7 days post infection than mock-

infected controls (**Fig. 2.4b**). Although GFAP expression varies among astrocyte subpopulations, recent work has demonstrated that GFAP is the most highly expressed transcript and protein in astrocytes isolated from the hippocampus[38]. Next, we determined whether an increase in astrocyte genesis during acute infection significantly contributes to alterations in the CNS immune profile after viral clearance. Analysis of *ex vivo*-isolated astrocytes at 25 d.p.i. demonstrated an increase in markers of A1, but not A2, reactive astrocyte markers, (**Fig. 2.4c, c′**). Thus, the slight increases in neuroprotective markers previously detected in whole hippocampal samples at the same time point (**Fig. 2.1c-e**) are likely contributed by other cell types. Analysis of panreactive markers[36] also detected increased expression of GFAP (**Fig. 2.4c′**). Identification of cellular sources of anti-neurogenic and proinflammatory cytokines in the CNS via transcriptional analysis of *ex vivo*-isolated astrocytes and microglia at 25 d.p.i. revealed astrocytes as the primary source of IL-1β, Caspase-1, and TNF (**Fig. 2.4d**). The purity of those cellular sources was confirmed by transcriptional analysis of cell type-specific markers, as previously reported[39]. Isolated astrocytes demonstrated significant enrichment of the astrocyte *Gfap* gene expression while isolated microglia show significant enrichment of microglial *Cx3cr1* and *Trem2* expression. Both ASCA-2 positive astrocytes and CD11b positive microglia had negligible expression of the neuronal gene *Rbfox3* (**Fig. 2.10**). Kinetic analysis of *Il1b* expression within hippocampi of WNV-NS5-E218A-infected mice showed persistent elevation of this anti-neurogenic cytokine at 25 d.p.i. (**Fig. 2.4e**). Immunohistochemical analysis of mock- and WNV-NS5-E218A-infected tissue at 25 d.p.i. (**Fig. 2.4f**) confirmed increases in numbers of activated, GFAP+ astrocytes (**Fig. 2.4g**) that are the primary cellular source of IL-1β protein expression in the recovering hippocampus (**Fig. 2.4h, i**). Taken altogether, these data indicate that WNND promotes the generation of A1 reactive astrocytes that express anti-neurogenic cytokines.

Il1r1$^{-/-}$ mice resist alterations in cell fate of early progenitors

To determine whether WNV-mediated reduction in neuroblast proliferation requires IL-1R1 signaling, mock- and WNV-NS5-E218A-infected *Il1r1*$^{-/-}$ mice were administered BrdU during the peak of encephalitis, followed by flow cytometric evaluation of hippocampal neuronal progenitors. In contrast to the reduction in neuroblast proliferation observed in neurogenic zones of wild type animals, *Il1r1*$^{-/-}$ mice exhibited normal neurogenesis in both the hippocampus (**Fig. 2.5a**) and SVZ (**Fig. 2.5b**). In addition, *Il1r1*$^{-/-}$ mice did not undergo the substantial increase in proliferating astrocytes observed in wild-type animals (**Fig. 2.5c**). Immunohistochemical identification of Ki67+ proliferating neural progenitor cells in conjunction with Mash1, which identifies early neural progenitor cells with neurogenic potential[40], within the DG revealed acute WNV-mediated decreases in wild-type animals, but not in animals deficient in IL-1R1 or Caspase 1 (*Casp1*$^{-/-}$), which cleaves pro-IL-1b to produce mature IL-1b (**Fig. 2.5d**). Acute viral loads did not differ between wild-type and *Il1r1*$^{-/-}$ animals at 6 d.p.i. in various brain regions (**Fig. 2.11a-c**), and there was no difference in persistent viral RNA at 25 d.p.i. in the hippocampus (**Fig. 2.11d**), confirming that virologic control of WNV-NS5-E218A was intact in *Il1r1*$^{-/-}$ animals. In addition, flow cytometric analysis of cells isolated from the hippocampus demonstrated similar numbers of various subpopulations of resident and infiltrating CD45^{+} cells in WNV-NS5-E218A infected wildtype and *Il1r1*$^{-/-}$ animals (**Fig. 2.11e-l**). These data support the notion that IL-1R1 signaling underlies derailment of neurogenesis during WNND.

Il1r1$^{-/-}$ mice exhibit synapse recovery and normal spatial learning

Given that *Il1r1*$^{-/-}$ mice are protected from derailed neurogenesis following WNV infection, we hypothesized that IL-1R1-deficient animals would exhibit improved synapse recovery following infection with WNV-NS5-E218A. Both WNV-NS5-E218A-infected wild-type and *Il1r1*$^{-/-}$ mice exhibit acute loss of presynaptic terminals at 7 d.p.i. (**Fig. 2.5e**), and wild-type animals continued to show decreased numbers of presynaptic terminals at 25 d.p.i. In contrast, *Il1r1*$^{-/-}$ animals displayed recovery of synapses at this time point (**Fig. 2.5f**). Given that adult neurogenesis and synaptic plasticity are critical for spatial learning, we allowed WNV-NS5-E218A-infected, *Il1r1*$^{-/-}$ mice to recover for a month beyond viral clearance (46 d.p.i.) and tested their ability to spatially locate and remember the location of a target hole in a Barnes maze over the course of 10 trials held twice daily for 5 days (**Fig. 2.6a**). While WNV-recovered, wild-type mice display significant deficits in spatial learning[14] (**Fig. 2.6b**), the performance of WNV-recovered *Il1r1*$^{-/-}$ mice was indistinguishable from mock-infected animals (**Fig 2.6c**). Area under the curve (AUC) analysis for each animal, which allows a comprehensive view of how individuals within the group performed across all 5 days of testing on the Barnes Maze, demonstrated that wild-type animals recovering from WNND had more severe memory impairments than mock-infected wild-type controls and WNND recovered *Il1r1*$^{-/-}$ animals (**Fig 2.6d**). To assess differences in exploratory behavior that may affect performance on the Barnes Maze spatial learning task, we performed Open Field testing (OFT) at 45 d.p.i., 1 day prior to the Barnes Maze (**Fig. 2.6a**). While the number of lines crossed during OFT were similar for mock- and WNV-infected mice of both genotypes, mock-infected *Il1r1*$^{-/-}$ animals crossed fewer lines than mock-infected wild-type controls (**Fig. 2.6e**). No differences in the number of center crosses were observed between all groups (**Fig. 2.6f**). These studies demonstrate a critical role for IL-1R1 in limiting synapse and cognitive recovery.

IL-1R antagonism prevents WNV-induced spatial learning deficits

In order to explore the potential for therapeutic intervention, we opted to test cognitive recovery in wild-type animals treated during acute infection with either vehicle or the IL-1R antagonist, Anakinra. As synapse elimination[14] and loss of neurogenesis occurs during acute infection, which is also when IL-1 expression was highest, we began treatment at 10 d.p.i., a time point during viral clearance[14] when the blood brain barrier was still permeable (**Fig. 2.12**). Mock- or WNV-NS5-E218A-infected animals received 5 daily intra-peritoneal doses of vehicle or Anakinra, and then recovered for 30 days prior to Barnes Maze testing at 46 d.p.i. (**Fig. 2.7a**). As expected, vehicle treated WNND recovered animals were significantly impaired in their ability to identify the location of the target hole during Barnes Maze testing (**Fig. 2.7b**). In contrast, animals treated with Anakinra were protected from WNV-induced spatial learning impairment (**Fig. 2.7c**). AUC analysis confirmed that WNND-recovered animals treated with Anakinra had improved performance on the Barnes Maze compared with vehicle treated animals (**Fig. 2.7d**). Finally, OFT at 45 d.p.i. demonstrated that there were no differences between any of the groups in exploratory behavior, locomotion, or number of center crosses (**Fig. 2.7f**). These studies identify a potential therapeutic target for the prevention of spatial learning defects that occur during recovery from WNND.

2.4 Discussion

The original designation of cytokines as immune modulators has expanded to include a variety of functions in nonlymphoid tissues, especially the CNS, where they play critical roles in neurodevelopment. Regulation of signaling by the gp130 family of cytokines through Janus Kinase/Signal Transducer and Activator of Transcription (JAK/STAT) pathways maintains the pool of neural stem and progenitor cells (NPCs), promoting neurogenesis of the latter[41]. During

development, IL-1R1 is also expressed on proliferating NPCs and IL-1b exerts an anti-proliferative, anti-neurogenic and pro-gliogenic effect on embryonic hippocampal NPCs *in vitro*[42,43]. Studies of viral encephalitis have demonstrated critical roles for innate cytokines expressed by infiltrating immune cells in T cell-mediated clearance of pathogen. However, their impact on CNS recovery and repair after viral clearance via actions on NPCs has not been elucidated. Our findings suggest that during the acute phase of viral infection, myeloid cell-derived IL-1 (ref.[10]) alters the proliferation and differentiation fates of neural progenitor cells, leading to a shift from neurogenesis to astrogenesis. Proinflammatory astrocytes then become the predominant source of the cytokine, which continues to inhibit neurogenesis, after myeloid cells retreat from the CNS[14]. Accordingly, mice deficient in IL-1R signaling are resistant to both derailment of neurogenesis as well as spatial memory impairments, which are observed in wild-type WNV-recovered mice. Because loss of neurogenesis is detected early in the course of infection, administration of IL-1R antagonist at 10 d.p.i., a time-point when the BBB is still permeable, was able to reverse the effects of IL-1 and improve spatial learning. Our data indicate that the combinatorial effect of synapse loss[14] and reduced neurogenesis can negatively impact hippocampal spatial learning and memory long beyond the initial episode of infection via a shift in sources of cytokines to neural cells.

Other neurotropic flaviviruses, including Japanese Encephalitis and Zika Virus, have been shown to directly infect neural progenitors, causing apoptosis of progenitors and progeny[44,45]. In agreement with previous studies[46], we found very few neural progenitor cells infected with WNV. However, transcriptional profiling detected altered expression of genes implicated in hippocampal neurogenesis during WNND recovery. These included increased expression of genes that encode CDKN1a, CDCA4, and CCND1, cell cycle progression inhibitors, and decreased expression of

genes that encode Epha5 and Sema6B, which regulate hippocampal axon pathfinding during neural development[47,48], were detected during WNND recovery. We also detected alterations to the Wnt signaling pathway, which can impact neural progenitor cell proliferation and motility, but also regulates synapse formation[49] and plasticity[50], potentially contributing to the failure of mice to recover from both neurogenesis derailment as well as WNV-mediated synapse loss[14]. The genetic signatures present during WNV recovery describes an environment which both impedes neural progenitor cell proliferation and the ability of immature and mature neurons to form new synapses.

While previous studies have detected IL-1R1 within the hippocampus[51], recent research highlighting astrocyte heterogeneity has not identified these cells as a first target of IL-1[52]. In contrast, numerous studies have implicated neural progenitor cells as a significant target of IL-1. IL-1a and IL-1b have both been shown to induce neural stem and progenitor cells to favor the astrocyte rather than neuronal lineage *in vitro*[42]. TNF, which is highly expressed in WNV-infected brains[5] in an IL-1R-dependent manner[10], has been shown in other contexts to direct neuronal progenitors towards an astrocyte fate via downstream STAT3 induction[53], suggesting that these may be part of the same anti-neurogenic pathway. *In vivo* studies using overexpression and stress models have shown that IL-1b decreases neurogenesis[43,54,55], and influences synaptic plasticity[56,57], processes that are vital for the development and retention of spatial memory. We found that abundance of IL-1b during acute infection altered lineage fate of neural stem cells within neurogenic zones of the CNS favoring astrocyte genesis. This led to a feed-forward cycle of inflammation, as astrocytes became the primary source of IL-1β in the recovering hippocampus. IL-1R1-deficient mice were protected from decreased neurogenesis following WNV infection, and retained the ability to learn a spatial memory task. Importantly, we demonstrated that the effect was specific to inflammasome-activated IL-1b by confirming that *Casp1*$^{-/-}$ animals were also

protected from decreased neurogenesis. In studies using cultured NPCs, IL-1b and TNF are both capable of altering lineage-fate to favor greater numbers of astrocytes and both of these pathways are dependent on downstream STAT3 activation[58]. While we focused on the role and necessity of IL-1R signaling, TNF, which was also upregulated by astrocytes at 25 d.p.i., may also contribute to the observed lineage fate-altering phenotype.

While multiple studies have described effects of cytokines released from astrocytes[59] and microglia[60] on memory and hippocampal neurogenesis, the precise contributions of each cell type *in vivo* remain ill-defined. In the current study, we found that astrocytes within WNV-recovered CNS express increased expression of *Il1b*, *Casp1* and *Tnf*, whereas microglia increased expression of *Ccl2*. Astrocytes display a regional heterogeneity[38,52], which can also reflect differences in homeostatic function, such as synaptogenesis[52], and response to infection, where cerebellar astrocytes are poised to quickly mount antiviral programs[61]. In addition to developmentally determined sub-populations[62,63], astrocytes display a remarkable plasticity and molecular identity determined in part by neuronal cues[64]. In response to different types of injury, reactive astrocytes can develop a recently described polarized phenotype termed A1 (infection induced, pro-inflammatory astrocytes) or A2 (ischemia induced, promoting tissue repair) that are distinguished by distinct genetic signatures[36]. In this study, A1 astrocytes were induced *in vivo* by lipopolysaccharide injection and the combination of IL-1a, TNF, and C1q was observed to promote A1 polarization *in vitro.* Our model of viral infection also exhibits elevated production of IL-1, TNF, and C1q[14]. Consistent with this, we also observed the *in vivo* development and persistence of astrocytes with panreactive and A1 markers. As proinflammatory astrocytes lose the ability to phagocytose due to a decrease in mRNA expression of the phagocytic receptors *Mertk* and *Megf10*, and fail to support synaptogenesis *in vitro* due to decreases in expression of *Gpc6* and *Sparcl1*,

factors that normally promote excitatory synapse formation[36]. Thus, the lack of recovery of synapses in our model could be explained by the generation of this subset of reactive astrocytes. Alternatively, lack of recovery could also be due to the loss of a specific astrocyte population that normally promotes synaptogenesis[52]. Although expansion of a synapse-promoting astrocyte population leads to seizures in the context of a reactive glioma[52], this population may be crucial for CNS repair in the setting of the diverse array of diseases recently associated with loss of synapses in addition to WNV encephalitis, including Alzheimer's disease[19], schizophrenia[20], and lupus[65]. Further studies are needed to more fully understand how homeostatic astrocyte populations respond to CNS injury, and whether this correlates with regional or functional identity. The discovery that newly derived, reactive astrocytes of a recently identified proinflammatory subset[36] are responsible for persistently decreased adult neurogenesis during WNV recovery also suggests cell-type specific studies will be required to elucidate these pathways in disease models.

There is a growing body of experimental evidence demonstrating the importance of homeostatic neuroimmune interactions for normal cognitive function (recently reviewed by[66,67]). However, the effects of immune mediators on brain function depend on their levels and locations; this phenomenon was classically demonstrated as a U-shaped curve relating the effect of IL-1 signaling on cognitive function in which either overexpression or complete blockade of IL-1 signaling both negatively impacted spatial learning[68]. Thus, in the context of neuroinflammation, increased expression of immune molecules may similarly lead to altered cognitive performance. Of note, we observed a trend towards recovery of neurogenesis in the SVZ that was absent in the hippocampus, an effect that has been reported previously in response to ionizing radiation[69], suggesting a differential responses to injury in these neurogenic niches. Interestingly, in a study of hypoxia driven neuroinflammation, hippocampal neurogenesis

decreased, while SVZ neurogenesis increased, an effect that was linked to IL-6 signaling[70]. Further work addressing the mechanism underlying differential responsiveness to cytokine signaling in neurogenic niches could shed light on basic aspects of neural precursor cell biology.

2.5 Methods

Animals

5-8 week-old male mice were used at the outset of all experiments. C57BL/6J mice were obtained from Jackson Laboratories. *Il1r1*$^{-/-}$ mice (> 10 generations backcrossed to C57BL/6) were obtained from Jackson Laboratories. Nestin-GFP mice (> 10 generations backcrossed to C57BL/6) were obtained from G. Enikolopov (Cold Spring Harbor Laboratories). All experimental protocols were performed in compliance with the Washington University School of Medicine Animal Safety Committee (protocol# 20140122).

Mouse models of WNV infection

Footpad: (WNV-NY99) The WNV strain 3000.0259 was isolated in New York in 2000 (Ebel et al., 2001) and passaged once in C6/36 *Aedes albopictus* cells to generate an insect cell–derived stock. 100 plaque-forming units (pfu) of WNV-NY99 were delivered in 50 ul to the footpad of anaesthetized mice.

Intracranial: "WNV-NS5-E218A," which harbors a single point mutation in the 2'O-methyl-transferase gene, was obtained from M. Diamond (Washington University) and passaged in Vero cells as described previously[41]. Deeply anaesthetized mice were administered 10^4 pfu of WNV-NS5-E218A or 10 pfu of WNV-NY99 in 10 ul of 0.5% FBS in HBSS into the brain's third ventricle

via a guided 29-gauge needle. “Mock” infected animals were deeply anesthetized and administered 10 ul of 0.5% FBS in HBSS into the brain’s third ventricle via a guided 29-gauge needle.

Stock titers of all viruses were determined by using BHK21 cells for viral plaque assay as previously described[42].

Microarray analysis.

Further analysis was performed on previously published hippocampal microarray gene expression data[14] (Gene Expression Omnibus #GSE72139) from Mock-infected and WNV-NS5-E218A animals at 25 days post infection. Expression data from selected genes ($P < 0.05$ or $P < 0.1$ for italicized genes, Two-tailed Students *t*-test) were converted to Z-scores for each individual gene and animal and are displayed as colorimetric heatmaps.

In vivo bromodeoxyuridine (BrdU) labeling.

BrdU (Sigma Aldrich) in sterile PBS was injected intraperitoneally (IP) for all experiments. For acute Immunohistochemical studies (harvests day 7-8 post-infection) mice were given 150 mg/kg of BrdU at 48 h prior to tissue harvest. For flow cytometric analyses, mice were given 100 mg/kg of BrdU at 48 h and again at 24 h prior to tissue harvest. For neuronal BrdU labeling, mice were given 75 mg/kg every 12 h beginning at 3 days post-infection and ending at 7 days post-infection for a total of 7 doses.

Antibodies

WNV (1:100 described previously[8]), NeuN (1:100, Cell Signaling, Cat 12943S, Clone D3S3I), BrdU (1:200, Abcam, Cat ab1893, polyclonal), CD45 (Biolegend, Cat 103114, Clone 30-F11), Doublecortin (1:150, Cell Signaling, Cat 4604S, polyclonal), GFAP (1:50 for flow cytometry; 1: 200 for IHC, BD, Cat 561483, Clone 1B4), IL-1b (R&D, Cat AF-401, polyclonal), Mash1 (BD, Cat 556604, Clone 24B72D11.1), Ki67 (Abcam, Cat AB15580, polyclonal), Synaptophysin (1:250, Synaptic Systems, Cat 101004, polyclonal). Secondary antibodies conjugated to Alexa-488, Alexa-555, or Alexa-647 (Invitrogen) were used at a1:400 dilution.

Immunohistochemistry

Following perfusion with ice-cold PBS and 4% paraformaldehyde (PFA), brains were immersion-fixed overnight in 4% PFA, followed by cryoprotection in 2 exchanges of 30% sucrose for 72 h, then frozen in OCT (Fisher). 9 um-thick fixed-frozen coronal brain sections were washed with PBS and permeabilized with 0.1% Triton X-100 (Sigma-Aldrich), and nonspecific Ab was blocked with 5-10% normal goat serum (Santa Cruz Biotechnology) for 1 h at 23°C. Mouse on Mouse kit (MOM basic kit, Vector) was used per manufacturers protocol when detecting synaptophysin (mouse, DAKO) to reduce endogenous mouse Ab staining. After block, slides were exposed to primary Ab or isotype matched IgG overnight at 4°C, washed with 0.2% FSG in PBS and incubated with secondary Abs for 1 h at 23°C. Nuclei were counterstained with DAPI (Invitrogen) and coverslips were applied with vectashield (Vector). Immunofluorescence was analyzed using a Zeiss LSM 510 laser-scanning confocal microscope and accompanying software (Zeiss). For each animal, 6-8 images were taken from 2-3 different coronal sections spaced at least 50 um apart. Positive immunofluorescent signals were quantified using the public domain NIH Image analysis software, ImageJ.

Flow cytometry

Cells were isolated from brains of WT mice at day 6, 15, or 30 days post-infection and stained with fluorescently conjugated antibodies to CD45, BrdU, and Doublecortin as previously described[37]. Briefly, animals were deeply anesthetized with a ketamine/xylazine mixture and perfused intracardially with ice cold dPBS (Gibco). Brains were aseptically removed, minced and enzymatic digested in HBSS (Gibco) containing collagenase D (Sigma, 50mg/ml), TLCK trypsin inhibitor (Sigma, 100 ug/ml), DNase I (Sigma, 100U/ul), HEPES ph 7.2 (Gibco, 1M), for 1hr at 23°C while shaking. The tissue was pushed through a 70 um strainer and spun down at 500*g* for 10min. The cell pellet was resuspended in a 37% percoll solution and spun at 1200*g* for 30min to remove myelin debris. Cells were washed in PBS, then resuspended in FACS buffer. Cells were blocked with TruStain fcX anti-mouse CD16/32 (Biolegend) for 5 min on ice, followed by incubation with fluorescently conjugated antibodies for 30 min on ice. Cells were then washed 2 times in PBS, fixed with 4% PFA for 10 min at 23°C and resuspended in FACS buffer. Data collection was performed with LSR-II (BD Biosciences) and analyzed with Flowjo software.

***Ex vivo* isolation of microglia and astrocytes with microbeads**

Animals were deeply anesthetized with a ketamine/xylazine mixture and perfused intracardially with ice cold dPBS (Gibco). Brains were aseptically removed, minced and enzymatic digested in HBSS (Gibco) containing collagenase D (Sigma, 50mg/ml), TLCK trypsin inhibitor (Sigma, 100 ug/ml), DNase I (Sigma, 100 U/ul), HEPES 7.2 (Gibco, 1M), for 1hr at 23°C while shaking. The tissue was pushed through a 70 um strainer and spun down at 500*g* for 10min. The cell pellet was resuspended in a 37% percoll solution and spun at 1200*g* for 30 min to remove myelin

debris. Cells were washed in PBS then resuspended in MACS buffer. $CD11b^+$ Microglia and $ACSA\text{-}2^+$ astrocytes were isolated using manual MACS sorting according to the manufacturer's instructions (Miltenyi Biotec). Non-specific labeling of CD11b+ microglia was prevented by incubating the cells with FcR blocking reagent prior to labeling the cells with ACSA-2 antibodies for magnetic isolation. The purified microglia and astrocytes were processed for real-time quantitative RT-PCR as described below.

Real-time quantitative RT-PCR

cDNA was synthesized using random hexamers, oligodT15, and MultiScribe reverse transcriptase (Applied Biosystems). A single reverse transcription master mix was used to reverse transcribe all samples in order to minimize differences in reverse transcription efficiency. The following conditions were used for reverse transcription: 25°C for 10 min, 48°C for 30 min, and 95°C for 5 min. Real-time quantitative RT-PCR was performed as previously described[14].

Behavioral Testing

Open field and Barnes Maze testing was performed as previously describe[14]. Briefly, mice were tested on the Barnes Maze over the course of 5 consecutive days, receiving two trials per day, spaced 30 minutes apart. For each trial, the mouse was given 3 minutes to explore the maze and find the target hole. Mice that did not enter the target hole within 3 minutes were gently guided into the hole. After each trial, the mouse remained in the target hole for exactly 1 minute, and then was returned to its home cage. The maze was decontaminated with 70% ethanol between each trial. The numbers of errors (nose pokes over non-target holes) were measured. One day prior to Barnes Maze testing, mice were tested via open field testing to monitor differences in exploratory

behavior. Each animal was given 5 minutes to explore an open field arena before returning to its home cage. Behavior was recorded using a camera (Canon Powershot SD1100IS), and a blinded experimenter scored the trials.

Anakinra Treatment

Anakinra (Kineret®, Sobi) was diluted in PBS to 10 mg/mL and animals were treated with 100 mg/kg/day of Anakinra or Vehicle (PBS) for 5 consecutive days by intraperitoneal (ip) injection. Animals were weighed daily to monitor for weight loss or adverse events, none of which were observed during the course of treatment.

Statistical Analysis

Statistical analyses were performed using Prism 7.0 (GraphPad Software). All data were analyzed using an unpaired student's t-test, one-way or two-way ANOVA with Bonferroni post-test to correct for multiple comparisons as indicated in the corresponding figure legends. A P value of $\leq$ 0.05 was considered significant.

2.6 Acknowledgements

This work was supported by NIH grants U19 AI083019, R01 NS052632, HDTRA11510032, (all to RSK). Experimental support was provided by the Speed Congenics Facility of the Rheumatic Diseases Core Center. Research reported in this publication was supported by the National Institute of Arthritis and Musculoskeletal and Skin Diseases, part of the National Institutes of Health, under Award Number P30AR048335. The content is solely the

responsibility of the authors and does not necessarily represent the official views of the National Institutes of Health.

2.7 References

1. Salimi, H., Cain, M.D. & Klein, R.S. Encephalitic Arboviruses: Emergence, Clinical Presentation, and Neuropathogenesis. *Neurotherapeutics* **13**, 514-534 (2016).
2. Lazear, H.M. & Diamond, M.S. New insights into innate immune restriction of West Nile virus infection. *Curr Opin Virol* **11**, 1-6 (2015).
3. Lambert, S.L., Aviles, D., Vehaskari, V.M. & Ashoor, I.F. Severe West Nile virus meningoencephalitis in a pediatric renal transplant recipient: successful recovery and long-term neuropsychological outcome. *Pediatr Transplant* **20**, 836-839 (2016).
4. Patel, H., Sander, B. & Nelder, M.P. Long-term sequelae of West Nile virus-related illness: a systematic review. *Lancet Infect Dis* **15**, 951-959 (2015).
5. Shrestha, B., Zhang, B., Purtha, W.E., Klein, R.S. & Diamond, M.S. Tumor necrosis factor alpha protects against lethal West Nile virus infection by promoting trafficking of mononuclear leukocytes into the central nervous system. *J Virol* **82**, 8956-8964 (2008).
6. Lazear, H.M.*, et al.* Interferon-lambda restricts West Nile virus neuroinvasion by tightening the blood-brain barrier. *Sci Transl Med* **7**, 284ra259 (2015).
7. Lazear, H.M., Pinto, A.K., Vogt, M.R., Gale, M., Jr. & Diamond, M.S. Beta interferon controls West Nile virus infection and pathogenesis in mice. *J Virol* **85**, 7186-7194 (2011).
8. Samuel, M.A. & Diamond, M.S. Alpha/beta interferon protects against lethal West Nile virus infection by restricting cellular tropism and enhancing neuronal survival. *J Virol* **79**, 13350-13361 (2005).
9. Shrestha, B.*, et al.* Gamma interferon plays a crucial early antiviral role in protection against West Nile virus infection. *J Virol* **80**, 5338-5348 (2006).
10. Durrant, D.M., Robinette, M.L. & Klein, R.S. IL-1R1 is required for dendritic cell-mediated T cell reactivation within the CNS during West Nile virus encephalitis. *J Exp Med* **210**, 503-516 (2013).
11. Ramos, H.J.*, et al.* IL-1beta signaling promotes CNS-intrinsic immune control of West Nile virus infection. *PLoS Pathog* **8**, e1003039 (2012).
12. Guarner, J.*, et al.* Clinicopathologic study and laboratory diagnosis of 23 cases with West Nile virus encephalomyelitis. *Hum Pathol* **35**, 983-990 (2004).
13. Leyssen, P.*, et al.* Acute encephalitis, a poliomyelitis-like syndrome and neurological sequelae in a hamster model for flavivirus infections. *Brain Pathol* **13**, 279-290 (2003).
14. Vasek, M.J.*, et al.* A complement-microglial axis drives synapse loss during virus-induced memory impairment. *Nature* **534**, 538-543 (2016).
15. Zhang, B., Patel, J., Croyle, M., Diamond, M.S. & Klein, R.S. TNF-alpha-dependent regulation of CXCR3 expression modulates neuronal survival during West Nile virus encephalitis. *J Neuroimmunol* **224**, 28-38 (2010).
16. Ceccaldi, P.E., Lucas, M. & Despres, P. New insights on the neuropathology of West Nile virus. *FEMS Microbiol Lett* **233**, 1-6 (2004).
17. Szretter, K.J.*, et al.* 2'-O methylation of the viral mRNA cap by West Nile virus evades ifit1-dependent and -independent mechanisms of host restriction in vivo. *PLoS Pathog* **8**, e1002698 (2012).
18. Michailidou, I.*, et al.* Complement C1q-C3-associated synaptic changes in multiple sclerosis hippocampus. *Ann Neurol* **77**, 1007-1026 (2015).
19. Hong, S.*, et al.* Complement and microglia mediate early synapse loss in Alzheimer mouse models. *Science* **352**, 712-716 (2016).

20. Sekar, A.*, et al.* Schizophrenia risk from complex variation of complement component 4. *Nature* **530**, 177-183 (2016).
21. Jarrard, L.E. On the role of the hippocampus in learning and memory in the rat. *Behav Neural Biol* **60**, 9-26 (1993).
22. Ming, G.L. & Song, H. Adult neurogenesis in the mammalian brain: significant answers and significant questions. *Neuron* **70**, 687-702 (2011).
23. Mishra, B.B., Gundra, U.M. & Teale, J.M. Expression and distribution of Toll-like receptors 11-13 in the brain during murine neurocysticercosis. *J Neuroinflammation* **5**, 53 (2008).
24. Lieberwirth, C., Pan, Y., Liu, Y., Zhang, Z. & Wang, Z. Hippocampal adult neurogenesis: Its regulation and potential role in spatial learning and memory. *Brain Res* **1644**, 127-140 (2016).
25. Cheffer, A., Tarnok, A. & Ulrich, H. Cell cycle regulation during neurogenesis in the embryonic and adult brain. *Stem Cell Rev* **9**, 794-805 (2013).
26. Riazi, K.*, et al.* Microglia-dependent alteration of glutamatergic synaptic transmission and plasticity in the hippocampus during peripheral inflammation. *J Neurosci* **35**, 4942-4952 (2015).
27. Wu, M.D., Montgomery, S.L., Rivera-Escalera, F., Olschowka, J.A. & O'Banion, M.K. Sustained IL-1beta expression impairs adult hippocampal neurogenesis independent of IL-1 signaling in nestin+ neural precursor cells. *Brain Behav Immun* **32**, 9-18 (2013).
28. del Rey, A., Balschun, D., Wetzel, W., Randolf, A. & Besedovsky, H.O. A cytokine network involving brain-borne IL-1beta, IL-1ra, IL-18, IL-6, and TNFalpha operates during long-term potentiation and learning. *Brain Behav Immun* **33**, 15-23 (2013).
29. Belarbi, K. & Rosi, S. Modulation of adult-born neurons in the inflamed hippocampus. *Front Cell Neurosci* **7**, 145 (2013).
30. Martinon, F., Burns, K. & Tschopp, J. The inflammasome: a molecular platform triggering activation of inflammatory caspases and processing of proIL-beta. *Mol Cell* **10**, 417-426 (2002).
31. Ben-Menachem-Zidon, O., Ben-Menahem, Y., Ben-Hur, T. & Yirmiya, R. Intra-hippocampal transplantation of neural precursor cells with transgenic over-expression of IL-1 receptor antagonist rescues memory and neurogenesis impairments in an Alzheimer's disease model. *Neuropsychopharmacology* **39**, 401-414 (2014).
32. Hein, A.M.*, et al.* Sustained hippocampal IL-1beta overexpression impairs contextual and spatial memory in transgenic mice. *Brain Behav Immun* **24**, 243-253 (2010).
33. Larson, S.J., Hartle, K.D. & Ivanco, T.L. Acute administration of interleukin-1beta disrupts motor learning. *Behav Neurosci* **121**, 1415-1420 (2007).
34. Cunningham, C. & Sanderson, D.J. Malaise in the water maze: untangling the effects of LPS and IL-1beta on learning and memory. *Brain Behav Immun* **22**, 1117-1127 (2008).
35. Heneka, M.T.*, et al.* NLRP3 is activated in Alzheimer's disease and contributes to pathology in APP/PS1 mice. *Nature* **493**, 674-678 (2013).
36. Liddelow, S.A.*, et al.* Neurotoxic reactive astrocytes are induced by activated microglia. *Nature* **541**, 481-487 (2017).
37. Sun, T., Vasek, M.J. & Klein, R.S. Congenitally acquired persistent lymphocytic choriomeningitis viral infection reduces neuronal progenitor pools in the adult hippocampus and subventricular zone. *PLoS One* **9**, e96442 (2014).
38. Chai, H.*, et al.* Neural Circuit-Specialized Astrocytes: Transcriptomic, Proteomic, Morphological, and Functional Evidence. *Neuron* **95**, 531-549 e539 (2017).
39. Feldmann, M., Pathipati, P., Sheldon, R.A., Jiang, X. & Ferriero, D.M. Isolating astrocytes and neurons sequentially from postnatal murine brains with a magnetic cell separation technique. *Journal of Biological Methods* **1**, 1-7 (2014).
40. Kim, E.J., Ables, J.L., Dickel, L.K., Eisch, A.J. & Johnson, J.E. Ascl1 (Mash1) defines cells with long-term neurogenic potential in subgranular and subventricular zones in adult mouse brain. *PLoS One* **6**, e18472 (2011).
41. Deverman, B.E. & Patterson, P.H. Cytokines and CNS development. *Neuron* **64**, 61-78 (2009).

42. Green, H.F., *et al.* A role for interleukin-1beta in determining the lineage fate of embryonic rat hippocampal neural precursor cells. *Mol Cell Neurosci* **49**, 311-321 (2012).
43. Wang, X., *et al.* Interleukin-1beta mediates proliferation and differentiation of multipotent neural precursor cells through the activation of SAPK/JNK pathway. *Mol Cell Neurosci* **36**, 343-354 (2007).
44. Das, S. & Basu, A. Japanese encephalitis virus infects neural progenitor cells and decreases their proliferation. *J Neurochem* **106**, 1624-1636 (2008).
45. Tang, H., *et al.* Zika Virus Infects Human Cortical Neural Progenitors and Attenuates Their Growth. *Cell Stem Cell* **18**, 587-590 (2016).
46. Shrestha, B., Gottlieb, D. & Diamond, M.S. Infection and injury of neurons by West Nile encephalitis virus. *J Virol* **77**, 13203-13213 (2003).
47. Tawarayama, H., Yoshida, Y., Suto, F., Mitchell, K.J. & Fujisawa, H. Roles of semaphorin-6B and plexin-A2 in lamina-restricted projection of hippocampal mossy fibers. *J Neurosci* **30**, 7049-7060 (2010).
48. Yue, Y., *et al.* Mistargeting hippocampal axons by expression of a truncated Eph receptor. *Proc Natl Acad Sci U S A* **99**, 10777-10782 (2002).
49. Bamji, S.X., *et al.* Role of beta-catenin in synaptic vesicle localization and presynaptic assembly. *Neuron* **40**, 719-731 (2003).
50. Yu, X. & Malenka, R.C. Beta-catenin is critical for dendritic morphogenesis. *Nat Neurosci* **6**, 1169-1177 (2003).
51. Cunningham, E.T., Jr., *et al.* In situ histochemical localization of type I interleukin-1 receptor messenger RNA in the central nervous system, pituitary, and adrenal gland of the mouse. *J Neurosci* **12**, 1101-1114 (1992).
52. John Lin, C.C., *et al.* Identification of diverse astrocyte populations and their malignant analogs. *Nat Neurosci* **20**, 396-405 (2017).
53. Peng, H., *et al.* HIV-1-infected and immune-activated macrophages induce astrocytic differentiation of human cortical neural progenitor cells via the STAT3 pathway. *PLoS One* **6**, e19439 (2011).
54. Koo, J.W. & Duman, R.S. IL-1beta is an essential mediator of the antineurogenic and anhedonic effects of stress. *Proc Natl Acad Sci U S A* **105**, 751-756 (2008).
55. Wu, M.D., *et al.* Adult murine hippocampal neurogenesis is inhibited by sustained IL-1beta and not rescued by voluntary running. *Brain Behav Immun* **26**, 292-300 (2012).
56. Prieto, G.A., *et al.* Synapse-specific IL-1 receptor subunit reconfiguration augments vulnerability to IL-1beta in the aged hippocampus. *Proc Natl Acad Sci U S A* **112**, E5078-5087 (2015).
57. Tong, L., *et al.* Brain-derived neurotrophic factor-dependent synaptic plasticity is suppressed by interleukin-1beta via p38 mitogen-activated protein kinase. *J Neurosci* **32**, 17714-17724 (2012).
58. Chen, E., *et al.* A novel role of the STAT3 pathway in brain inflammation-induced human neural progenitor cell differentiation. *Curr Mol Med* **13**, 1474-1484 (2013).
59. Vallieres, L., Campbell, I.L., Gage, F.H. & Sawchenko, P.E. Reduced hippocampal neurogenesis in adult transgenic mice with chronic astrocytic production of interleukin-6. *J Neurosci* **22**, 486-492 (2002).
60. Smith, P.L., Hagberg, H., Naylor, A.S. & Mallard, C. Neonatal peripheral immune challenge activates microglia and inhibits neurogenesis in the developing murine hippocampus. *Dev Neurosci* **36**, 119-131 (2014).
61. Daniels, B.P., *et al.* Regionally distinct astrocyte interferon signaling promotes blood-brain barrier integrity and limits immunopathology during neurotropic viral infection. *J Clin Invest* **in press**(2017).
62. Muroyama, Y., Fujiwara, Y., Orkin, S.H. & Rowitch, D.H. Specification of astrocytes by bHLH protein SCL in a restricted region of the neural tube. *Nature* **438**, 360-363 (2005).

63. Tsai, H.H., *et al.* Regional astrocyte allocation regulates CNS synaptogenesis and repair. *Science* **337**, 358-362 (2012).
64. Farmer, W.T., *et al.* Neurons diversify astrocytes in the adult brain through sonic hedgehog signaling. *Science* **351**, 849-854 (2016).
65. Bialas, A.R., *et al.* Microglia-dependent synapse loss in type I interferon-mediated lupus. *Nature* **546**, 539-543 (2017).
66. Filiano, A.J., Gadani, S.P. & Kipnis, J. How and why do T cells and their derived cytokines affect the injured and healthy brain? *Nat Rev Neurosci* **18**, 375-384 (2017).
67. Tay, T.L., Savage, J.C., Hui, C.W., Bisht, K. & Tremblay, M.E. Microglia across the lifespan: from origin to function in brain development, plasticity and cognition. *J Physiol* **595**, 1929-1945 (2017).
68. Goshen, I., *et al.* A dual role for interleukin-1 in hippocampal-dependent memory processes. *Psychoneuroendocrinology* **32**, 1106-1115 (2007).
69. Hellstrom, N.A., Bjork-Eriksson, T., Blomgren, K. & Kuhn, H.G. Differential recovery of neural stem cells in the subventricular zone and dentate gyrus after ionizing radiation. *Stem Cells* **27**, 634-641 (2009).
70. Covey, M.V., Loporchio, D., Buono, K.D. & Levison, S.W. Opposite effect of inflammation on subventricular zone versus hippocampal precursors in brain injury. *Ann Neurol* **70**, 616-626 (2011).

2.8 Figures

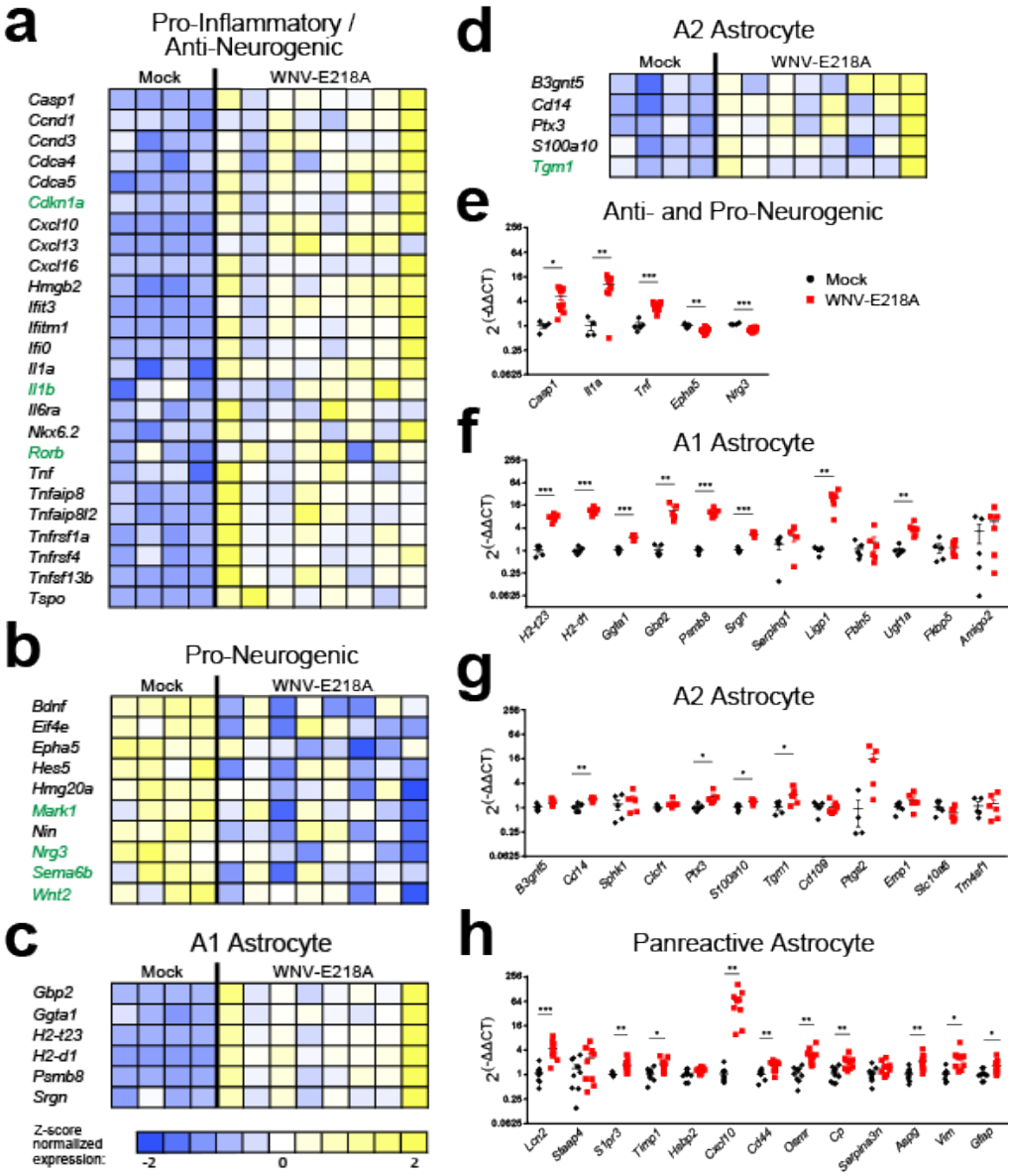

Fig. 2.1. Gene transcripts that impact neurogenesis and markers of proinflammatory astrocytes are altered in WNV-recovered mice. (**a-d**) Heat maps show relative expression by z-score of altered genes generated by microarray analysis of hippocampal RNA collected at 25 days post infection (d.p.i.) from Mock, and WNV-NS5-E218A infected, recovering mice. All genes listed in black font show significant fold change ($P < 0.05$ by two-tailed Student's t-test) while those in green are trending toward significance ($0.05 < P < 0.1$ by two-tailed Student's t-Test). (**e-h**) Validation of microarray hits by QPCR in an independent sample of hippocampal RNA collected at 25 d.p.i. from mock and WNV-NS5-E218A infected, recovering mice. *, $P < 0.05$; ** $P < 0.01$, *** $P < 0.001$, by two-tailed Student's t-test. Each symbol represents an individual mouse; data are mean ± s.e.m. . Data are pooled from 2 independent experiments with 4-10 mice per condition in each. Panels of gene-expression markers include genes that are pro and anti-neurogenic (**e**), A1 & A2 astrocyte markers (**f-g**) and panreactive astrocyte markers (**h**).

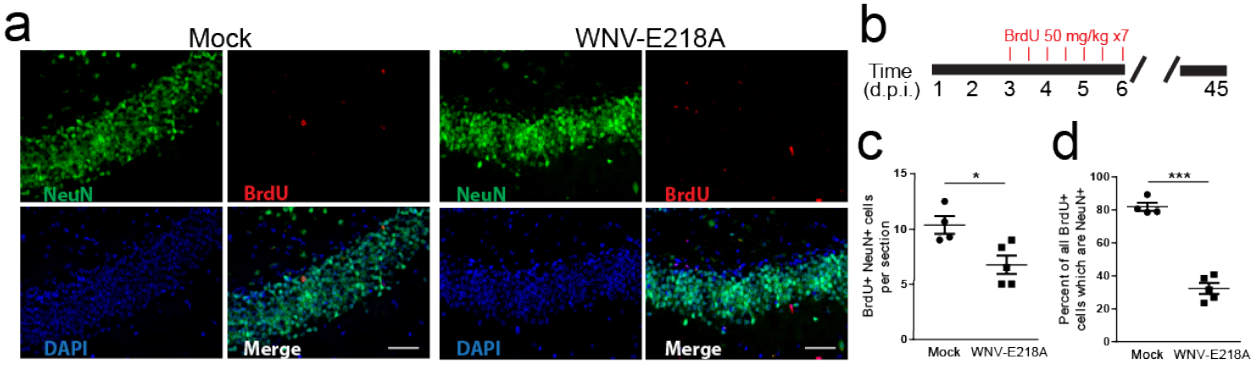

Fig 2.2 Fewer new neurons are born within the dentate gyrus during WNV-NS5-E218A recovery. (**a**) Representative image of the dentate gyrus of Mock and WNV-NS5-E218A infected animals at 45 d.p.i., following *in vivo* BrdU labeling during acute infection. BrdU (red), NeuN (green), and DAPI (blue). (**b**) Experimental design. Mice were given BrdU by intraperitoneal injection every 12 hours for 3.5 days (7 injections) beginning at 4 d.p.i., then animals were sacrificed at 45 d.p.i. for immunohistochemical analysis. (**c, d**) Quantification of $BrdU^{+}NeuN^{+}$ cells per section of dentate gyrus depicted in panel **a** (**c**), and normalized to the number of $BrdU^{+}$ cells. *, $P < 0.05$ by two-tailed, Student's t-test. ***, $P < 0.001$. Each symbol represents an individual mouse; small horizontal lines indicate the mean (± s.e.m). Data are representative of one experiment.

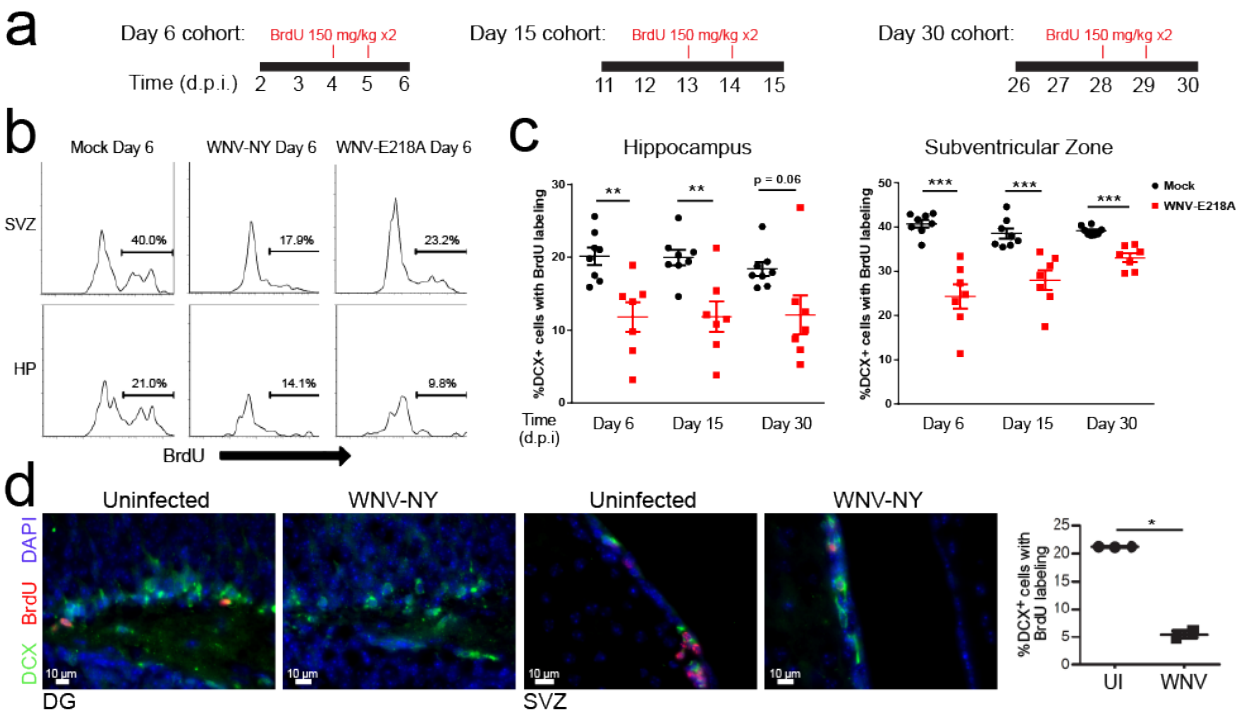

Fig 2.3 Deficits in adult neurogenesis during WNV infection. (**a**) Experimental design. Mock, WNV-NY99 or WNV-NS5-E218A mice were given an i.p. BrdU injection (100 mg/kg) at 24 and 48 hours prior to harvest at 6, 15, or 30 d.p.i. (**b**) Cells were isolated from subventricular zone (SVZ) or hippocampus (HP) and proliferation rates of neuroblasts (% BrdU incorporation) was measured by flow cytometry. Representative plots showing BrdU+ cells after gating on doublecortin+ (DCX) cells (see **Supplementary Fig. 1**) in mock, WNV-NY-99 and WNV-NS5-E218A intracranially infected animals. (**c**) Quantification of proliferating neuroblasts (%DCX+ cells labeled with BrdU) in the hippocampus and subventricular zone at 6, 15, and 30 d.p.i. following *in vivo* BrdU labeling as shown in **a**. (**d**) Representative images and quantification of immunostaining for proliferating neuroblasts in the SVZ and HP following footpad infection with WNV-NY99. *, $P < 0.05$, **, $P < 0.005$, ***, $P < 0.001$ by two-tailed student's t-test. Quantification in **c** and **d** was normalized to age-matched mock-infected controls to compensate for age-related alterations in neurogenesis. Each symbol represents an individual mouse; small horizontal lines indicate the mean (± s.e.m.). Data are pooled from 2 independent experiments with 3-5 mice per condition per time point (**c**) or representative of one experiment with 5 mice (**d**).

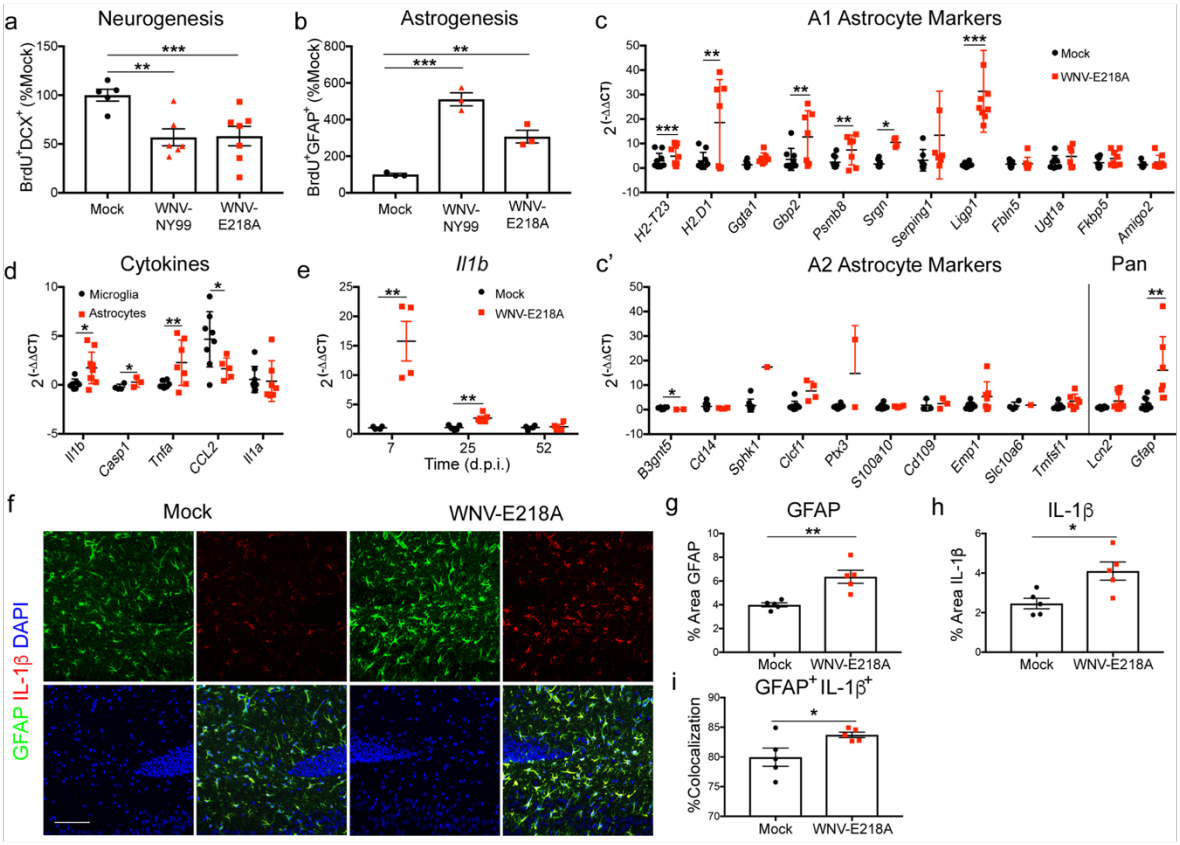

Fig 2.4. Greater numbers of astrocytes are born within the hippocampus during acute WNV encephalitis which adopt a proinflammatory phenotype and express IL-1β. (**a,b**) Mock, WNV-NY99 and WNV-NS5-E218A infected mice were given an i.p. BrdU injection at 24 and 48 hours prior to harvest at 6 d.p.i. Cells were isolated from dissected hippocampi and stained for flow cytometry. Quantification of neurogenesis ($BrdU^+DCX^+$) and astrogenesis ($BrdU^+GFAP^+$) was normalized to mock. Gene expression analysis of (**c**) A1, and (**c'**) A2 and panreactive astrocyte markers in *ex vivo* isolated astrocytes from mock and WNV-NS5-E218A whole brains by qPCR. (**d**) Gene expression analysis of cytokines in *ex vivo* isolated microglia and astrocytes from WNV-NS5-E218A whole brains by qPCR, normalized to mock-infected samples of the respective cell types. (**e**) Gene expression of *Il1b* by qPCR of RNA isolated from hippocampal tissue collected at 7, 25, and 52 d.p.i. from mock and WNV-NS5-E218A infected animals. (**f-i**) Immunostaining for IL-1□ in hippocampus of mock and WNV-NS5-E218A infected animals collected at 25 d.p.i. Representative images are shown in **f,** percent area of GFAP in **g,** percent area of IL-1□ in **h,** and percent area of *Il-1b* $^+GFAP^+$ normalized to total IL-1□$^+$ area in **i**. *, $P < 0.05$, **, $P < 0.005$, ***, $P < 0.001$ by two-tailed student's t-test. Each symbol represents an individual mouse; small horizontal lines or bar height represent the mean (± s.e.m.). Data are representative of one experiment (**a,b,e-i**), or pooled from three independent experiments with at least 3 mice per group (**c, c', d**).

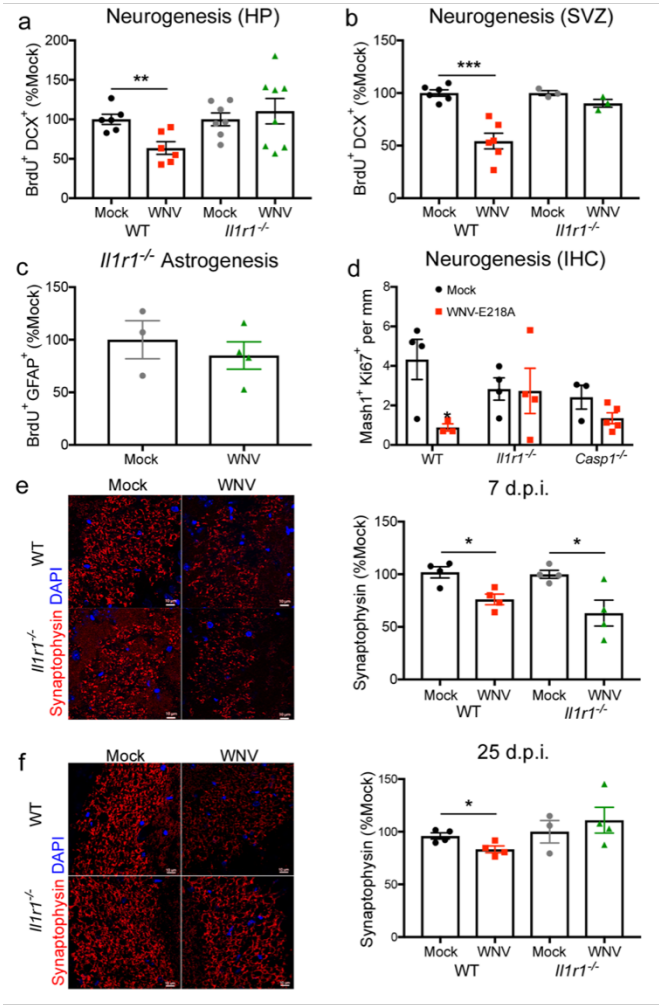

Fig 2.5. IL-1R1$^{-/-}$ mice resist WNV-mediated alterations in neuroblast proliferation and recover synapses earlier than wildtype controls. (**a,b**) Mock and WNV-NS5-E218A infected wild-type (WT) and *Il1r1*$^{-/-}$ animals were assessed for alterations in neurogenesis at 6 d.p.i. following *in vivo* BrdU labeling at 24 and 48 hours prior to harvest. Quantification of BrdU^{+}DCX+ cells by flow cytometry are shown for the hippocampus (HP) in **a** and the subventricular zone (SVZ) in **b**, normalized to age-matched mock infected controls. (**c**) Mock and WNV-NS5-E218A infected *Il1r1*$^{-/-}$ animals were assessed for alterations in astrogenesis at 6 d.p.i. following *in vivo* BrdU labeling at 24 and 48 hours prior to harvest. Quantification of BrdU+GFAP+ cells by flow cytometry are shown for the hippocampus, normalized to age-matched mock infected controls. (**d**) Hippocampal neurogenesis in Mock and WNV-NS5-E218A infected WT, *Il1r1*$^{-/-}$, and *Caspase-1*$^{-/-}$ (*Casp1*$^{-/-}$) was analyzed by immunohistochemistry (IHC) at 6 d.p.i. Quantification of the number of Mash1^{+}Ki67^{+} cells per mm of dentate gyrus analyzed. (**e-f**) Immunostaining of synapses in mock and WNV-NS5-E218A infected WT at *Il1r1*$^{-/-}$ animals at 7 d.p.i. in **e** and 25 d.p.i. in **f**. Quantification shows percent area of synaptophysin in the CA3 of the hippocampus. Synaptophysin (red) and DAPI (blue). *, $P < 0.05$, **, $P < 0.005$, ***, $P < 0.001$ by two-tailed student's t-test. Each symbol represents an individual mouse; height of bar indicates the mean (± s.e.m.). Data are pooled from 2 independent experiments (**a,b**) or representative of one experiment (**e-f**) with 4-5 mice/group.

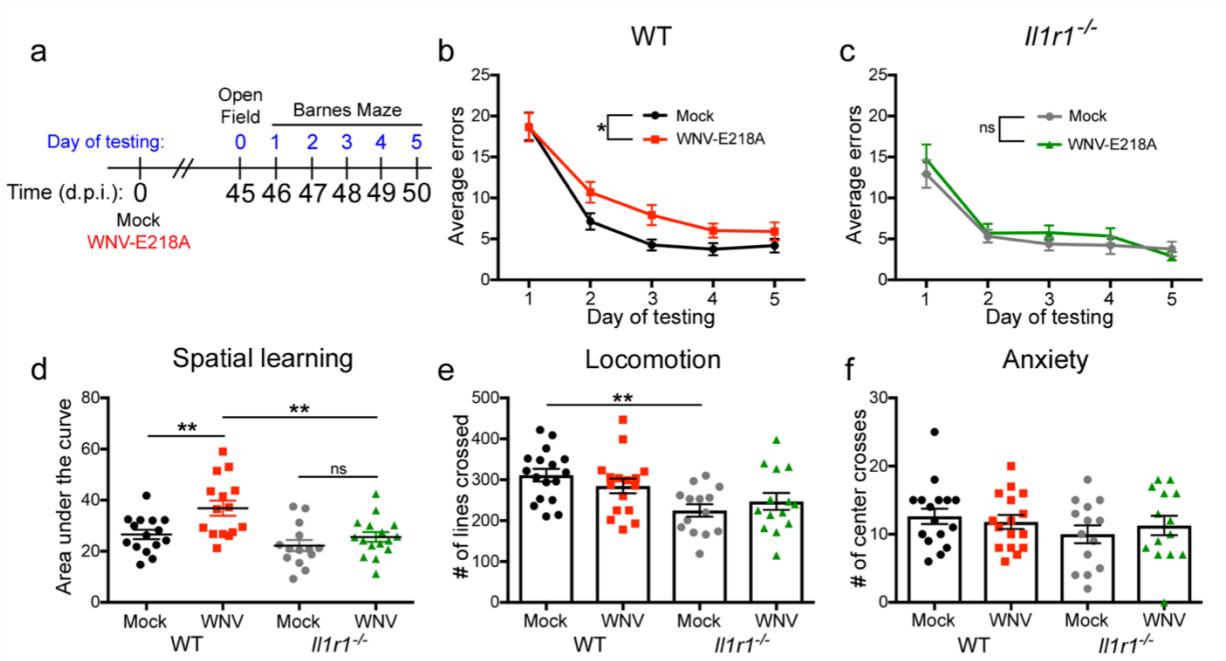

Fig 2.6. *Il1r1*$^{-/-}$ WNV-NS5-E218A-infected mice are protected from virus-induced spatial learning deficits on the Barnes Maze behavior task. (**a**) Experimental design. Mock or WNV-NS5-E218A infected wild-type (WT) and ***Il1r1***$^{-/-}$ underwent behavioral testing beginning at 45 d.p.i. Open field testing was performed at 45 d.p.i., followed by 5 consecutive days of Barnes Maze testing. (**b**) Barnes maze performance of WT mice, showing average errors per trial of each group for each day of testing. (**c**) Barnes maze performance of ***Il1r1***$^{-/-}$ mice. (**d**) Barnes Maze performance of mock and WNV-NS5-E218A infected mice, quantified as area under the curve for each individual animal within each group. (**e**) Open Field testing showing the number of lines crossed in 5 minutes of testing for each animal. (**f**) Open Field testing showing the number of times an animal crossed the center of the arena in 5 minutes of testing for each animal. For Barnes Maze, ns = not significant ($P > 0.05$), *, $P < 0.05$ by two-way ANOVA for effect of WNV. ns = not significant ($P > 0.05$), *, $P < 0.05$, **, $P < 0.005$ by one-way ANOVA with Bonferroni's multiple comparisons test to compare groups. Each symbol represents an individual mouse; small horizontal lines or height of bars represents the mean (± s.e.m.). Data are pooled composite experiments with at least 4 animals per group.

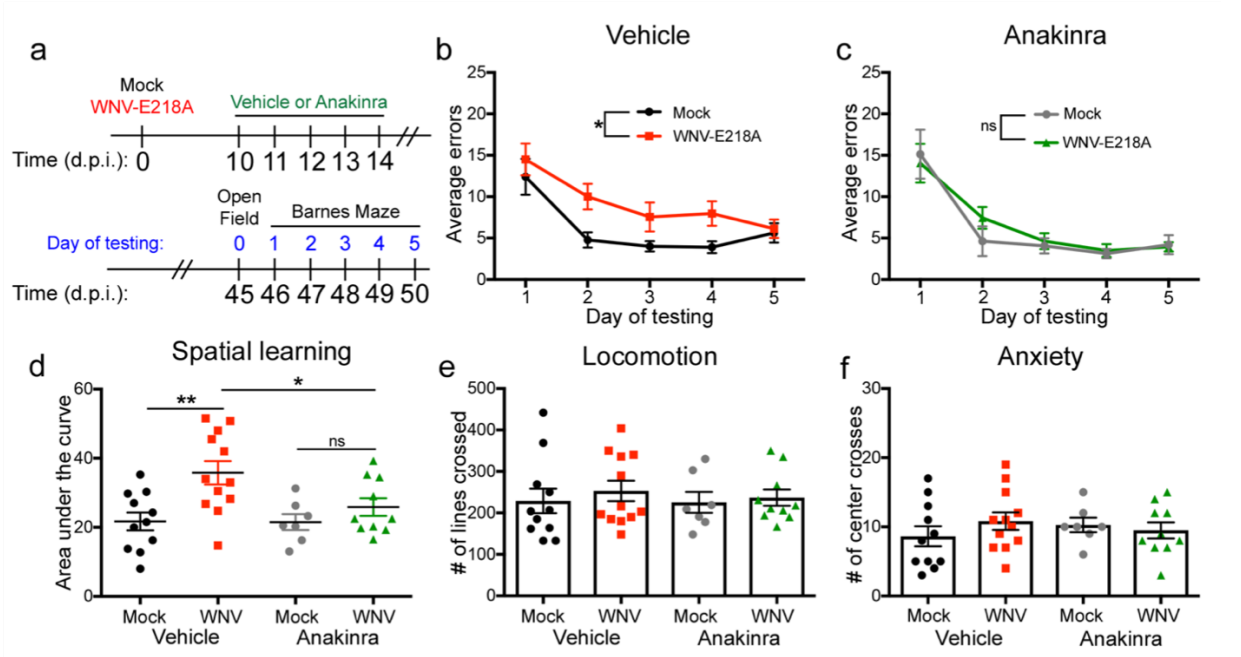

Fig 2.7. WNV-NS5-E218A-infected mice treated with Anakinra are protected from virus-induced spatial learning deficits on the Barnes Maze behavior task. (**a**) Experimental design. Mock or WNV-NS5-E218A infected wild-type (WT) mice were treated with 5 consecutive doses of 100mg/kg/day of Anakinra or vehicle by intraperitoneal (ip) injection beginning at 10d.p.i. Animals were allowed to recover for an additional 30 days post treatment, followed by behavior testing at 45 d.p.i. Open Field testing was performed at 45 d.p.i., followed by 5 consecutive days of Barnes Maze testing. (**b**) Barnes maze performance of vehicle treated WT mice, showing average errors per trial of each group for each day of testing. (**c**) Barnes maze performance of Anakinra treated wildtype mice. (**d**) Barnes Maze performance of mock and WNV-NS5-E218A infected mice, quantified as area under the curve for each individual animal within each group. (**e**) Open Field testing showing the number of lines crossed in 5 minutes of testing for each animal. (**f**) Open Field testing showing the number of times an animal crossed the center of the arena in 5 minutes of testing for each animal. For Barnes Maze, ns = not significant ($P > 0.05$), *, $P < 0.05$ by two-way ANOVA for effect of WNV. ns = not significant ($P > 0.05$), *, $P < 0.05$, **, $P < 0.005$ by one-way ANOVA with Bonferroni's multiple comparisons test to compare groups. Each symbol represents an individual mouse; small horizontal lines or height of bars represents the mean (± s.e.m.). Data are pooled composites of 3 independent experiments, with at least 3 animals per group.

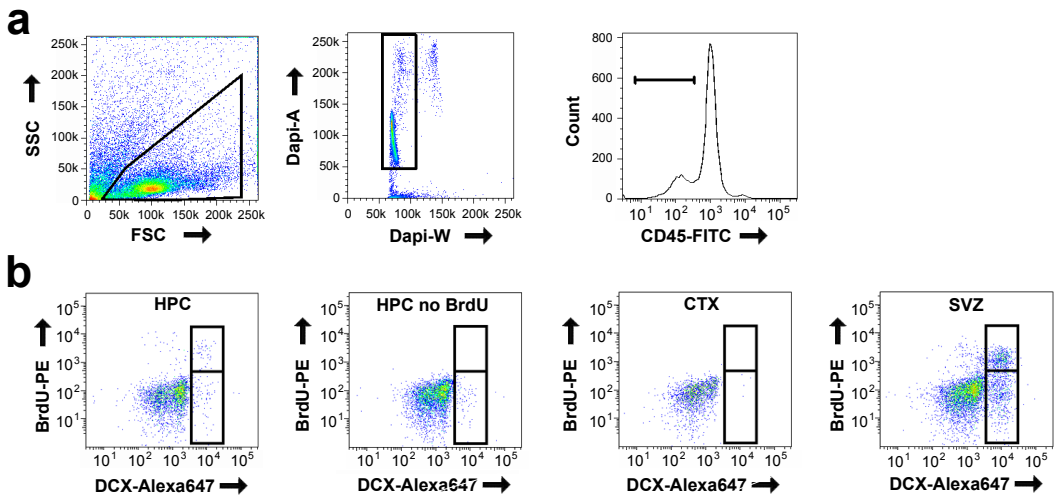

Fig 2.8 Flow cytometry gating strategy

(a) Following isolation and staining with Dapi and antibodies to CD45, Doublecortin, and BrdU, doublets were excluded, and the CD45-negative population was utilized for further gates. **b** Percentage of $BrdU^{+}$ neuroblasts, through expression of the marker, DCX, was calculated and example plots shown from Hippocampus (HPC), Hippocampus from an animal which did not receive BrdU injection (HPC no BrdU), Cortex (CTX), and Subventricular Zone (SVZ).

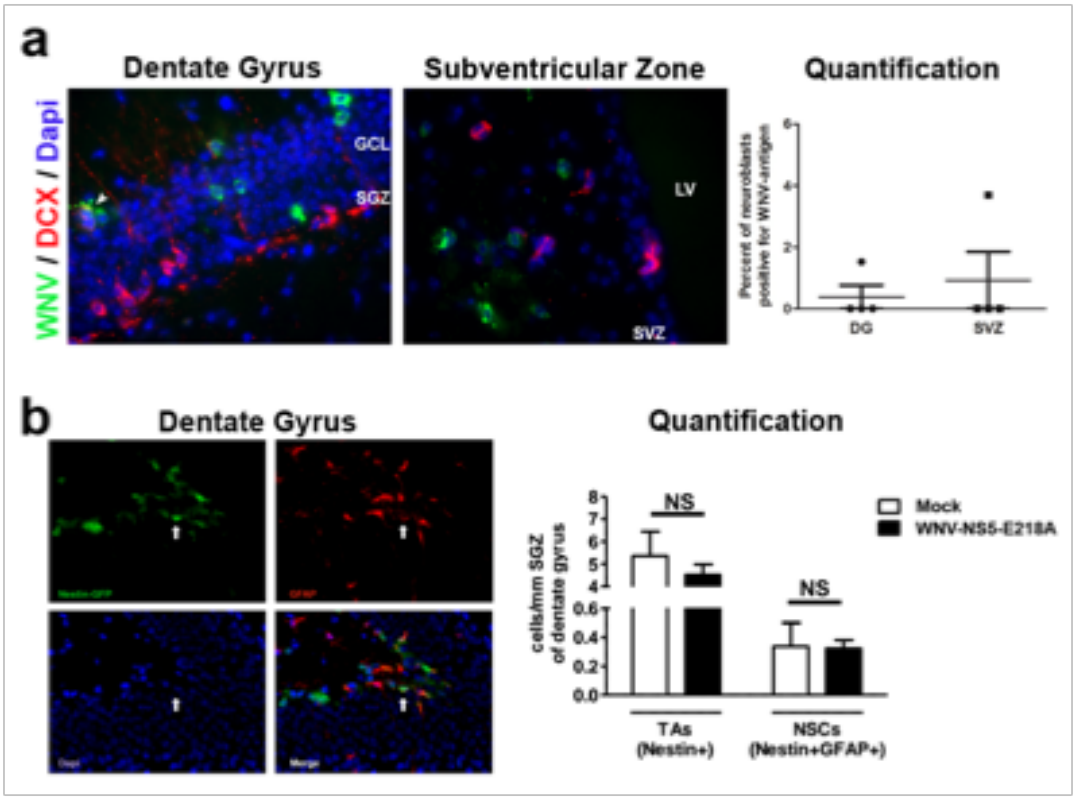

Fig 2.9 WNV permissivity of DCX+ neuroblasts *in vivo*

a 5 week old mice were infected via the footpad with 100 pfu of wild type WNV(NY99) and harvested for tissue collection on day 8 post infection. Immunohistochemistry is shown for West Nile antigen and the neuroblast marker, doublecortin (DCX) within the Dentate gyrus (DG) and Subventricular Zones (SVZ). Many WNV+ neurons can be seen within the granule cell layer (GCL) of the DG and the striatum neighboring the SVZ, however only 1 out of 4 animals showed any WNV and DCX-double positive cells (shown by white arrowhead, Left), resulting in a mean % of infection of less than 1% of total DCX^+ cells. Within the DG, infected DCX^+ cells were always located within the GCL—indicating that they are more mature neuroblasts or immature neurons. **b**Immunostaining for GFP and GFAP in mock and WNV-NS5-E218A nestin-GFP reporter animals. Representative images of the dentate gyrus are shown on the left and quantification of Nestin+ transit amplifying (TA) and $Nestin^+GFAP^+$ neural stem cells (NSC) on the right. Nestin-GFP (green), GFAP (red) and DAPI (blue). ns = not significant ($P > 0.05$).

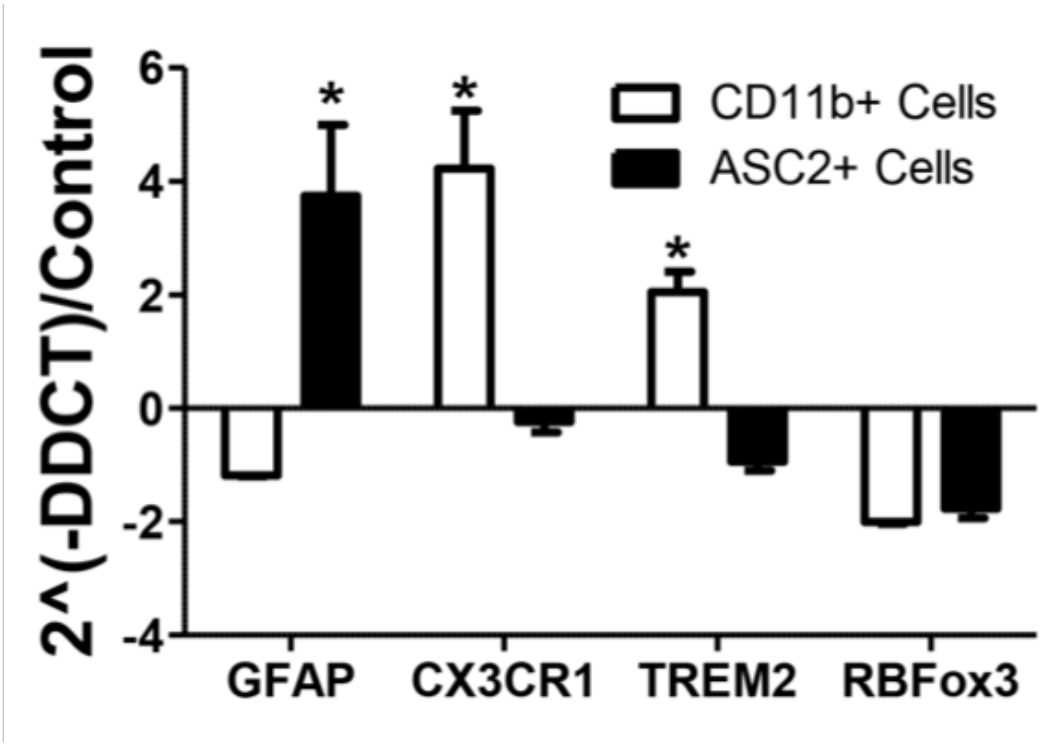

Fig 2.10 Determination of astrocyte and microglia purity

qRT-PCR analysis of expression of cell type specific astrocyte (GFAP), microglia (Cx3CR1, Trem2), and neuronal (RBFox3) transcripts in *ex vivo* isolated astrocytes ($ASC2^+$ cells) and microglia ($CD11b^+$ cells). *, $P < 0.05$ using two-way ANOVA followed by Bonferonni post test.

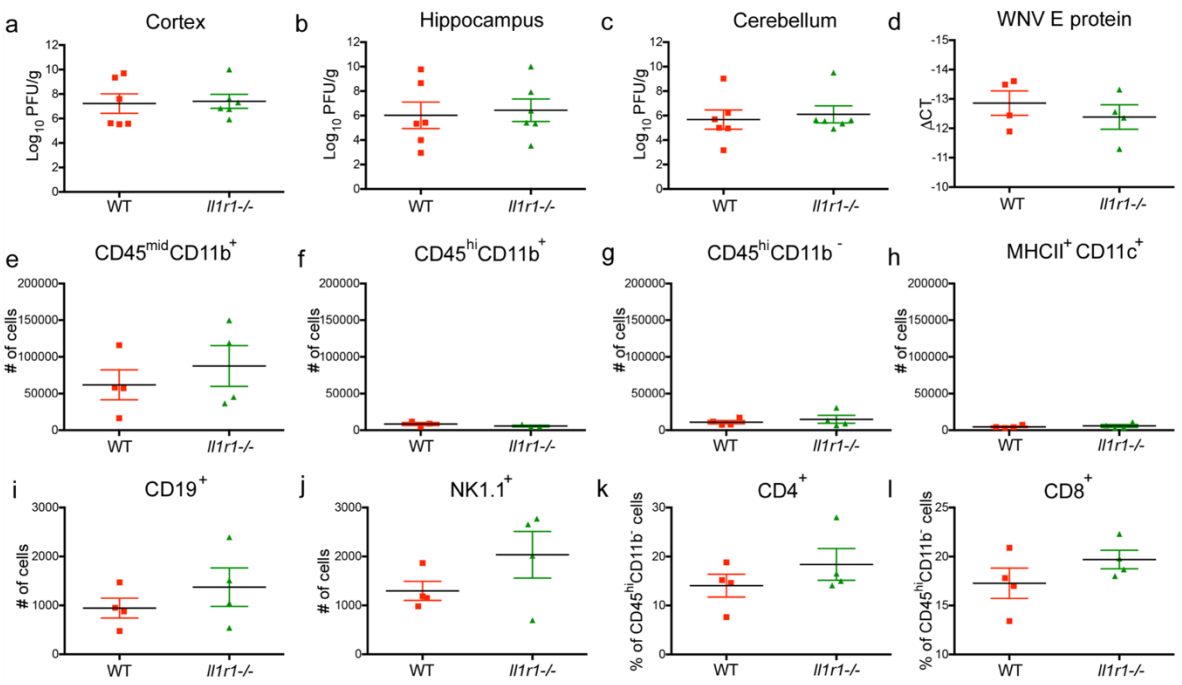

Fig 2.11 Lack of IL-1 signaling does not affect viral control of immune cell infiltrates to the CNS

a-c Plaque assay of CNS tissue from WNV-NS5-E218A infected wildtype (WT) and *Il1r1*$^{-/-}$ animals at 6 d.p.i. **d** qPCR analysis of WNV envelope protein at 25 d.p.i. in hippocampus from WNV-NS5-E218A WT and *Il1r1* $^{-/-}$ mice. **e-l** Flow cytometric analysis of stained single cell populations isolated from hippocampus of WT and *Il1r1* $^{-/-}$ mice at 6 d.p.i. ns = not significant ($P > 0.05$ using two tailed student's t test).

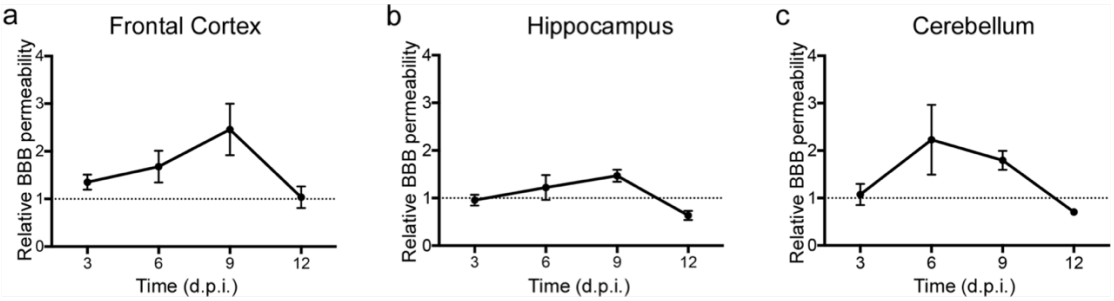

Fig 2.12 Blood brain barrier opening peaks at 6 dpi, and closes by 12 dpi

a-c Relative blood brain barrier permeability of the frontal cortex, hippocampus, and cerebellum at 3, 6, 9, and 12 d.p.i. was assessed by an *in vivo* sodium fluorescein assay to determine optimal time for drug administration. d.p.i.: Days Post Infection.

Chapter 3: T cells promote microglia-mediated synaptic elimination and cognitive dysfunction during recovery from neuropathogenic flaviviruses

This chapter is adapted from a manuscript published in Nature Neuroscience:

Garber C, Soung A, Vollmer LL, Kanmogne M, Last A, Brown, J, Klein RS. T cells promote microglia-mediated synaptic elimination and cognitive dysfunction during recovery from neuropathogenic flaviviruses. *Nat Neurosci*. 2019;22(8):1276-1288. doi:10.1038/s41593-019-0427-y.

C.G., A.S., and R.S.K. designed the experiments. C.G., A.S., L.L.V., M.K., A.L., and J.B. performed experiments. C.G., A.S., L.L.V., M.K., and R.S.K analyzed the data. R.S.K., C.G., and A.S. wrote the paper. All authors read and edited the manuscript.

3.1 Abstract

T cells clear virus from the CNS and dynamically regulate brain functions, including spatial learning, through cytokine signaling. Here we determined whether hippocampal T cells that persist after recovery from infection with West Nile virus (WNV) or Zika virus (ZIKV) impact hippocampal-dependent learning and memory. Using newly established models of viral encephalitis recovery in adult animals, we show that in mice that have recovered from WNV or ZIKV infection, T cell-derived interferon-γ (IFN-γ) signaling in microglia underlies spatial-learning defects via virus-target-specific mechanisms. Following recovery from WNV infection, mice showed presynaptic termini elimination with lack of repair, while for ZIKV, mice showed extensive neuronal apoptosis with loss of postsynaptic termini. Accordingly, animals deficient in

$CD8^+$ T cells or IFN-γ signaling in microglia demonstrated protection against synapse elimination following WNV infection and decreased neuronal apoptosis with synapse recovery following ZIKV infection. Thus, T cell signaling to microglia drives post-infectious cognitive sequelae that are associated with emerging neurotropic flaviviruses.

3.2 Introduction

Among the most debilitating consequences of arboviral infections of the CNS is impairment in cognitive function that occurs despite recovery from acute encephalitis. Mosquito-borne infections with flaviviruses, in particular and including WNV and Japanese encephalitis virus, are linked to significant long-term cognitive sequelae, including decreases in psychomotor speed and in verbal and visuospatial learning, which not only persist but also worsen for years after recovery from encephalitis[1]. In addition, the recently emerged and related flavivirus ZIKV may cause a range of neurological complications in adults, including encephalopathy, and meningomyelitis or encephalomyelitis, which may be associated with defects in memory and cognition with unknown long-term outcomes for survivors[2]. In the adult CNS, WNV targets fully differentiated neurons[3], whereas Japanese encephalitis virus targets immature neurons[4] and ZIKV may additionally target microglia[5] and neural progenitors[6] depending on the strain. That recovery from infection with these viruses may all correlate with reduced learning abilities, despite their differential tropism for neural cell subtypes, suggests that events triggered acutely may be generalizable for a broader category of memory disorders.

The formation and consolidation of memories occur primarily in the hippocampus and depends on the integrity of a trisynaptic circuit between the entorhinal cortex, the hippocampal dentate

gyrus (DG) and the cornu ammonis (CA). In particular, excitatory connections between CA3 pyramidal neurons support the formation of spatial memories in adult rodents[7]. Accordingly, memory disorders, including those associated with Alzheimer's disease (AD), Parkinson's disease, and post-viral encephalitis cognitive sequelae, are all associated with disruptions in circuit integrity via synapse elimination or neuronal loss within the hippocampus[8–10]. Microglial function is critical for synaptic plasticity and for maintenance of adult neurogenesis within neurogenic niches[11,12]. While mechanisms contributing to hippocampal dysfunction are incompletely understood, recovery from WNV infection clearly involves alterations in the homeostatic functions of microglia and astrocytes. This is because reactive changes in these cells persist for weeks after clearance of the infectious virus, which lead to complement-mediated synapse elimination within the CA3 region[10]and interleukin-1 (IL-1)-mediated inhibition of synaptic repair[13].

Activation of microglia and astrocytes in the acutely infected CNS promotes the parenchymal entry of antiviral T cells, which exert virological control via cytokine-mediated, non-cytolytic mechanisms. T cell cytokines such as IFN-γ may also influence microglial biology. In brain tissues of patients with multiple sclerosis, Parkinson's disease, or AD, infiltrating T cells are found in proximity to activated microglia[14–16], and transition into AD dementia correlates with increased numbers of microglial majorhisto-compatibility complex II $(MHCII)^{+}$ cells[17]. IFN-γ influences social interactions[18], synapse formation[19], neurogenesis[20], and learning and memory[21], primarily through regulatory mechanisms. Thus, IFN-γ-deficient animals show increased rates of hippocampal neurogenesis and synapse formation and hyperconnectivity in the pre-frontal cortex[18,19], all of which are partially reversed by an injection of recombinant IFN-γ into the cerebrospinal fluid. Such effects suggest that IFN-γ dynamically influences circuit plasticity in

adult animals. Resident memory T (T_{rm}) cells, which reside in non-lymphoid tissues at sites of prior antigen exposure, produce IFN-γ to coordinate rapid recall responses following re-challenge[22]. Although there is evidence to indicate that IFN-γ^+ T cells may induce microglial activation, the functional implications of a parenchymal population of T cells that persist in the CNS after clearance of viral infections remain unknown.

In this study, we demonstrate that antiviral T cells that persist within the hippocampus after recovery from flaviviral infection are the most proximal trigger of spatial-learning defects. Using newly established in vivo models of recovery from flaviviral encephalitis caused by either a mutant WNV (WNV-NS5-E218A) or ZIKV (Zika-Dakar virus) infection, we determined that $CD8^+$ T cell-derived IFN-γ is required for microglial activation and impaired spatial learning in the post-infectious CNS. We show that WNV and ZIKV differentially target forebrain regions within adult mice, especially with regard to the hippocampus, which exhibited dramatic differences in neuropathology. However, while both flaviviruses led to the persistence of IFN-γ^+CD8^+ T cells and microglial activation in the hippocampus following recovery, WNV infection was associated with the elimination of presynaptic termini, while ZIKV promoted the loss of neuronal nuclei and postsynaptic termini. Subpopulations of these T cells expressed CD 103, a marker associated with the formation of brain T_{rm} cells, which suggests that the newly formed T_{rm} cells might contribute to these effects. Although IFN-γ receptor (IFNGR)-deficient mice (*Ifngr1*$^{-/-}$) infected with either WNV or ZIKV exhibited no acute defects in CNS virological control, spatial learning was preserved. *Ifngr1*$^{-/-}$ and *Cd8*$^{-/-}$ mice exhibited early recovery of presynaptic termini expressing synaptophysin during recuperation from WNV infection. For ZIKV, *Ifngr1*$^{-/-}$ and *Cd8*$^{-/-}$ mice exhibited decreased neuronal apoptosis with recovery of postsynaptic termini that was most pronounced in the CA regions following viral clearance.

Microglial-specific deletion of IFNGR protected mice against spatial-learning deficits and blocked alterations in synapses or neuronal numbers induced during recovery from infection with either virus. These results indicate that T cell and microglial interactions are critical for triggering post-infectious cognitive dysfunction through effects on hippocampal circuitry.

3.3 Results

ZIKV preferentially targets the adult hippocampus.

To address the mechanisms of cognitive recovery from neuroinvasive infection with ZIKV, we developed a model of ZIKV infection recovery in adult mice. Direct intracranial inoculation of 8-week-old C57BL/6J (wild-type (WT)) mice with ZIKV-Dakar (Dakar 41525, Senegal, 1984), which shows increased pathogenicity, including higher levels of inflammatory cytokine induction in mice, compared with Asian strains[23], led to weight loss but 100% survival (Fig. 3.1a,,b).b). This was comparable to our established recovery model of infection with a mutant WNV[10], a strain in which a point mutation in NS5, a nonstructural protein that encodes a 2'-*O*-methyltransferase, prevents viral recognition by tetratricopeptide repeats 1 (IFIT1), which normally acts to block translation of virion-delivered virus-specific RNAs[24]. ZIKV replicated to high levels in the hippocampus and cortex, and, to a lesser extent, in the cerebellum (Fig. 3.1c). Quantitative PCR (qPCR) analysis of hippocampal tissue during acute ZIKV infection and recovery demonstrated robust induction of *Cxcl10*, *Tnfa*, and *Il1a* (Fig. 3.1d), which are molecules known to play important roles during WNV infection of the CNS[25]. Detection of ZIKV or WNV envelope protein (*E*) mRNA via in situ hybridization revealed dramatic differences in viral tropism within forebrain regions. Robust levels of ZIKV *E* mRNA were

detected within all regions of the hippocampi of all animals examined. By comparison, *E* mRNA in WNV-infected mice was variably detected in multiple areas throughout forebrain and hindbrain regions (Fig. 3.1e; Fig. 3.9a,b). Immunohistochemical (IHC) detection of viral proteins within cellular targets of both viruses revealed that both WNV and ZIKV primarily targeted mature neurons (Fig. 3.1f; Fig. 3.9c,d); however, ZIKV E protein was also detected within $NeuN^+$ cells near the neurogenic subgranular zone of the DG, suggesting that there is additional targeting of immature neurons (Fig. 3.9e,f). These data suggest that direct intracranial infection with ZIKV leads to high viral titers in the hippocampus and induces a neuroinflammatory immune response in animals that survive infection, providing a robust model for recovery from neurotropic viral infection.

ZIKV infection of the adult CNS is associated with loss of neurons.

Expression of cytokines and chemoattractant molecules within the virally infected CNS promotes the recruitment and activation of antiviral T cells, which may persist after viral clearance with unknown consequences[26]. A transcriptional microarray analysis of hippocampal gene expression during recovery of WNV (25 days post-infection (d.p.i.)) indeed identified pathways associated with adaptive immune responses. Genes involved in antigen processing and presentation and in chemokine signaling[10] were identified, which suggests that cytokines and chemoattractant molecules persist beyond acute infection. Indeed, flow cytometry analysis of $CD45^+$ cells in the hippocampus during acute infection and after recovery from ZIKV and WNV encephalitis revealed a large population of infiltrating lymphocytes ($CD45^{hi}CD11b^-$), which were primarily $CD8^+$ T cells, that persisted despite viral clearance (Fig. 3.10). Intraparenchymal

T cells and activated astrocytes and microglia were detected robustly at all time points within the hippocampus during recovery from ZIKV infection (Fig. 3.2a,c), whereas these cells were at the highest levels at 25 d.p.i. with WNV (Fig. 3.2b,d). Consistent with prior work[10], WNV infection did not lead to neuronal loss in the hippocampus (Fig. 3.2b,d), although ZIKV infection led to a significant decrease in $NeuN^+$ cells during acute infection that plateaued by 25 d.p.i. (Fig. 3.2a,c). These data suggest these flaviviruses exert distinct immunopathological effects during recovery.

Antiviral $CD8^+IFN\gamma^+$ T cells associate with microglia in the post-infected hippocampus.

An analysis of infiltrating CNS T cells in mice at 25 d.p.i. with WNV or ZIKV revealed significantly increased percentages of $CD8^+$ T cells expressing the integrin CD103, which has been associated with CNS T_{rm} cell formation[26] (Fig. 3.2e,f). Percentages of $CD45^{mid}CD11b^+CX3CR1^+CCR2^-$ microglia expressing MHCII, a marker associated with microglial activation that is induced by the T cell cytokine IFN-γ, were also significantly increased (Fig. 3.2g,h). Consistent with this, the qPCR analysis revealed that hippocampal *Ifng* expression increased following WNV and ZIKV infection, and remained significantly elevated during recovery (Fig. 3.3a,c). An analysis of IFN-γ-YFP (yellow fluorescent protein) reporter mice at 25 d.p.i. demonstrated that $CD3^+$ T cells expressed the bulk of IFN-γ in hippocampus at this time point, with $IBA1^+$ microglia representing an additional source (Fig. 3.3b,d). Flow cytometry analysis of $CD45^+IFN\text{-}\gamma^+$ cells isolated from the hippocampus of IFN-γ-Thy1.1 reporter mice at 25 d.p.i. confirmed that ~15% of the cells were $CD45^{mid}CD11b^+$ microglia, while ~80% were $CD45^{hi}CD11b^-$ lymphocytes, specifically $CD8^+$ T

cells (Fig. 3.3e–g). An analysis of $CD8^+IFN\text{-}\gamma^+$cells confirmed that a subpopulation of these cells expressed CD103, while detection of NS4B, the predominant CD8 epitope in WNV-infected mice[27], via tetramer staining confirmed virus specificity (Fig. 3.3f,g; Fig. 3.11). In addition, $IFN\text{-}\gamma^+CD8^+$ T cells were observed in close proximity to $CX3CR1^+$ microglia at 25 d.p.i. (Fig. 3.3h,i). An additional flow cytometry analysis of mice at 52 d.p.i. confirmed that $CD8^+IFN\text{-}\gamma^+$ T cells persisted in the hippocampus 1 month after viral clearance (Fig. 3.11). These data show that antiviral T cells reside in the hippocampus following flavivirus infection, and may influence the reactivity of resident neural cell populations through cytokine signaling.

ZIKV- and WNV-infected mice show IFN-γ-mediated deficits in spatial learning post recovery.

While IFN-γ is critical for virological control within the CNS, it is also a dynamic regulator of circuit plasticity[18]. Thus, we hypothesized that IFN-γ signaling between T cells and resident CNS cells may underlie post-infectious cognitive sequelae. Mock, WNV, or ZIKV infection of *Ifngr1*$^{-/-}$and WT mice did not reveal significant differences in survival, weight loss, or clinical score between these animal models (Fig. 3.12a–f). Consistent with the clinical course, the kinetics of infectious viral replication in most brain regions of the CNS were similar between WT and *Ifngr1*$^{-/-}$ mice following WNV and ZIKV infection (not shown), with the exception of the cerebella in *Ifngr1*$^{-/-}$ animals, for which WNV clearance was significantly delayed, but cleared in both genotypes by 24 d.p.i. (Fig. 3.12g–i). Mock-, WNV-or ZIKV-infected *Ifngr1*$^{-/-}$and WT mice underwent cognitive behavioral testing 1 month following viral clearance (Fig. 3.4a). WT mice exhibited spatial-learning deficits on the Barnes maze following

WNV infection, as previously described[10,13], as did those recovering from ZIKV infection, while *Ifngr1*$^{-/-}$ mice were protected, showing similar learning curves to mock-infected controls (Fig. 3.4b,c). To control for alterations in anxiety or movement that could impact performance in hippocampus-dependent tasks, we also performed open-field tests (OFTs). While WNV infection did not alter exploratory or anxiety-like behaviors during the OFT in WT or *Ifngr1*$^{-/-}$ mice (Fig. 4e,g), ZIKV-infected WT and *Ifngr1*$^{-/-}$ mice crossed more lines during the OFT than mock-infected controls (Fig. 3.4d), but did not show differences in anxiety (Fig. 3.4f). As this increase in locomotion was observed in both genotypes, this change in behavior is unlikely to explain the difference in the Barnes maze deficits observed between WT and *Ifngr1*$^{-/-}$ mice.

T cell-derived IFN-γ is required to achieve an antiviral state following antigen re-exposure[22], which is an important functional outcome for T_{rm} cell generation. Of interest, we found that there was decreased expression of the T_{rm} cell marker CD103 in a subpopulation of $CD45^{hi}CD11b^{-}CD8^{+}$ T cells in the hippocampus of *Ifngr1*$^{-/-}$ animals post recovery from infection compared with WT controls, with minimal CD103 expression in $CD4^{+}$ T cells (Fig. 3.13a,b). We also found high levels of CCR2 on a subpopulation of $CD45^{hi}CD11b^{-}CD8^{+}$ T cells in the hippocampus of mice that had recovered from infection, the expression of which did not change in the absence of IFN-γ signaling (Fig. 3.13c,d). Importantly, CCR2 expression by $CD3^{+}$ T cells has been demonstrated in human spinal cord tissue from cases of WNV encephalomyelitis[28]; however, the functional consequence of CCR2 expression by T cells in the CNS remains unknown. Together, these data suggest that IFN-γ signaling negatively affects cognitive recovery from neurotropic viral infections, which is unlikely to be due to differences in clinical disease or virological control.

IFNGR signaling is required for neuronal apoptosis during recovery from ZIKV infection.

Given the dramatic hippocampal targeting and neuronal loss observed following ZIKV infection (Figs. 3.1 and 3.2), we determined whether the altered survival of neural cells might underlie spatial-learning deficits. At 25 d.p.i. with ZIKV, *Ifngr1*$^{-/-}$ and Cd8$^{-/-}$ mice exhibited significantly higher levels of NeuN compared with similarly infected WT animals, in which levels were reduced by ~30% of mock-infected controls (Fig. 3.5a–c). In comparison, WT, *Ifngr1*$^{-/-}$, and *Cd8*$^{-/-}$ mice had similar levels of detection of NeuN following recovery from WNV infection (Fig. 3.5e–g). Consistent with prior studies[10], we observed no ongoing neuronal loss in WT animals post recovery from WNV infection (Fig. 3.5e–g). Consistent with the observed loss of NeuN^{+} cells, TdT-mediated dUTP nick end labeled (TUNEL)$^{+}$ cells in the DG, CA3, and CA1 regions of the hippocampus of ZIKV-infected WT animals were significantly increased post recovery compared with mock-and ZIKV-infected *Ifngr1*$^{-/-}$ animals post recovery (Fig. 3.5h). Of note, levels of apoptosis within the DG were considerably lower and more variable than that observed in other hippocampal regions (Fig. 3.5a,d,h). Within the CA3, which is a region critical for spatial learning, detection of NeuN^{+}TUNEL^{+} cells was significantly lower in ZIKV-infected *Ifngr1*$^{-/-}$ and *Cd8*$^{-/-}$mice compared with similarly infected WT animals after viral clearance (Fig. 3.5i,j). ZIKV did not target GAD67^{+} GABAergic neuronal populations, which suggests that the virus may not target interneurons (Fig. 3.14a). In contrast, there were no significant differences in NeuN^{+}TUNEL^{+} cells in the hippocampus of WT and *Ifngr1*$^{-/-}$ mice post recovery from mock infection or WNV infection (Fig. 3.5k). ZIKV also did not alter the number of new neurons born within the DG during recovery from infection, which suggests that impairment in neurogenesis is not a contribution to long-term deficits (Fig. 3.14b). However, increased neuronal loss and apoptosis persisted up to 52 d.p.i. in ZIKV-infected WT mice post

recovery compared with mock-and ZIKV-infected *Ifngr1*$^{-/-}$ mice post recovery (Fig. 3.5l; Fig. 3.14d). These data indicate that WNV and ZIKV lead to differential effects on neurons, including pathology, that contribute to defects in spatial learning.

IFNGR is required for synapse elimination during recovery from WNV infection via IL-1.

Prior studies have demonstrated that WNV infection leads to acute and chronic loss of synaptophysin^{+} presynaptic terminals, but preservation of Homer1^{+} postsynaptic terminals, which ceased by 52 d.p.i.[10]. In addition, expression of IL-1β by reactive astrocytes inhibits the recovery of presynaptic termini and is associated with spatial-learning deficits during recovery from WNV infection[13]. Given the synapse recovery observed in *Ifngr1*$^{-/-}$ mice and the demonstration that IFN-γ influences IL-1β expression[29], we examined levels of this cytokine in WNV-infected *Ifngr1*$^{-/-}$ mice post recovery. Consistent with prior studies[13], we detected increased IL-1β expression by GFAP^{+} astrocytes in the hippocampus of WNV-infected WT mice post recovery, which was significantly decreased in *Ifngr1*$^{-/-}$ animals at 25 d.p.i. (Fig. 3.6a). As previously reported[10], WNV-infected WT animals showed decreased synaptophysin^{+} presynaptic terminals within the CA3 at 7 and 25 d.p.i., while WNV-infected *Ifngr1*$^{-/-}$ and *Cd8*$^{-/-}$ animals demonstrated limited evidence of synapse elimination at either time point (Fig. 3.6b,c; Fig. 3.14e). This result suggests that IFNGR is required for synapse elimination during WNV infection. In contrast, and consistent with acute and chronic loss of NeuN^{+} perikarya, ZIKV infection led to loss of Homer1^{+} post-synaptic terminals in WT and *Ifngr1*$^{-/-}$ animals at 7 d.p.i., with preservation of synaptophysin $^{+}$ and vGlut^{+} presynaptic terminals (Fig. 3.14c,f,g). ZIKV-infected WT animals continued to exhibit decreased numbers of Homer1^{+} postsynaptic terminals

within the CA3 at 25 and 52 d.p.i., while ZIKV-infected *Ifngr1*$^{-/-}$ animals exhibited recovery of postsynaptic termini by 52 d.p.i. (Fig. 3.6d,e). ZIKV-infected WT and *Ifngr1*$^{-/-}$ animals also both displayed significantly increased IL-1β expression by GFAP^{+} astrocytes in the hippocampus compared with mock-infected controls post recovery (Fig. 3.15a). Of note, IL-1β expression was not detected within IBA1^{+} cells at 25 d.p.i. (not shown). These data suggest that persistent alterations in postsynaptic termini contribute to spatial-learning deficits in ZIKV-infected mice independent of IL-1β signaling.

IFNGR signaling potentiates microglial engulfment of postsynaptic termini and perikaryal in ZIKV-infected animals.

Phagocytic roles for microglia are well established and include removal of both apoptotic newborn cells in the neurogenic niche of the hippocampus and non-apoptotic TBR2^{+} neural progenitors in the developing cerebral cortex, in addition to synapse pruning and elimination, the latter of which requires the upregulation of markers of microglial activation[30]. We therefore wondered whether T cell-derived IFN-γ signaling is required for synapse elimination or neuronal loss following WNV or ZIKV infection, respectively, via specific effects on microglia. Indeed, both WNV and ZIKV infection led to increased expression of IBA1 at 25 d.p.i. in WT mice, which did not occur in similarly infected *Ifngr1*$^{-/-}$ animals (Fig. 3.7a,b). Importantly, no differences in numbers of CD45^{hi}CD11b^{+}CX3CR1^{+}CCR2^{-} microglia cells or expression of TMEM119, a recently described homeostatic marker for microglia, were observed in WNV-and ZIKV-infected WT and *Ifngr1*$^{-/-}$animals post recovery (Fig. 3.15b–e). This result is consistent with prior data demonstrating that viral infections do not promote microglial proliferation[10].

Flow cytometry analysis of $CD45^{mid}CD11b^{+}CX3CR1^{+}CCR2^{-}$ microglia revealed increased expression of MHCII in WNV-and ZIKV-infected WT animals post recovery; this increased expression was significantly attenuated in *Infgr1*$^{-/-}$ animals (Fig. 3.15f,g). This finding confirms that IFN-γ contributes to microglial activation in the post-infectious CNS. Three-dimensional reconstructions of $IBA1^{+}$ cells from sections of ZIKV-infected mice at 25 d.p.i. revealed $Homer1^{+}$ puncta (Supplementary Video 1) and $NeuN^{+}$ nuclei (Supplementary Video 2) within microglia. Colocalization of Homer1 or NeuN, lysosomal-associated membrane protein 1 (LAMP1), and IBA1 revealed increased numbers of postsynaptic termini within the lysosomes of $IBA1^{+}$ cells, which were significantly reduced in *Ifngr1*$^{-/-}$ mice at 25 d.p.i. (Fig. 3.7c–f). These data suggest that microglia may be critically involved in responses to T cell-derived IFN-γ that drive cognitive impairment after infection with either WNV or ZIKV.

Micrgolial-specific deletion of IFNGR protects animals against spatial-learning defects.

Given the shared alteration in microglial activation observed in both WNV-and ZIKV-infected animals post recovery in the absence of IFN-γ signaling, we utilized a conditional deletion paradigm to determine whether IFN-γ signaling within microglia of mice post recovery was responsible for the observed spatial-learning deficits. *Cx3cr1*^{CreER}*Ifngr*$^{fl/fl}$ (referred to as Cre^{+}hereafter) animals and *Cx3cr1*^{CreER}*Ifngr*$^{fl/fl}$ (referred to as Cre^{-} hereafter) litter-mate controls were mock-infected or infected with WNV or ZIKV, and then treated with tamoxifen 1 week after infectious viral clearance (at 19 and 21 d.p.i.). Animals were allowed to recover for 3 weeks to achieve specific deletion of *Ifngr* in long-lived microglia while allowing time for short-lived CX3CR1-expressing myeloid populations to turnover[31] (Fig. 3.16a–d), at which time cognitive

behavior testing was performed (Fig. 3.8a). Similar to WT animals, tamoxifen-treated Cre^{-}animals displayed significant spatial-learning deficits on the Barnes maze following WNV and ZIKV infection (Fig. 3.8b,c). In contrast, tamoxifen-treated Cre^{+} animals performed similarly to mock-infected controls (Fig. 3.8b,c). OFTs confirmed no differences in locomotor activity or anxiety between experimental groups, with the exception of an increase in activity in ZIKV-infected WT animals, as previously shown (Fig. 3.8d–g). Importantly, microglial-specific deletion of *Ifngr* after viral clearance was sufficient to prevent elimination of synaptophysin^{+} presynaptic termini and neuronal apoptosis in WNV-and ZIKV-infected mice, respectively (Fig. 3.8h,i). A lack of increased microglial MHCII expression was also observed in WNV-and ZIKV-infected Cre^{+} mice post recovery (Fig. 3.16e,f), confirming that IFN-γ signaling in microglia during recuperation promotes their continued activation. Together, these data suggest that IFN-γ signaling in microglia contributes to microglial activation and spatial-learning deficits following clearance of infectious WNV and ZIKV from the CNS.

3.4 Discussion

Antiviral T cells persist within the CNS for months to years after neurotropic viral infections[26]. The extent to which these tissue-resident cells impact on normal brain function is unclear; however, studies of acutely infected mice suggest that $CD8^{+}$ T cells may damage neuronal structures, such as dendrites, during viral clearance[32]. Here, we developed a novel murine model to evaluate mechanisms of cognitive decline following adult ZIKV infection. We found that ZIKV preferentially targets and induces the loss of neurons throughout the hippocampus, which was also associated with the loss of postsynaptic Homer1^{+} termini. In contrast, the related WNV, which infects neurons throughout the CNS, led to elimination of synpato-physin^{+} presynaptic

termini, which was most pronounced within the CA3 region of the hippocampus, as previously described[10,13]. Survival after infection with either virus was associated with the recruitment of antiviral $CD4^+$ and $CD8^+$ T cells, the latter of which persisted in the virus-cleared CNS, expressed CD103, and became a predominant source of IFN-γ. While IFN-γ^+CD4^+ T cells also persisted, targeted deletion of IFN-γ signaling or CD8 was sufficient for reversing the effects of WNV and ZIKV infection on synapses and apoptosis, respectively. IFN-γ signaling was required for synapse elimination during WNV infection and for the loss of neuronal cell bodies and recovery of synapses after ZIKV infection. Levels of IFN-γ remained elevated after viral clearance, and IFN-γ signaling was required for microglial activation and cognitive dysfunction during recovery from infection with either virus. Microglia-specific deletion of *Ifngr* prevented the development of WNV-or ZIKV-induced hippocampal-dependent learning and memory deficits, suggesting that T cell signaling to microglia is a pivotal event in the development of post-infectious cognitive dysfunction after recovery from flavivirus encephalitis (Fig. 3.17). We used an inducible CX3CR1-Cre line (*Cx3cr1* -Cre^{ERT}) and administered tamoxifen 1 week after viral clearance (~20 d.p.i.), when macrophages are no longer present in the CNS (Fig. 3.10). We therefore designed this experiment to limit the possibility that non-microglial myeloid cells were participating in the process. Nevertheless, as CXC3R1 is not a specific microglial marker, non-microglial cells could possibly contribute to the results obtained.

Infection with ZIKV appears to target the hippocampus in our model. The pathogenesis of ZIKV infection is poorly understood, and there is considerable debate regarding the putative receptors that enable ZIKV infection of various cell types. Several entry receptors, including the innate immune receptor DC-SIGN, the transmembrane protein TIM-1, and TAM receptors (Tyro3, Axl, and Mertk), a family of phosphatidylserine receptors, have been extensively studied for their

potential role as flavivirus entry receptors[33]. However, a more recent study investigating different infection routes of ZIKV, including subcutaneous, transplacental, vaginal, and intracranial infections in WT and TAM receptor null mice, showed no difference in viral titers[34]. TAM receptors, at least in mice, are therefore not essential for ZIKV infection, but may play roles in viral tropism. Studies examining *Tyro3* expression in the rodent CNS, however, have demonstrated that it is specifically expressed within the neocortex, especially within the hippocampus[35]. Thus, although Tyro3 is not required for ZIKV infection, the high level of hippocampal expression of this receptor could potentially contribute to ZIKV targeting this CNS region. ZIKV also led to extensive and ongoing neuronal apoptosis in the hippocampus, which was attenuated in the absence of IFN-γ. This is consistent with studies of mice with CNS autoimmune disease, in which IFN-γ is observed to directly induce apoptosis of oligodendrocytes[36]. Alternatively, activated microglia can promote apoptosis by inducing phosphatidylserine exposure and subsequent phagocytosis of neurons by Mertk[37]. The differential extent of neuronal apoptosis and recovery in ZIKV-infected WT, *Ifngr1*$^{-/-}$, and *Cd8*$^{-/-}$ mice supports reports that a threshold number of neurons may be needed to achieve spatial learning[38]. Resolution of neuroinflammation may involve FasL-mediated apoptosis of T cells[39], which may explain the increased numbers of TUNEL^{+} cells that are not neurons.

The persistence of presynaptic termini after ZIKV infection suggests that synaptic boutons of injured axons of hippocampal neurons may be resistant to the rapid loss incurred by other cortical neurons[40]. This also suggests that microglial activation following viral infection does not universally lead to elimination of presynaptic termini, even among closely related virus family members, and that mechanisms leading to microglial-mediated phagocytosis of synapses or neuronal nuclei may be distinct[41]. Elimination of presynaptic termini following WNV infection

requires the complement component C3 and its receptor C3aR[10]. Astrocytic C3 induces C3aR-mediated phagocytosis in a model of AD, but this is attenuated with prolonged exposure to C3 (ref. [42]), which may explain the lack of elimination of presynaptic termini in the setting of the observed robust and persistent ZIKV-induced astrogliosis.

Loss of IFN-γ signaling also led to attenuation of astrocyte activation during recovery from WNV, but not ZIKV, infection. The lack of astrocyte activation in *Ifngr1*$^{-/-}$ animals protected animals against astrocyte IL-1β production[13], which limits synapse repair during recovery from WNV infection[13]. This effect could be caused by a direct loss of IFN-γ signaling in astrocytes, or it could be secondary to the lack of microglial activation[43]. In our model, the latter explanation is more probable given that specific deletion of *Ifngr* in microglia was sufficient to protect animals against spatial-learning deficits, and prior work has demonstrated that in *Csflr*$^{-/-}$ mice, which lack microglia, lipopolysaccharide injection fails to activate astrocytes[44]. These studies suggest that signaling between microglia and astrocytes critically regulates ongoing neuroinflammation following viral clearance. That spatial learning is preserved in ZIKV-infected *Ifngr1*$^{-/-}$ animals post recovery despite widespread astrocyte reactivity and IL-1β production, which is pathogenic in WNV-infected animals post recovery, adds to the growing body of work demonstrating that heterogeneity in astrocyte reactivity can promote or prevent CNS repair in a disease-specific manner[44].

Although the full spectrum of clinical complications after infection with ZIKV remains unclear, the incidence of neurological manifestations is increasing, including reports of cognitive sequelae[45,46]. Our study also detected increased motor activity in ZIKV-infected mice post recovery. Of interest, neuropsychiatric symptoms, including hyperactivity and hypomania, have been reported in a young adult presenting with ZIKV encephalitis[46]. This finding suggests that

ZIKV targeting of the hippocampus may influence cognitive functions beyond spatial learning. Cognitive dysfunction after recovery from WNV infection was first reported in the United States approximately 8 years after its emergence in the New York area[47], and numerous clinical studies since that time have documented persistent psychological and cognitive sequelae following WNV infection[1]. Moreover, the induced cognitive sequelae may worsen over time[1]. In humans, male sex is independently associated with developing neuroinvasive disease and death, especially in older individuals[48]. While no studies have addressed sex differences in cognitive outcomes, higher survival rates of female patients could impact potential findings. In our study, we used both male and female animals in numbers powered to assess cognitive dysfunction but not sex differences. Further studies of both humans and rodents are needed to examine sexually dimorphic features of neurological sequelae after flavivirus encephalitis.

The differential effect of global versus cell-specific deletion of IFNGR on locomotor activity in ZIKV-infected mice suggests that cell-specific roles for this receptor in motor activity may occur during recovery. In addition to microglia, IFNGR is also expressed by astrocytes, neurons, and brain microvasculature, which may each exhibit regional differences in their levels of expression and/or signaling pathways. Given that ZIKV also targets axons in the pyramidal tract (Fig. 3.1e), it is possible that effects on motor activity are mediated by any of these cell types within this brain region. As microglial-specific deletion of IFNGR abolished hyperactivity, it is possible that IFNGR signaling in microglia specifically limits the effects of the virus on motor function. As the effect was not abolished in mice with global IFNGR deletion, it is possible that IFNGR signaling of other cell types might override the effects of microglia. Additional studies examining regional and cell-specific differences in IFNGR signaling are needed to determine the mechanism of this effect.

In summary, our studies demonstrate that re-establishing circuit integrity through recovery of lost synapses or neurons is critical for restoring hippocampal function after injury, and identify IFN-γ signaling to microglia as a proximal regulator of this repair in the post-infectious CNS. Given the recent association of herpesviral infections[49] and T cells[50] within the CNS parenchyma of patients with AD, the mechanisms uncovered in our study could have implications for other types of memory disorders.

3.5 Methods

Animals

Male and female mice (8–10 weeks old) were used for each experiment. C57BL/6J, *Ifngr1*$^{-/-}$, Ifngr$^{fl/fl}$ and CX3CR1-Cre^{ERT} mice were obtained from Jackson Laboratories. Transgenic animals were backcrossed more than ten generations to C57BL/6 mice at Jackson Laboratories. IFN-γ-YFP (C57BL/6 background) and IFN-γ-Thy1.1 (C57BL/6 background) were obtained from H. Shin at Washington Univeristy in St. Louis. CX3CR1^{GFP}CCR2^{RFP} mice were obtained from R. Ransohoff and the Lerner Research Institute and crossed in-house to *Ifngr1*$^{-/-}$ mice to generate *Ifngr1*$^{-/-}$CX3CR1^{GFP}CCR2^{RFP} reporter mice. All experiments followed the guidelines approved by the Washington University School of Medicine Animals Safety Committee (protocol no. 20170064).

Mouse models of WNV infection.

WNV-NS5-E218A and ZIKV-Dakar strains utilized for intracranial infections were obtained from M. Diamond at Washington University in St Louis. WNV-NS5-E218A contains a single point mutation in the gene encoding 2'-*O*-methyltransferase. Mice were deeply anesthetized and

intracranially administered 1 X 10^4 plaque-forming units (p.f.u.) of WNV-NS5-E218A or ZIKV-Dakar. Viruses were diluted in 10 µl of 0.5% fetal bovine serum in Hank's balanced salt solution (HBBS) and injected into the third ventricle of the brain with a guided 29-guage needle. Mock-infected mice were intracranially injected with 10 µl of 0.5% in HBSS into the third ventricle of the brain with a guided 29-guage needle. BHK21 cells were used for viral plaque assays to determine stock titers of both viruses (described below).

Measurement of viral burden.

WNV-or ZIKV-infected mice were killed and tissues were collected, weighed, homogenized with zirconia beads in a MagNA Lyser instrument (Roche Life Science) in 500 µl of PBS, and stored at −80 °C until virus titration. Thawed samples were clarified by centrifugation (2,000 × *g* at 4 °C for 10 min), and then diluted serially before infection of BHK21 cells. Plaque assays were overlaid with low-melting point agarose, fixed 4 days later with 10% formaldehyde, and stained with crystal violet. Viral burden was expressed on a $\log_{10}$ scale as p.f.u. per gram of tissue. During initial development of the adult ZIKV infection and recovery model (Fig. 3.9), viral burden was determined by qPCR with reverse transcription (qRT-PCR). RNA was extracted using a RNeasy Mini kit (Qiagen). ZIKV levels were determined by one-step qRT-PCR on an Applied Biosystems ViiA7 Real-Time PCR system using standard cycling conditions. A standard curve was produced using serial tenfold dilutions of ZIKV RNA, and viral burden was expressed as viral RNA equivalents per gram of tissue.

Immunohistochemistry.

Mice were anesthetized and perfused with ice-cold Dulbecco's PBS (Gibco) followed by ice-cold 4% paraformaldehyde (PFA). Brains were post-fixed overnight in 4% PFA followed by cyroprotection in 30% sucrose (three exchanges for 24 h), then frozen in OCT compound (Fischer). Coronal tissue sections (10 μm) were washed with PBS and permeabilized with 0.1–0.3% Triton X-100 (Sigma-Aldrich). Nonspecific antibodies were blocked with 5% normal goat serum (Sigma-Aldrich) at room temperature for 1 h. To reduce endogenous mouse antibody staining when detecting ZIKV, a Mouse on Mouse kit (MOM basic kit, Vector) was used as per the manufacturer's instructions. Slides were then incubated in primary antibody (described below) or isotype-matched IgG overnight at 4 °C. Following washes in PBS, slides were then incubated in secondary antibodies at room temperature for 1 h, and nuclei were counterstained with 4,6-diamidino-2-phenylindole (DAPI; Invitrogen). Coverslips were applied with ProLong Gold Antifade Mountant (Thermo Fisher). Immunofluorescent images were acquired using a Zeiss LSM 880 confocal laser scanning microscope and processed using software from Zeiss. Immunofluorescent signals were quantified using the software ImageJ.

Antibodies for immunohistochemistry.

The following primary antibodies were used for IHC analyses: WNV (1:100, polyclonal[25]), ZIKV (1:50; gift from M. Diamond (St. Louis, MO), ZV-13), NeuN (1:1,000; Cell Signaling, cat no. 12943S, clone D3S3I), BrdU (1:200; Abcam, cat. no. ab1893, polyclonal), doublecortin (1:125; Cell Signaling, cat. no. 4604S, polyclonal), GFAP (1:250; Thermo, cat. no. 13–0300, clone 2.2B10), IL-1β (1:100; R&D, cat. no. AF-401, polyclonal), CD3 (1:250; R&D, cat. no. MAB4841, clone 17A2), CD11c (1:50; Novus, cat. no. NB110– 97871, clone AP-MAB0806), GFP (1:500; Abcam, cat. no. ab13970, polyclonal), IBA1 (1:200; Wako, cat. no. 019–19741, polyclonal),

TMEM119 (1:200; Abcam, cat. no. ab209064, clone 28–3), TUNEL (Roche In situ Cell Death kit Red), and synaptophysin (1:250; Synaptic Systems, cat. no. 101004, polyclonal). Secondary antibodies conjugated to Alexa-488 (Invitrogen, cat. no. A-21206, polyclonal) or Alexa-555 (Invitrogen, cat. no. A-21435, polyclonal) were used at a 1:400 dilution.

Three-dimensional reconstruction of confocal z-stack images.

Confocal z-stack images were taken using a Zeiss LSM 880 laser scanning microscope with Airyscan at ×63 magnification, and consisted of at least eight images. Images were transformed into three-dimensional reconstruction videos using the image analysis software Volocity 3D image.

RNAscope in situ hybridization.

Mice were anesthetized and perfused with ice-cold PBS. Brains were then immersion-fixed overnight in 4% PFA followed by three exchanges of 30% sucrose for 24 h. Brains were embedded in OCT compound (Fischer) and 10-µm sagittal tissue sections were prepared. RNAscope 2.5 HD Assay-Brown was performed as per the manufacturer's instructions. Probes against WNV and ZIKA mRNA (ACD) were used. Viral tropism was analyzed using a ZEISS Axio Imager Z2 fluorescence microscope.

Flow cytometry.

Cells from the hippocampus and cortex of mice were isolated at indicated d.p.i. and stained with fluorescence-conjugated antibodies (described below) as previously described[13]. Briefly, mice were anesthetized and perfused with ice-cold Dulbecco's PBS (Gibco). Hippocampal and cortex brain tissue were dissected out, minced, and enzymatically digested at room temperature for 1 h with shaking. The digestion buffer contained collagenase D (Sigma, 50 mg ml^{-1}), TLCK trypsin inhibitor (Sigma, 100 μg ml^{-1}), DNase I (Sigma, 100 U μl^{-1}), HEPES buffer, pH 7.2 (Gibco, 1 M) in HBSS (Gibco). The tissue was then pushed through a 70-μm strainer and pelleted by a 500 × *g*spin cycle for 10 min. To remove myelin debris, cells were resuspended in 37% Percoll and spun at 1,200 × g for 30 min. Cells were then resuspended in FACS buffer. TruStain fcX anti-mouse CD16/32 (BioLegend, cat. no. 101320, clone 93) was used to block the cells for 5 min at 4 °C, followed by cell surface staining for 15 min at 4 °C. Cells were washed twice in FACS buffer, fixed with 4% PFA, and resuspended in 2% PFA for data acquisition. Data were collected using a Fortessa X-20 instrument and analyzed with the software Flowjo.

Antibodies for flow cytometry.

The following antibodies were used for flow cytometry: CD45 (PE/Cy7, BioLegend, cat. no. 103114, clone 30-F11), CD11b (Brilliant Violet 605, BioLegend, cat. no. 101257, clone M1/70), I-A/I-E (MHC-II, APC/Cy7, BioLegend, cat. no. 107628, clone M5/114.15.2), CD4 (Alexa Fluor 700, BioLegend, cat. no. 100536, clone RM4–5), CD8 (PerCP/Cy5.5, BioLegend, cat. no. 100734, clone 53–6.7), NK1.1 (Brilliant Violet 421, BioLegend, cat. no. 108741, clone PK136), CD103 (APC, BioLegend, cat. no. 121414, clone 2E7), Thy1.1 (PE, BioLegend, cat. no. 202524,

clone OX-7), CD119 (IFNGR, Biotin, BD Biosciences, cat. no. 558771, clone GR20), and streptavidin (PE, BD Biosciences, cat. no. 554061).

Behavioral testing.

Animals underwent open-field and Barnes maze testing as previously described[13]. Briefly, mice were given 3 min to explore the Barnes maze platform and to find the target hole. If a mouse did not find the target hole within the test period, it was gently guided in the hole. At the end of a trial, the mice remained in the target hole for 1 min before being placed back into their home cage between trials. Each mouse received two trials per day over the course of five consecutive days. The number of errors (or number of nose pokes over non-target holes) was recorded. Before Barnes maze testing, animals performed the OFT as a measure of exploratory behavior. Each mouse was given 5 min to explore an empty arena before being placed back into its home cage. Both the Barnes maze platform and the open-field arena were decontaminated with 70% ethanol between trials and/or mice. All trials were video recorded using a camera (Canon Powershot SD1100IS) and scored by experimenters blinded to the treatment conditions.

Statistical analysis.

Unpaired Student's *t*-test or one-way or two-way analysis of variance (ANOVA) with appropriate post-test to correct for multiple comparisons, in which the means of all groups were compared pairwise, were performed as indicated in the figure legends. Prism 7.0 (GraphPad Software) was used for generating graphs and statistical analyses. *P* values of ≤ 0.05 were

considered significant. To determine sample sizes for virological and immunological studies, a power analysis was performed using the following values: probability of type I error = 0.05, power = 80%, fivefold hypothetical difference in mean, and population variance of 25-fold (virological studies) or 12-fold (immunological studies). Sample sizes for behavioral testing experiments were predetermined by the power analysis. For all experiments, animals were randomly assigned to mock, WNV or ZIKV infection. Investigators were blinded to group allocation during data collection and analyses.

3.7 References

1. Murray KO et al. Survival analysis, long-term outcomes, and percentage of recovery up to 8 years post-infection among the Houston West Nile virus cohort. PLoS One 9, e102953 (2014).
2. Mehta R. et al. The spectrum of neurological disease associated with Zika and chikungunya viruses in adults in Rio de Janeiro, Brazil: a case series. PLoS Negl. Trop. Dis. 12, e0006212 (2018).
3. Shrestha B, Gottlieb D. & Diamond MS Infection and injury of neurons by West Nile encephalitis virus. J. Virol. 77, 13203–13213 (2003).
4. Ogata A. et al. Japanese encephalitis virus neurotropism is dependent on the degree of neuronal maturity. J. Virol. 65, 880–886 (1991).
5. Lum FM et al. Zika virus infects human fetal brain microglia and induces inflammation. Clin. Infect. Dis. 64, 914–920 (2017).
6. Garcez PP et al. Zika virus impairs growth in human neurospheres and brain organoids. Science352, 816–818 (2016).
7. Neunuebel JP & Knierim JJ CA3 retrieves coherent representations from degraded input: direct evidence for CA3 pattern completion and dentate gyrus pattern separation. Neuron 81, 416–427 (2014).
8. Hong S. et al. Complement and microglia mediate early synapse loss in Alzheimer mouse models. Science 352, 712–716 (2016).

9. Lui H. et al. Progranulin deficiency promotes circuit-specific synaptic pruning by microglia via complement activation. Cell 165, 921–935 (2016).

10. Vasek MJ et al. A complement-microglial axis drives synapse loss during virus-induced memory impairment. Nature 534, 538–543 (2016).

11. Parkhurst CN et al. Microglia promote learning-dependent synapse formation through brain-derived neurotrophic factor. Cell 155, 1596–1609 (2013).

12. Sierra A. et al. Microglia shape adult hippocampal neurogenesis through apoptosis-coupled phagocytosis. Cell Stem Cell 7, 483–495 (2010).

13. Garber C. et al. Astrocytes decrease adult neurogenesis during virus-induced memory dysfunction via IL-1. Nat. Immunol. 19, 151–161 (2018).

14. Brochard V. et al. Infiltration of CD4+ lymphocytes into the brain contributes to neurodegeneration in a mouse model of Parkinson disease. J. Clin. Invest 119, 182–192 (2009).

15. Grebing M. et al. Myelin-specific T cells induce interleukin-1beta expression in lesion-reactive microglial-like cells in zones of axonal degeneration. Glia 64, 407–424 (2016).

16. Togo T. et al. Occurrence of T cells in the brain of Alzheimer's disease and other neurological diseases. J. Neuroimmunol. 124, 83–92 (2002).

17. Paz J, Yao H, Lim HS, Lu XY & Zhang W The neuroprotective role of attractin in neurodegeneration. Neurobiol. Aging 28, 1446–1456 (2007).

18. Filiano AJ et al. Unexpected role of interferon-gamma in regulating neuronal connectivity and social behaviour. Nature 535, 425–429 (2016).

19. Kim IJ, Beck HN, Lein PJ & Higgins D. Interferon gamma induces retrograde dendritic retraction and inhibits synapse formation. J. Neurosci. 22, 4530–4539 (2002).

20. Li L, Walker TL, Zhang Y, Mackay EW. & Bartlett PF Endogenous interferon gamma directly regulates neural precursors in the non-inflammatory brain. J. Neurosci. 30, 9038–9050 (2010).

21. Monteiro S. et al. Absence of IFNgamma promotes hippocampal plasticity and enhances cognitive performance. Transl. Psychiatry 6, e707 (2016).

22. Schenkel JM et al. T cell memory. Resident memory CD8 T cells trigger protective innate and adaptive immune responses. Science 346, 98–101 (2014).

23. Tripathi S. et al. A novel Zika virus mouse model reveals strain specific differences in virus pathogenesis and host inflammatory immune responses. PLoS Pathog. 13, e1006258

(2017).

24. Daffis S. et al. 2’-O methylation of the viral mRNA cap evades host restriction by IFIT family members. Nature 468, 452–456 (2010).

25. Durrant DM, Robinette ML & Klein RS IL-1R1 is required for dendritic cell-mediated T cell reactivation within the CNS during West Nile virus encephalitis. J. Exp. Med. 210, 503–516 (2013).

26. Wakim LM, Woodward-Davis A. & Bevan MJ Memory T cells persisting within the brain after local infection show functional adaptations to their tissue of residence. Proc. Natl Acad. Sci. USA107, 17872–17879 (2010).

27. Kaabinejadian S. et al. Immunodominant West Nile virus T cell epitopes are fewer in number and fashionably late. J. Immunol. 196, 4263–4273 (2016).

28. Mahad D. et al. Modulating CCR2 and CCL2 at the blood-brain barrier: relevance for multiple sclerosis pathogenesis. Brain 129, 212–223 (2006).

29. Eigenbrod T, Bode KA & Dalpke AH Early inhibition of IL-1beta expression by IFN-gamma is mediated by impaired binding of NF-kappaB to the IL-1beta promoter but is independent of nitric oxide. J. Immunol. 190, 6533–6541 (2013).

30. Ebner F. et al. Microglial activation milieu controls regulatory T cell responses. J. Immunol. 191, 5594–5602 (2013).

31. Goldmann T. et al. Origin, fate and dynamics of macrophages at central nervous system interfaces. Nat. Immunol. 17, 797–805 (2016).

32. Kreutzfeldt M. et al. Neuroprotective intervention by interferon-gamma blockade prevents $CD8^+$ T cell-mediated dendrite and synapse loss. J. Exp. Med 210, 2087–2103 (2013).

33. Nowakowski TJ et al. Expression analysis highlights AXL as a candidate Zika virus entry receptor in neural stem cells. Cell Stem Cell 18, 591–596 (2016).

34. Hastings AK et al. TAM receptors are not required for Zika virus infection in mice. Cell Rep. 19, 558–568 (2017).

35. Prieto AL, O’Dell S, Varnum B. & Lai C. Localization and signaling of the receptor protein tyrosine kinase Tyro3 in cortical and hippocampal neurons. Neuroscience 150, 319–334 (2007).

36. Ottum PA, Arellano G, Reyes LI, Iruretagoyena M. & Naves R. Opposing roles of interferon-gamma on cells of the central nervous system in autoimmune neuroinflammation. Front. Immunol. 6, 539 (2015).

37. Neher JJ et al. Phagocytosis executes delayed neuronal death after focal brain ischemia. Proc. Natl Acad. Sci. USA 110, E4098–E4107 (2013).

38. Nakatomi H. et al. Regeneration of hippocampal pyramidal neurons after ischemic brain injury by recruitment of endogenous neural progenitors. Cell 110, 429–441 (2002).

39. Wang X, Haroon E, Karray S, Martina D. & Schluter D. Astrocytic Fas ligand expression is required to induce T-cell apoptosis and recovery from experimental autoimmune encephalomyelitis. Eur. J. Immunol. 43, 115–124 (2013).

40. Canty AJ et al. Synaptic elimination and protection after minimal injury depend on cell type and their prelesion structural dynamics in the adult cerebral cortex. J. Neurosci. 33, 10374–10383 (2013).

41. Vilalta A. & Brown GC Neurophagy, the phagocytosis of live neurons and synapses by glia, contributes to brain development and disease. FEBS J 285, 3566–3575 (2018).

42. Lian H. et al. Astrocyte-microglia cross talk through complement activation modulates amyloid pathology in mouse models of Alzheimer's disease. J. Neurosci. 36, 577–589 (2016).

43. Savarin C. et al. Astrocyte response to IFN-gamma limits IL-6-mediated microglia activation and progressive autoimmune encephalomyelitis. J. Neuroinflamm. 12, 79 (2015).

44. Liddelow SA et al. Neurotoxic reactive astrocytes are induced by activated microglia. Nature541, 481–487 (2017).

45. Nicastri E, Castilletti C, Balestra P, Galgani S. & Ippolito G. Zika virus infection in the central nervous system and female genital tract. Emerg. Infect. Dis. 22, 2228–2230 (2016).

46. Zucker J. et al. Zika virus-associated cognitive impairment in adolescent, 2016. Emerg. Infect. Dis. 23, 1047–1048 (2017).

47. Sejvar JJ The long-term outcomes of human West Nile virus infection. Clin. Infect. Dis. 44, 1617–1624 (2007).

48. Borchardt SM, Feist MA, Miller T. & Lo TS Epidemiology of West Nile virus in the highly epidemic state of North Dakota, 2002–2007. Public Health Rep. 125, 246–249 (2010).

49. Readhead B. et al. Multiscale analysis of independent Alzheimer's cohorts finds disruption of molecular, genetic, and clinical networks by human herpesvirus. Neuron 99, 64–82 e67 (2018).

50. Unger MS et al. Doublecortin expression in CD8+ T-cells and microglia at sites of amyloid-beta plaques: a potential role in shaping plaque pathology? Alzheimers Dement. 14, 1022–1037 (2018).

3.8 Figures

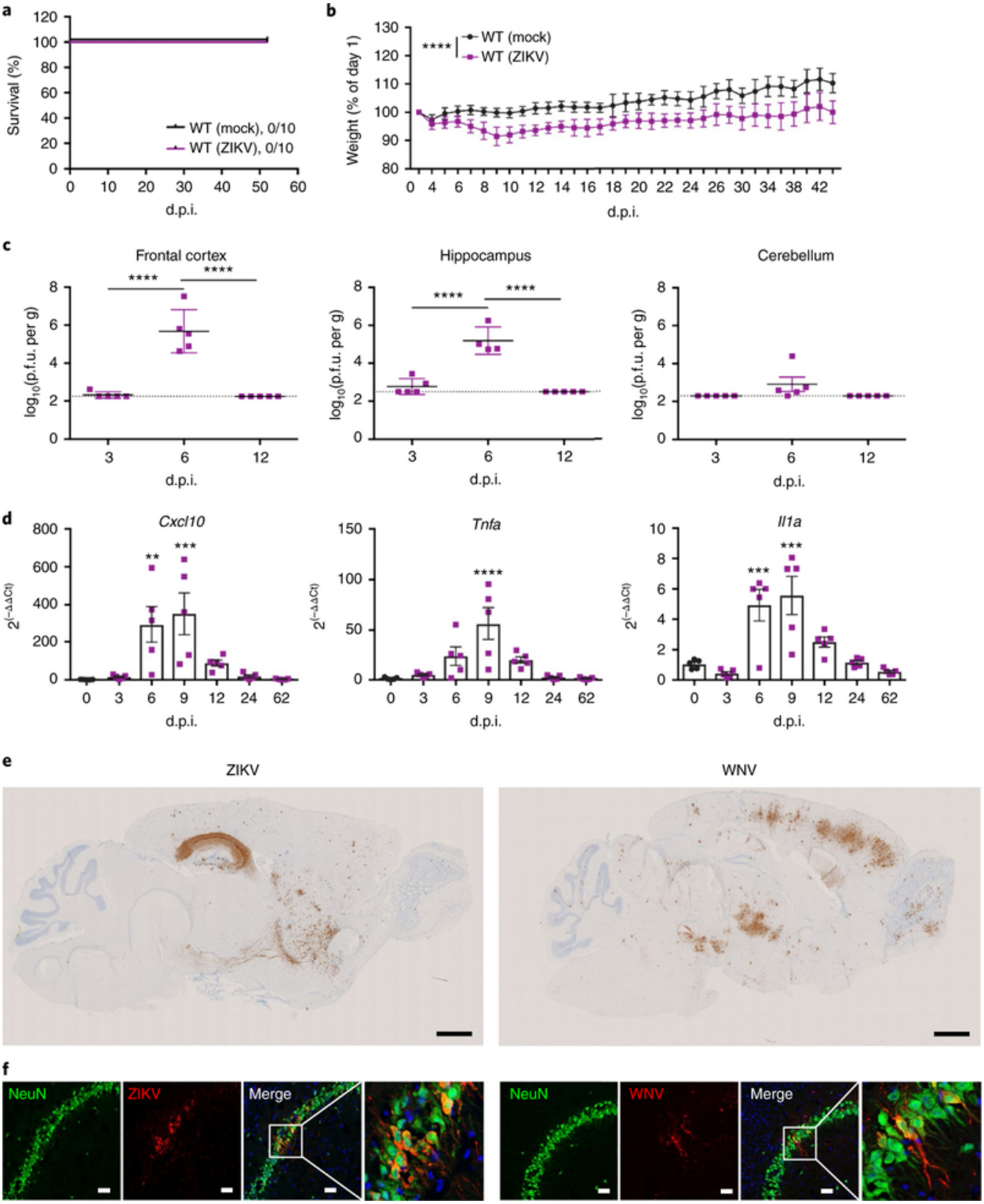

Figure 3.1. ZIKV targets the hippocampus.

a-d, Establishing a mouse model of adult ZIKV infection and recovery. **a**, ZIKV infection did not cause lethality in adult mice. **b**, ZIKV infection led to weight loss, expressed as the percentage of day 0 body weight. Data were pooled from two independent experiments (n = 10 mice per group; P< 0.0001). **c**, ZIKV replicated in the CNS of WT mice. Viral burden was quantified via standard plaque assays (n = 5 mice per group; P = 0.0001 for the frontal corext and hippocampus). P.f.u., plaque-forming units. **d**, ZIKV infection induced cytokine responses in the hippocampus. qPCR analysis of indicated mRNA isolated from the hippocampus at the indicated d.p.i. (n = 5 mice per group). *Cxcl10* (left to right), P= 0.0048 and 0.0007; *Tnfa*, P< 0.0001; *Il1a* (left to right), P = 0.0010 and 0.0002. **e,f**, ZIKV and WNV target different regions of the CNS during acute infection, but similarly infect mature neurons in the hippocampus. **e**, In situ hybridization for viral RNA at 7 d.p.i. revealed dramatic differences in the neurotropism of WNV and ZIKV. ZIKV consistently targeted the hippocampus, with sparse infection of the cortex and striatum. Conversely, WNV RNA was present throughout the CNS, including the olfactory bulb, cortex, hippocampus, and cerebellum. Representative images shown (n = 4 mice per group) here, with additional images shown in Supplementary Fig 1. Scale bars,1,000 μm. **f**, ZIKV and WNV target mature neurons in the hippocampus. Representative immunostaining of the CA3 region of the hippocampus for NeuN (green), viral antigen (red), and DAPI (blue). Data are representative of one independent experiment. Scale bar, 20 μm. For **b-d**, data represent the mean ± s.d. and were analyzed by two-way (**b**) or one-way (**c** and **d**) ANOVA, and corrected for multiple comparisons. **P< 0.005, ***P< 0.001, ****P<0.0001.

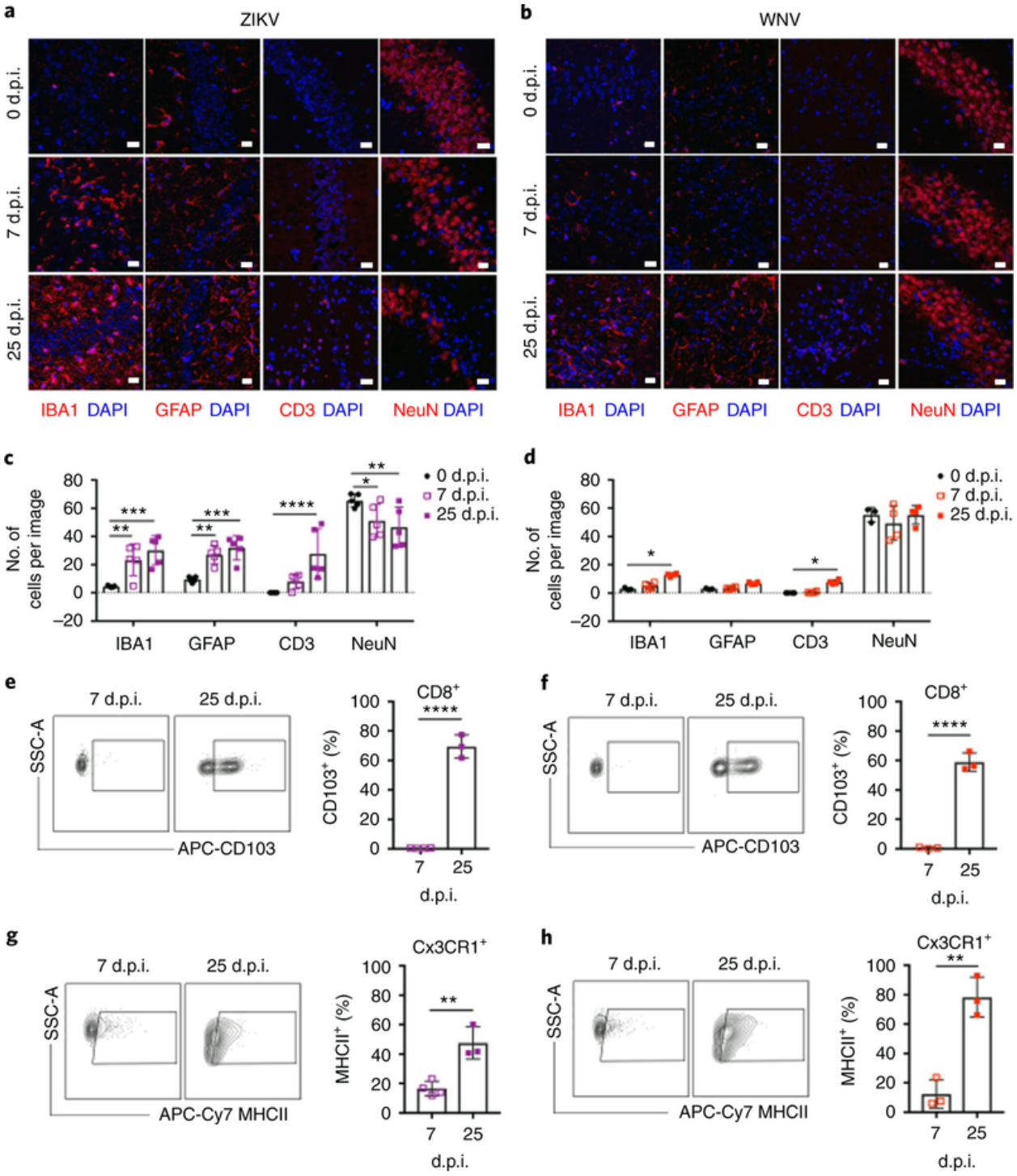

Figure 3.2. ZIKV induces neuroinflammation and neuronal loss in the hippocampus.

a-d, ZIKV and WNV induce differential neuropathology in the hippocampus of WT mice. IHC analysis revealed that the number of microglia (IBA1$^+$), astrocytes (GFAP$^+$), and T cells (CD3$^+$) increases in the hippocampus after infection with either virus, but the number of neurons

(NeuN^{+}) decreases following ZIKV infection. **a,b**, Representative images shown. Scale bars, 20 μm. **c,d**, The number of cells were quantified as indicated. For **c**, *n = 3* (0 d.p.i.) or 5 (7, 25 d.p.i.) mice per group. IBA1, $P = 0.0051$ (0 versus 7d.p.i.) and $P = 0.0001$ (0 versus 25d.p.i.); GFAP, $P = 0.0086$ (0 versus 7d.p.i.) and $P = 0.0008$ (0 versus 25 d.p.i.); CD3, $P = 0.0001$ (0 versus 25 d.p.i.); NeuN, $P = 0.0342$ (0 versus 7d.p.i.) and $P = 0.0046$ (0 versus 25 d.p.i.). For **d**, $n = 3$ (0,25) or 4 (7d.p.i.) mice per group. IBA1, $P = 0.0125$; CD3, $P = 0.0367$. **e-h**, T cells persist in the hippocampus after viral clearance, and microglia demonstrate persistent activation. Flow cytometry analysis of cells isolated from the hippocampus of CC3CR1^{GFP}CCR2^{RFP}reporter animals at the indicated d.p.i. (gating strategy shown in Supplementary Fig 2). Data are representative of two independent experiments. **e,f**, ZIKV (**e**) and WNV (**f**) infection leads to increased expression of CD103 in CD45^{hi}CD11b^{-}CD8^{+} T cells ($n = 3$ mice per group; $P<0.0001$). **g,h**, CD45^{mid}CD11b^{+}Cx3CR1^{+}CCR2^{-} microglia isolated from the hippocampus of ZIKV-infected (**g**) and WNV-infected mice (**h**) express high levels of MHCII at 25 d.p.i. ($n = 3$ mice per group; $P = 0.0035$ (**g**) and $P = 0.0023$ (**h**)). For **c-h**, data represent the mean±s.d. and were analyzed by two-way ANOVA, corrected for multiple comparisons (**c** and **d**) or by unpaired two-sided *t*-test (**e-h**). *$P<0.05$, **$P< 0.005$, ***$P< 0.001$, ****$P< 0.0001$.

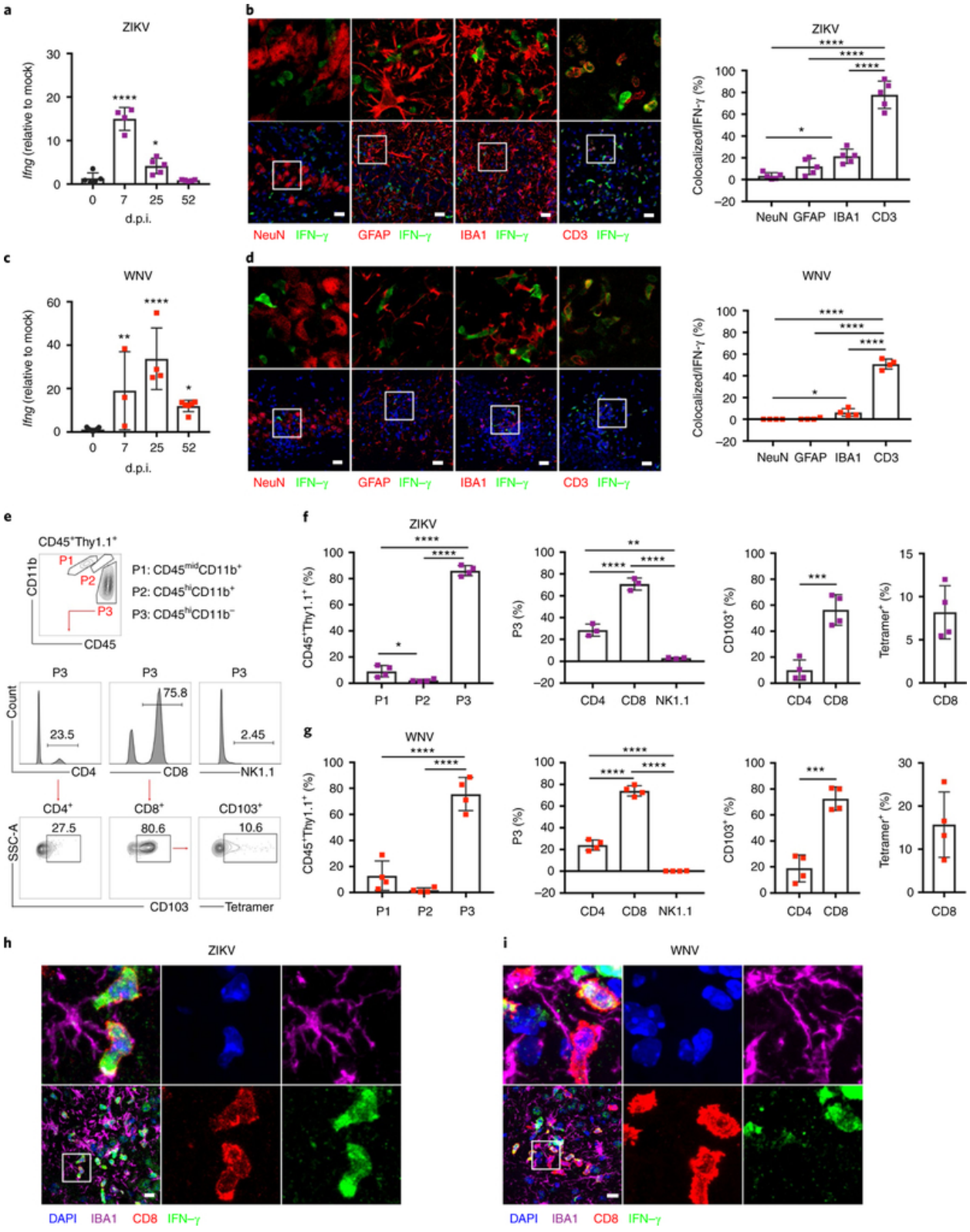

Figure 3.3. T cells express IFN-γ in the post-infected hippocampus.

a,c, qPCR analysis of *Ifng* expression in the hippocampus at the indicated d.p.i. For **a**, $n = 4$ (0, 7 d.p.i.) or 5 (25, 52 d.p.i.) mice per group. For **c**, n = 4 (0, 25d.p.i.), 3 (7 d.p.i.), or 5 (52 d.p.i.) mice per group. For **a** (left to right), $P = 0.0001$ and $P= 0.0376$. For **c** (left to right), $P = 0.0021$, $P= 0.0001$, and $P = 0.0145$. **b-g**, IFN-γ is primarily expressed by $CD3^+CD8^+$ T cells at 25 d.p.i. **b,d**, Immunostaining (left) and quantitation (right) of hippocampi at 25d.p.i. from IFN-γ-YFP reporter mice for IFN-γ (YFP) and cell-type-specific markers for neurons (NeuN), astrocytes (GFAP), microglia (IBA1), and T cells (CD3) to identify the source of IFN-γ in the hippocampi of infected mice post recovery. Images in the upper panel are magnifications of the boxed area in the corresponding images in the lower panel. Scale bars, 20 μm. For **b**, $n = 5$ mice per group; $P = 0.0143$ (NeuN versus GFAP) and $P< 0.0001$ (for other comparisons). For **d**, $n = 4$ mice per group; $P = 0.0439$ (NeuN versus GFAP) and $P< 0.0001$ (for other comparisons). **e-g**, $CD45^+$IFN-γ^+ cells isolated from the hippocampus of IFN-γ-Thy1.1 reporter mice at 25d.p.i. e, Gating strategy. Cells were gated via CD45 and CD11b to identify putative microglial (P1: $CD45^{mid}CD11b^+$), macrophage (P2: $CD45^{hi}CD11b^+$), and lymphocyte (P3: $CD45^{hi}CD11b^-$) populations among IFN-γ-expressing cells. Population P3 was further analyzed for CD4, CD8, and NK1.1 expression. IFN-γ^+CD4^+ and IFN-γ^+CD8^+ T cells were further analyzed for CD103 expression, and IFN-γ^+CD8^+ T cells were analyzed for virus specificity via NS4B tetramer staining. **f,g**, Quantification of indicated populations ($n = 4$ mice per group). For **f**, $P = 0.0402$ (P1 versus P2), $P< 0.0001$ (for other comparisons), $P= 0.0011$ (P3: CD4 versus CD8), and $P = 0.0006$ ($CD103^+$: CD4 versus CD8). For **g**, $P< 0.0001$ (for other comparisons) and $P = 0.0002$ ($CD103^+$: CD4 versus CD8). Full gating strategy and absolute numbers are provided in Supplementary Fig 3. **h,i**, IFN-γ^+CD8^+ T cells are closely associated with microglia in the post-infectious CNS. Representative immunostaining of the CA3 region of the hippocampus for IFN γ, CD8, IBA1, and DAPI. Data are representative of one independent experiment. For **a-d**, **f**, and **g**, data represent the mean±s.d. and were analyzed by one-way ANOVA and corrected for multiple comparisons. *P<0.05, **P< 0.005, ***P<0.001, ****P<0.0001.

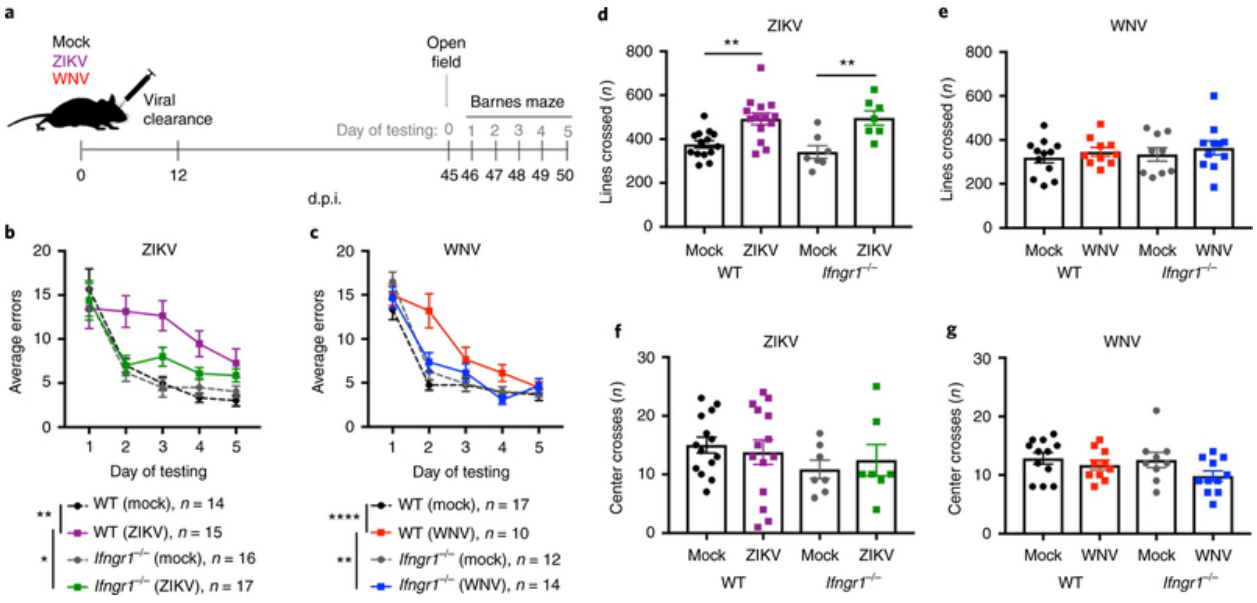

Figure 3.4 Loss of IFN-γ signaling protects animals against spatial-learning deficits.

a-g, WT mice display spatial-learning deficits 1 month after viral clearance. *lfngr1*$^{-/-}$ animals are protected against these deficits. Data were pooled from four independent experiments, with the sample size for each group indicated in **b** and **c. a**, Schematic of the model of viral infection and recovery. **b,c**, Average errors on the Barnes maze (sample sizes are indicated). For **b**, P = 0.0012 (WT mock versus ZIKV) and P = 0.0381 (*lfngr1*$^{-/-}$ mock versus ZIKV). For **c**, P<0,0001 (WT mock versus ZIKV) and P= 0.0186 (*lfngr1*$^{-/-}$ mock versus ZIKV). **d-g**, Open-field data to assess locomotor activity (lines crossed; **d,e**) and anxiety (center crosses; **f,g**) in 5 min when exploring an open-field arena (for sample sizes, see the corresponding colors in **b** and **c**). For **d** (left to right), P = 0.0032 and P= 0.0059. For **b-g**, data represent the mean±s.e.m. and were analyzed by two-way ANOVA, and corrected for multiple comparisons. *P<0.05, **P< 0.005, ****P< 0.0001.

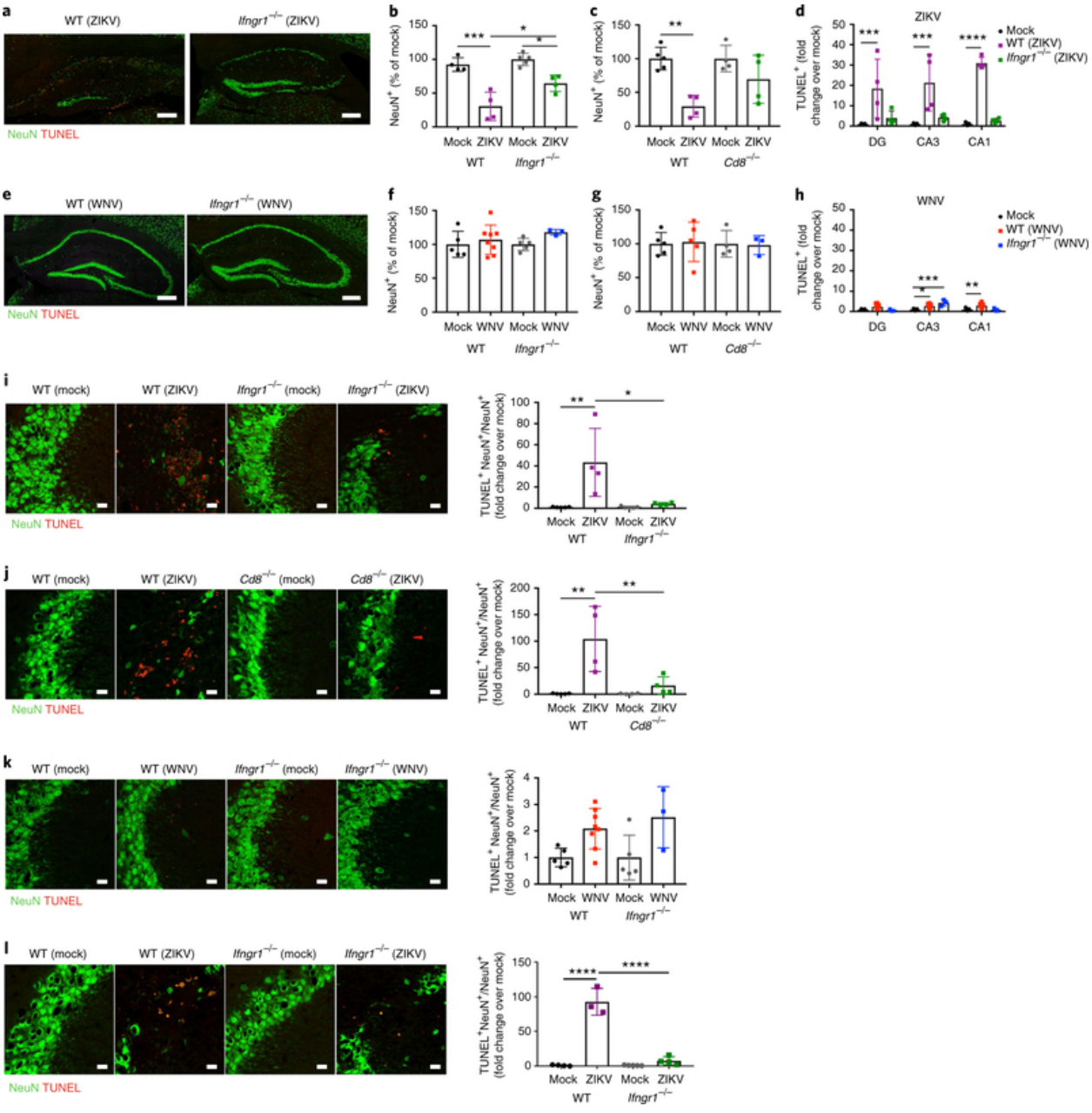

Figure 3.5 IFN-γ promotes neuronal apoptosis in ZIKV-infected animals post recovery.

a-h, ZIKV, but not WNV, infection leads to decreased numbers of hippocampal neurons at 25 d.p.i. More neurons were found in infected *Ifngrl*$^{-/-}$ and *Cd8*$^{-/-}$ mice post recovery. **a-c,e-g**, Representative images (**a**,e) and quantitation (b,c,f,g) of neurons in the hippocampus. Data were pooled from two to three independent experiments. For b, $n = 4$ (WT mock, WT ZIKV, *Ifngrl*$^{-/-}$ ZIKV) or 5 (*Ifngr7*$^{-/-}$ mock) mice per group. For **c**, $n = 5$ (WT mock) or 4 (WT ZIKV, *Ifngrl*$^{-/-}$ mock, *Ifngrl*$^{-/-}$ ZIKV) mice per group. For **f**, $n = 5$ (WT mock, *Ifngr7*$^{-/-}$ mock), 7 (WT WNV), or 3 (*Ifngr1*$^{-/-}$ ZIKV) mice per group. For **g**, $n = 5$ (WT mock, WT ZIKV), 4

(*Ifngrl*$^{-/-}$ mock), or 3 (*Ifngrl*$^{-/-}$ ZIKV) mice per group. For **b**(left to right), *P*= 0.001, *P*= 0.0111, and ***P*** = 0.0214. For **c**, *P*= 0.0032. Scale bars, 200μm. **d,h**, Quantitation of TUNEL^{+} cells in multiple regions of the hippocampus at 25 d.p.i. following ZIKV and WNV infection of WT and *Ifngrl*$^{-/-}$ mice. Note that levels of apoptosis were much lower in WNV-infected animals post recovery. Data were pooled from two independent experiments (*n* = 4 mice per group). For **d** (left to right), *P* = 0.0009, *P = 0.0001,* and *P = 0.0001.* For **h** (left to right), *P* = 0.0138, *P*= 0.0002, and *P* = 0.0068. **i,j**, ZIKV infection leads to significant increases in TUNEL^{+}NeuN^{+} cells, which is not observed in *Ifngrl*$^{-/-}$ or *Cd8*$^{-/-}$ mice post recovery. Data were pooled from two independent experiments. For **i**, *n* = 5 mice per group; *P* = 0.0049 and *P* = 0.0134 (left to right). For **j**, *n* = 4 mice per group; *P* = 0.0014 and *P* = 0.0081 (left to right). **k**, Quantitation of TUNEL^{+}NeuN^{+} cells at 25 d.p.i. with WNV. Data were pooled from two independent experiments (*n* = 5 (WT mock, *Ifngrl*$^{-/-}$ mock), 7 (WT WNV), or 3 (*Ifngrl*$^{-/-}$ WNV) mice per group). l, Quantitation of TUNEL^{+}NeuN^{+} in ZIKV-infected WT versus *Ifngrl*$^{-/-}$ mice at 52d.p.i. Data were pooled from two independent experiments (*n* = 4 mice per group; *P*< 0.0001). Scale bars, 20 μm. For **b-d**, **f-l**, data represent the mean±s.d. and were analyzed by two-way ANOVA, and corrected for multiple comparisons (**b-h**). **P*<0.05, ***P*<0.005, ****P*<0.001.

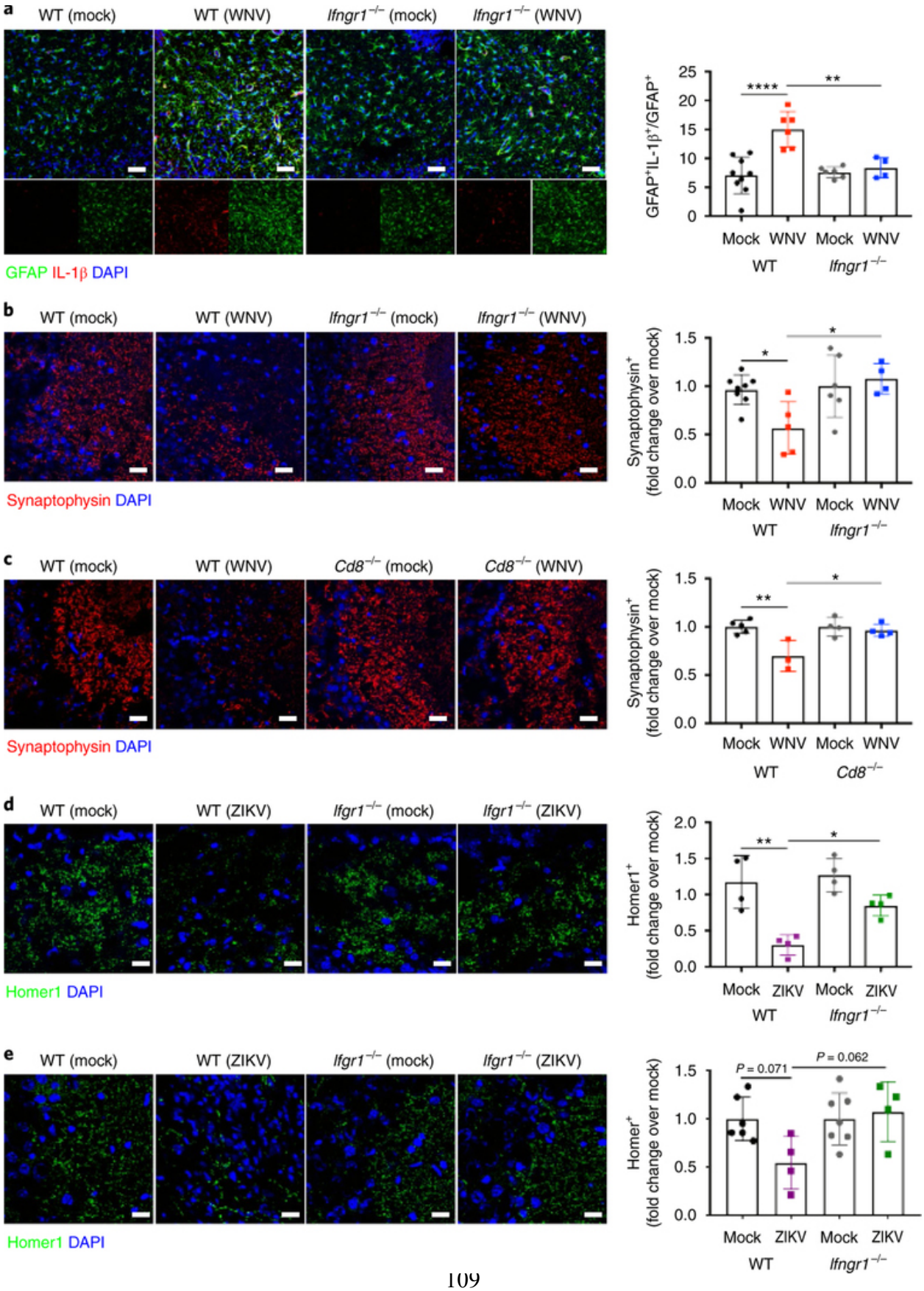
a
WT (mock)
WT (WNV)
Ifngr1−/− (mock)
Ifngr1−/− (WNV)
GFAP IL-1β DAPI
GFAP+IL-1β+/GFAP+
****
**
Mock WNV Mock WNV
WT
Ifngr1−/−
b
WT (mock)
WT (WNV)
Ifngr1−/− (mock)
Ifngr1−/− (WNV)
Synaptophysin DAPI
Synaptophysin+ (fold change over mock)
*
*
Mock WNV Mock WNV
WT
Ifngr1−/−
c
WT (mock)
WT (WNV)
Cd8−/− (mock)
Cd8−/− (WNV)
Synaptophysin DAPI
Synaptophysin+ (fold change over mock)
**
*
Mock WNV Mock WNV
WT
Cd8−/−
d
WT (mock)
WT (ZIKV)
Ifgr1−/− (mock)
Ifgr1−/− (ZIKV)
Homer1 DAPI
Homer1+ (fold change over mock)
**
*
Mock ZIKV Mock ZIKV
WT
Ifngr1−/−
e
WT (mock)
WT (ZIKV)
Ifgr1−/− (mock)
Ifgr1−/− (ZIKV)
Homer1 DAPI
Homer+ (fold change over mock)
P = 0.071
P = 0.062
Mock ZIKV Mock ZIKV
WT
Ifngr1−/−

Figure 3.6 IFNGR is required for repair of presynaptic and postsynaptic termini in flavivirus-infected animals post recovery.

a-c, WNV infection induces astrocyte IL-1β production, which leads to delayed recovery of synapses in the hippocampus at 25 d.p.i. in WT mice, but *Ifngrl*$^{-/-}$ and *Cd8*$^{-/-}$ animals display early recovery of presynaptic termini. **a**, Representative immunostaining (left) and quantitation (right) of the hippocampus. Data were pooled from three independent experiments (n = 9 (WT mock), 6 (WT WNV, *Ifngrl*$^{-/-}$ mock), or 4 *(Ifngrl*$^{-/-}$ WNV) mice per group; P<0.0001 (left) and P= 0.0040 (right)). Scale bar, 50 μm. **b,c**, Representative immunostaining (left) and quantitation (right) of the hippocampus at 25d.p.i. Data were pooled from three independent experiments. For **b**, n = 9 (WT mock), 6 (WT WNV, *Ifngrl*$^{-/-}$ mock), or 4 *(Ifngrl*$^{-/-}$ WNV) mice per group; P = 0.0311 (left) and P = 0.0169 (right). For **c**, n = 5 (WT mock), 3 (WT WNV), or 4 *(Ifngrl*$^{-/-}$ Mock, *Ifngrl*$^{-/-}$ WNV) mice per group; P = 0.0048 (left) and P = 0.0157 (right). Scale bars, 50 μm. **d,e**, ZIKV infection leads to chronic loss of Homer1^{+} postsynaptic terminals at 25 and 52 d.p.i. in WT mice, but *Ifngrl*$^{-/-}$ animals display recovery. **d**, Representative immunostaining (left) and quantitation (right) of the hippocampus at 25d.p.i. Data were pooled from two independent experiments (n = 4 mice per group; P= 0.0011 (left) and P = 0.0311 (right)). Scale bar, 10μm. **e**, Representative immunostaining (left) and quantitation (right) of the hippocampus at 52 d.p.i. Data were pooled from two independent experiments (n = 6 (WT mock), 4 (WT WNV, *Ifngrl*$^{-/-}$ WNV), or 7 (*Ifngrl*$^{-/-}$ Mock) mice per group). Scale bar, 10 μm. For all panels, data represent the mean±s.d. and were analyzed by two-way ANOVA, and corrected for multiple comparisons. *P<0.05, **P<0.005, ****P<0.0001.

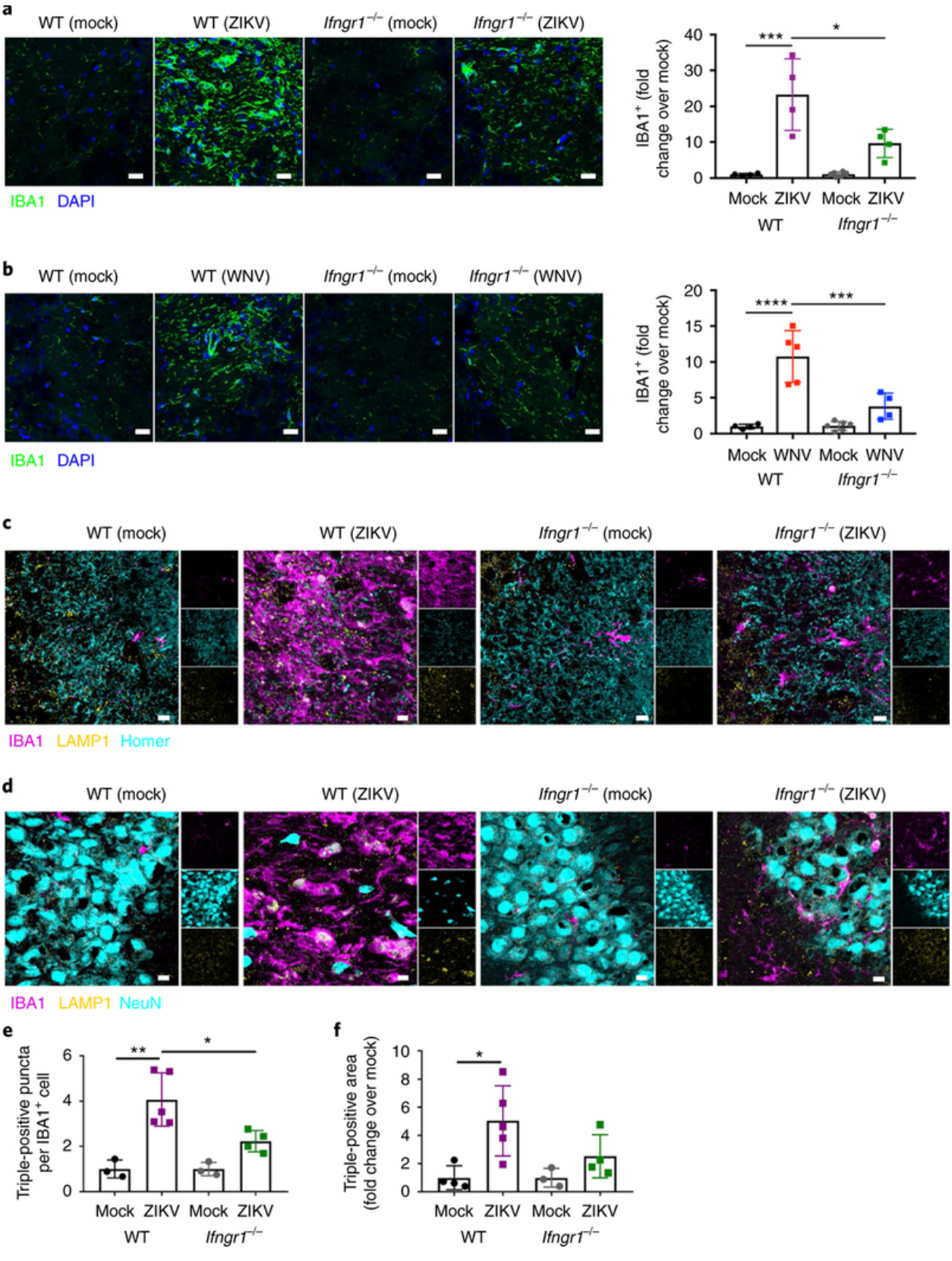
a
WT (mock)
WT (ZIKV)
Ifngr1−/− (mock)
Ifngr1−/− (ZIKV)
IBA1 DAPI
IBA1+ (fold change over mock)
***
*
Mock ZIKV Mock ZIKV
WT
Ifngr1−/−
b
WT (mock)
WT (WNV)
Ifngr1−/− (mock)
Ifngr1−/− (WNV)
IBA1 DAPI
IBA1+ (fold change over mock)
****
***
Mock WNV Mock WNV
WT
Ifngr1−/−
c
WT (mock)
WT (ZIKV)
Ifngr1−/− (mock)
Ifngr1−/− (ZIKV)
IBA1 LAMP1 Homer
d
WT (mock)
WT (ZIKV)
Ifngr1−/− (mock)
Ifngr1−/− (ZIKV)
IBA1 LAMP1 NeuN
e
Triple-positive puncta per IBA1+ cell
**
*
Mock ZIKV Mock ZIKV
WT
Ifngr1−/−
f
Triple-positive area (fold change over mock)
*
Mock ZIKV Mock ZIKV
WT
Ifngr1−/−

Figure 3.7. IFN-γ potentiates microglial engulfment of postsynaptic termini and neurons in ZIKV-infected animals post recovery.

a,b, WNV or ZIKV infection induces increased expression of IBA1 in the hippocampus at 25d.p.i., which is significantly reduced in *Ifngrl*$^{-/-}$ mice. Representative immunostaining (left) and quantitation (right) of the hippocampus at 25d.p.i. Data were pooled from two independent experiments. For **a**, $n = 4$ mice per group; P=0.0001 (left) and $P = 0.0102$ (right). For **b**, $n = 4$ (WT mock, WT WNV, *Ifngrl*$^{-/-}$WNV) or 6 (*Ifngrl*$^{-/-}$ mock) mice per group; $P < 0.0001$ (left) and $P = 0.0010$ (right). Scale bars, 50 μm. c,e, IBA1^{+} microglia engulf postsynaptic termini at 25d.p.i., which is significantly reduced in *Ifngrl*$^{-/-}$mice. Representative immunostaining, with single-channel images on the right (**c**) and quantitation (**e**) of the hippocampus of infected mice post recovery. Data were pooled from two independent experiments (n= 3 (WT Mock, *Ifngrl*$^{-/-}$ Mock), 5 (WT ZIKV), or 4 (*Ifngrl*$^{-/-}$ ZIKV) mice per group; P= 0.0011 (left) and $P = 0.0209$ (right)). Scale bars, 10 μm. **d,f**, IBA1^{+} microglia engulf NeuN^{+} perikarya at 25d.p.i., which is reduced in *Ifngrl*$^{-/-}$ mice. Representative immunostaining, with single-channel images on the right (**d**) and quantitation (**f**) of the hippocampus of infected mice post recovery. Data were pooled from two independent experiments ($n = 4$ (WT Mock, *Ifngrl*$^{-/-}$ ZIKV), 5 ($n =$ WT ZIKV), or 3 (*Ifngrl*$^{-/-}$Mock) mice per group; $P = 0.0190$). Scale bars, 10μm. For **a, b, e**, and **f**, data represent the mean±s.d. and were analyzed by two-way ANOVA, corrected for multiple comparisons. *P<0.05, ***P< 0.001, ****P< 0.0001.

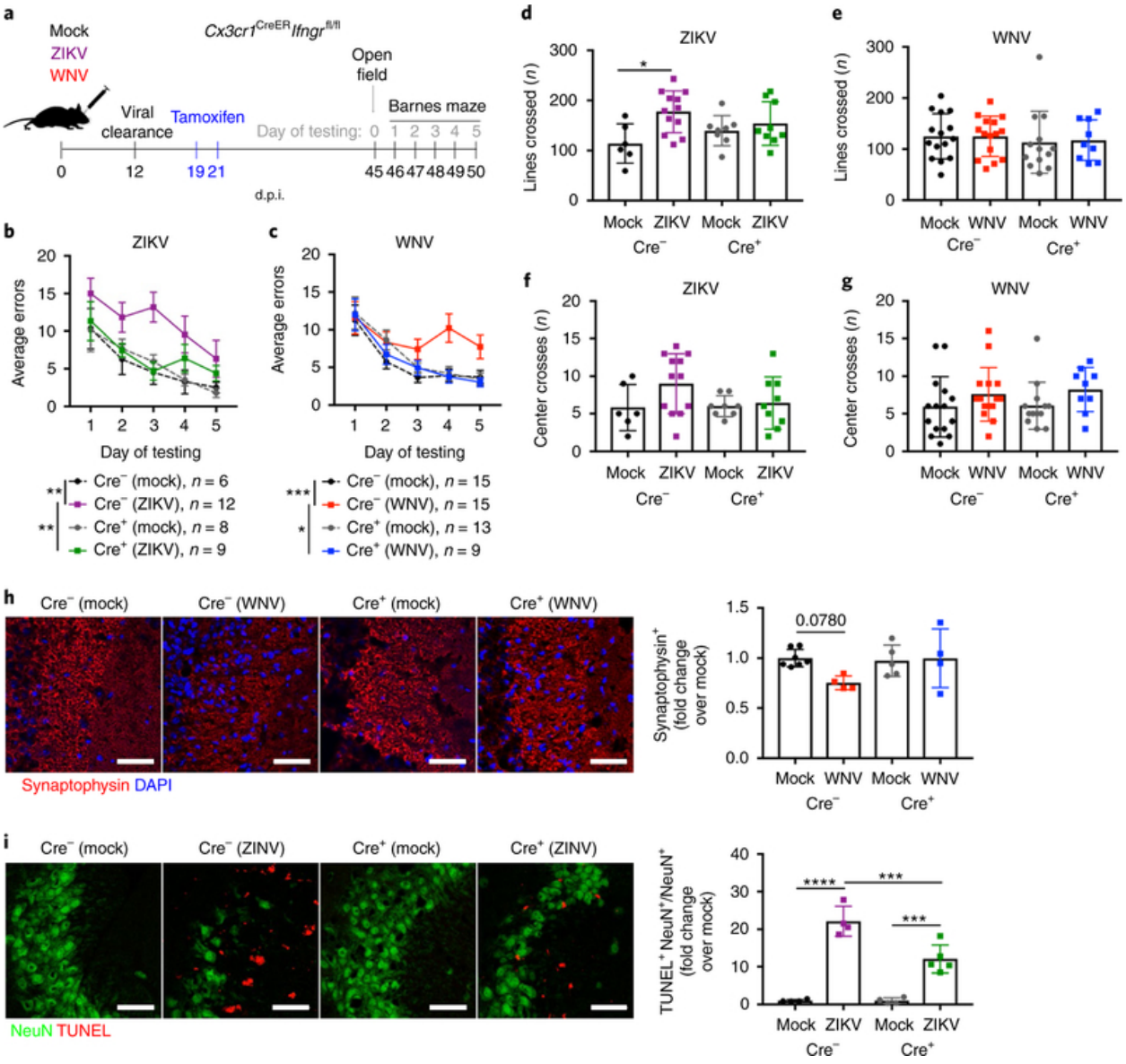

Figure 3.8 Loss of IFN-γ signaling in microglia during recovery protects animals against spatial-learning deficits.

a-g, Specific deletion of IFNGR in microglia after viral clearance is sufficient to protect animals against WNV-or ZIKV-induced spatial-learning deficits. **a**, Experimental design. *Cx3cr1*^{CreER}*Ifngr*$^{fl/fl}$ (Cre^{+}) animals were generated, and *Cx3cr1*^{CreER}*Ifngr*$^{fl/fl}$ (Cre^{-}) littermates were used as controls. Mice were challenged intracranially with mock, WNV, or ZIKV at 8 weeks of age. All mice were treated with tamoxifen at 19 and 21 d.p.i. to induce Cre-recombinase expression and achieve deletion of *Ifngr* in CX3CR1^{+} microglia. Behavioral testing began on 45 d.p.i. with OFTs, followed by 5 consecutive days of Barnes maze testing. **b,c**, Average errors on the Barnes maze. Data were pooled from four independent experiments, and

sample sizes are as listed. For **b**, P= 0.0011 (Cre^- mock and ZIKV) and P = 0.0073 (Cre^+ mock and ZIKV). For **c**, P = 0.003 (Cre^- mock and ZIKV) and P= 0.0207 (Cre^+ mock and ZIKV). **d-g**, OFT data to assess locomotor activity (lines crossed; **d,e**) and anxiety (center crosses; **e,g**) in 5 min when exploring an open-field arena. Data were pooled from four independent experiments (for sample sizes, see the corresponding colors in **b** and **c**); P = 0.0146 (**d**). **h,i**, Specific deletion of *Ifngr* in microglia after viral clearance is sufficient to protect animals against WNV-or ZIKV-mediated synapse and neuronal loss, respectively. Cre^+ and Cre^- littermates were infected with mock, WNV, or ZIKV and treated with tamoxifen as described above, but tissue was collected at 25 d.p.i. for IHC analysis of synaptophysin or NeuN and TUNEL positivity. Data were pooled from two independent experiments. For **h**, n = 7 (Cre^- Mock), 4 (Cre^- WNV, Cre^+ WNV), or 5 (mock Cre^+) mice per group. For **i**, n = 4 (Cre^- mock, Cre^- ZIKV, Cre^+ mock) or 5 (Cre^+ ZIKV) mice per group. Scale bars, 20 μm. Data represent the mean±s.e.m. (**b** and **c**) or mean±s.d. (**d-i**) and were analyzed by two-way ANOVA, and corrected for multiple comparisons (**a-i**). *P<0.05, **P< 0.005, ***P< 0.001, ****P< 0.0001.

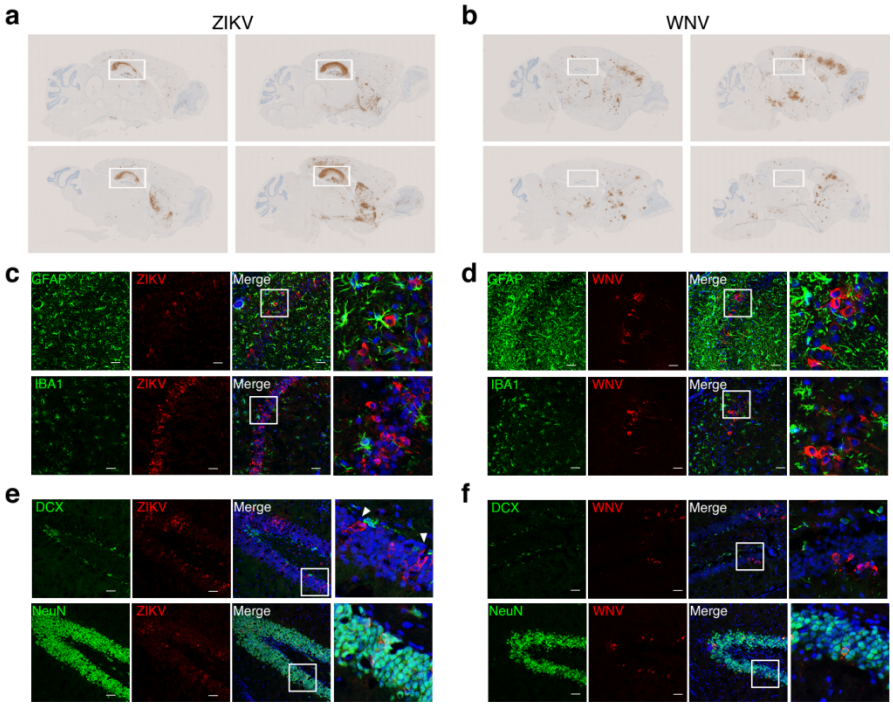

Figure 3.9. ZIKV targets the hippocampus.

(**a,b**) ZIKV preferentially targets the hippocampus (white box). Additional representative images of *in situ* hybridization for viral RNA (RNA-ISH) at 7 dpi as in Fig 1e, (n=4 mice per group). (**c,d**) Neither WNV nor ZIKV targets astrocytes (GFAP+) or microglia (IBA1+) in the CA3 region of the hippocampus. (**e,f**) Neither WNV nor ZIKV targets neural progenitor cells (DCX+) but does infect NeuN+ cells in the dentate gyrus of the hippocampus. Scale bar 20 μm.

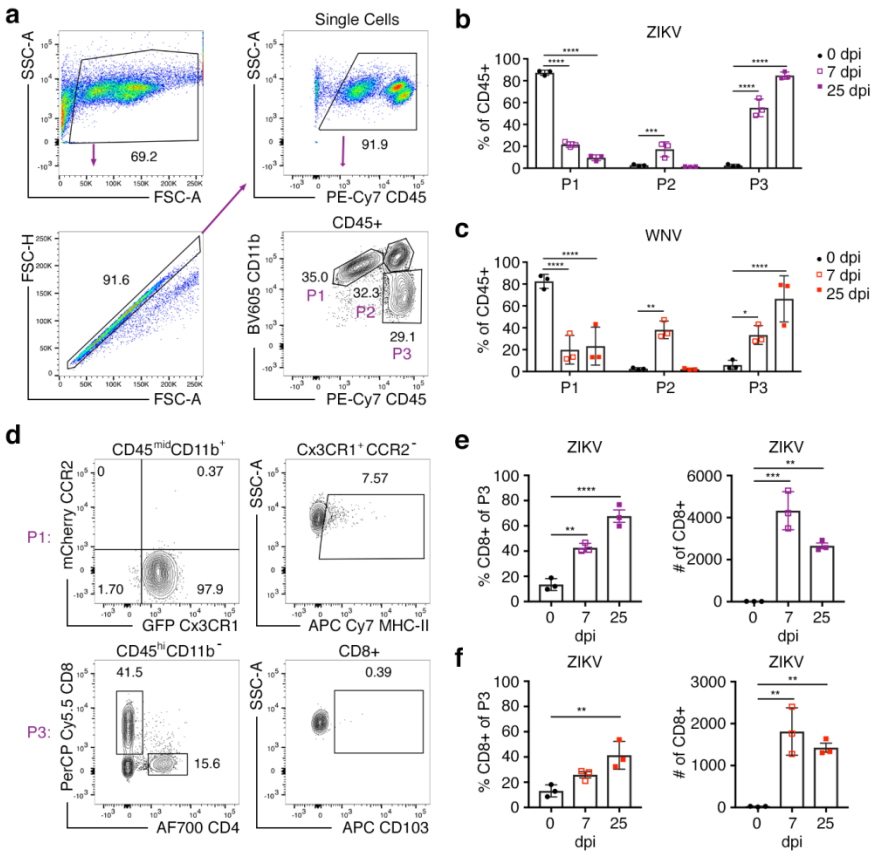

Figure 3.10. Kinetics of immune cell infiltration to the hippocampus.

Cx3CR1^{GFP}CCR2^{RFP} reporter animals were infected with WNV or ZIKV at 8 weeks old. Cells were isolated from the hippocampus at indicated dpi. (**a**) Gating strategy to identify putative microglia (P1: CD45^{mid}CD11b^{+}), macrophage (P2: CD45^{hi}CD11b^{+}), and lymphocyte (P3: CD45^{hi}CD11b^{-}) populations. (**b,c**) Quantification of indicated populations at 0, 7, and 25 dpi revealed infiltration of putative macrophage and lymphocyte populations by 7 dpi, the latter of which persisted in the hippocampus at 25 dpi. Data are representative of two independent experiments (n=3 mice per group, mean ± SD). (**d**) Additional gates were applied to P1 and P3 populations to assess MHC-II expression in CD45^{mid}CD11b^{+}Cx3CR1^{+}CCR2^{-} microglia populations and CD103 expression in CD45^{hi}CD11b^{-} CD8^{+} T cells (quantification in main Figure 2). (**e,f**) CD45^{hi}CD11b^{-} CD8^{+} T cells (identified by gating strategy in a,d) enter the hippocampus by 7 dpi and persist to 25 dpi (n=3 mice per group, mean ± SD). Data was analyzed by two-way (b,c) or one-way (e,f) ANOVA, and corrected for multiple comparisons. *,P<0.05, **, P<0.005, ***, P<0.001, ****, P<0.0001.

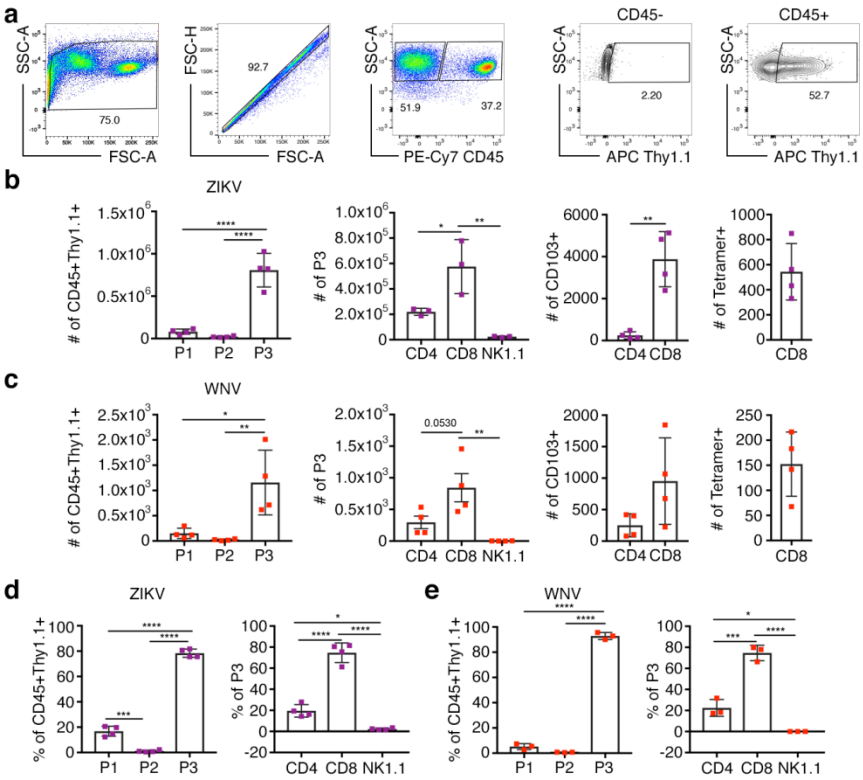

Figure 3.11 IFN-γ$^+$ T cells persist in the hippocampus.

Most of the IFNg$^+$ cells in the hippocampus during recovery are CD8$^+$ T cells, and these persist in the hippocampus for at least a month after viral clearance. IFNγ-Thy1.1 reporter mice were infected with ZIKV or WNV and cells were isolated from the hippocampus at 25 or 52 dpi for flow cytometric analysis. (**a**) Representative gating strategy to identify CD45$^+$IFNg$^+$ cells, which were further analyzed according to the gating strategy shown in main Figure 3. (**b,c**) Data from main Figure 3f,g represented as number of cells (n=4 mice per group, mean ± SD). (**d,e**) Analysis of CD45$^+$IFNγ$^+$ cells at 52 dpi showed that CD45^{hi}CD11b$^-$ CD8$^+$ T cells persist in the hippocampus at least one month after viral clearance. Data are representative of two independent experiments (n=3-4 mice per group, mean ± SD). Data was analyzed by one-way ANOVA, and corrected for multiple comparisons. *,P<0.05, **, P<0.005, ***, P<0.001, ****, P<0.0001.

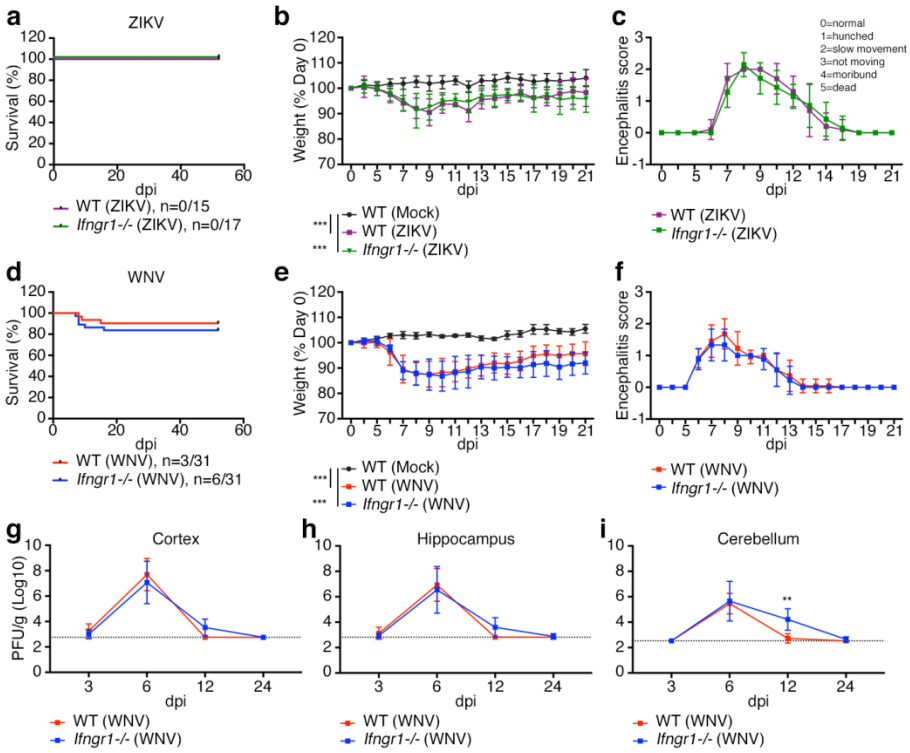

Figure 3.12 *Ifngr1*$^{-/-}$ mice display similar clinical course and viral burden as WT mice.

(**a-f**) Loss of IFNγ signaling does not affect survival, weight loss, or clinical score. (a,d) Survival analysis (n indicated in the figure). (b,e) No difference in weight loss following infection, expressed as % of day 0 body weight (b: n=4 WT (mock), 10 WT (WNV), 5 *Ifngr1*$^{-/-}$ (WNV); e: n=20 WT (mock), 15 WT (ZIKV), 16 *Ifngr1*$^{-/-}$ (ZIKV); mean ± SD). (c,f) No difference in clinical score following infection (n as in b,e; mean ± SD). (**g-i**) Loss of IFNγ signaling does not influence replication or clearance of infectious virus, with the exception of slight delay in the cerebellum. Viral burden was quantified via standard plaque assays. Data are pooled from two independent experiments (n=5-15 mice per group; mean ± SD). Data was analyzed by log rank (Mantel-Cox) test (a,d) or two-way ANOVA (b,c,e-i) and corrected for multiple comparisons. **, P<0.005.

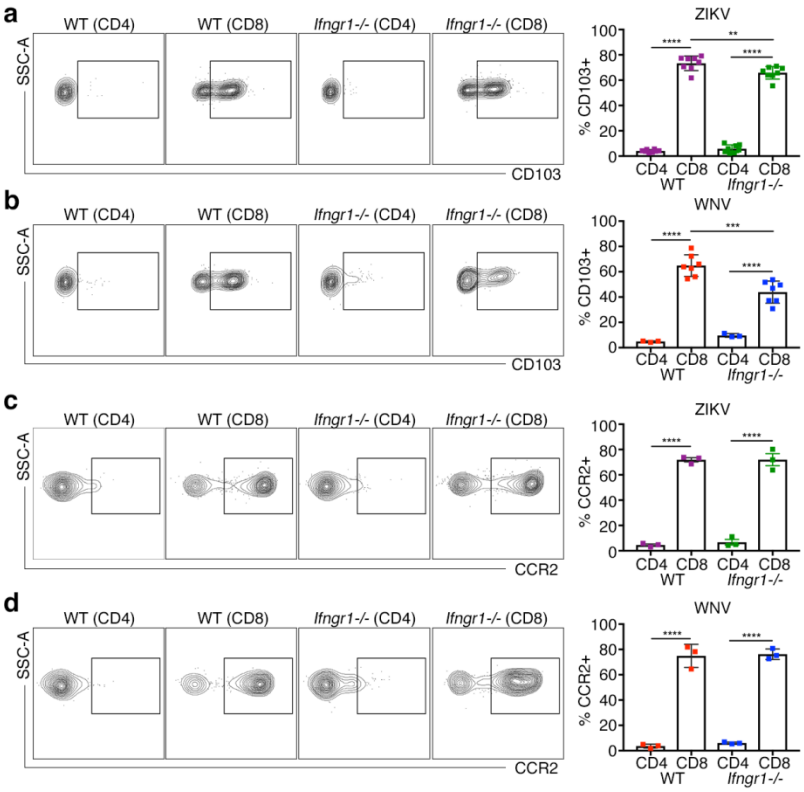

Figure 3.13 *Ifngr1*$^{-/-}$ mice have slight decrease in CD103^{+}CD8^{+} T cells, which express high levels of CCR2.

(**a,b**) Loss of IFNγ signaling led to a small but significant decrease in CD103 expression of CD45^{hi}CD11b^{-}CD8^{+} T cells isolated from the hippocampus at 25 dpi. Flow cytometric analysis of cells isolated from the hippocampus of Cx3CR1^{GFP}CCR2^{RFP} or *Ifngr1*$^{-/-}$Cx3CR1^{GFP}CCR2^{RFP} animals as in Fig. 2e-f (gating strategy in Supplementary Fig 2). Data are pooled from two independent experiments (n=3-8 mice per group; mean ± SD). (**c,d**) Loss of IFNγ signaling did not influence CCR2 expression, which was high increased in CD45^{hi}CD11b^{-}CD8^{+} T cells isolated from the hippocampus at 25 dpi. Flow cytometric analysis of cells isolated from the hippocampus of Cx3CR1^{GFP}CCR2^{RFP} or *Ifngr1*$^{-/-}$Cx3CR1^{GFP}CCR2^{RFP} animals as in Fig. 2e-f (gating strategy in Supplementary Fig 2). Data are pooled from two independent experiments (n=3-8 mice per group; mean ± SD). Data was analyzed by two-way ANOVA and corrected for multiple comparisons (a-d). **, P<0.005, ***, P<0.001, ****, P<0.0001.

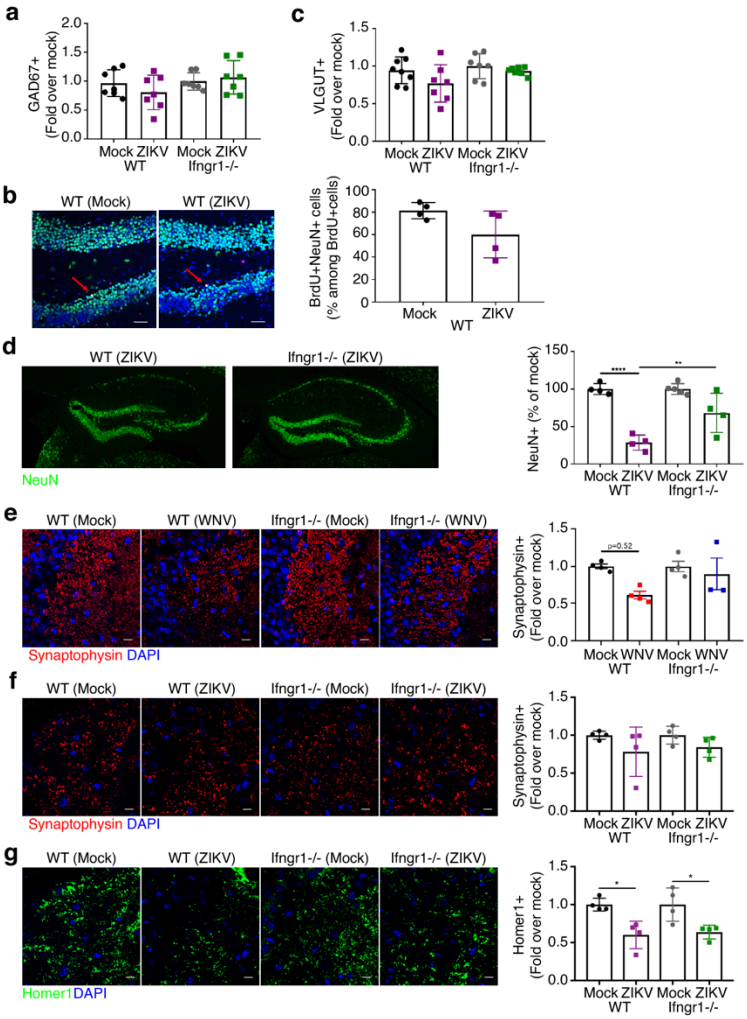

Figure 3.14 Decreases in post-synaptic terminals and increase in apoptotic neurons are observed during ZIKV acute infection and long-term recovery.

(**a,c**) ZIKV infection does not target glutamatergic termini (Vglut1) or GABAergic (GAD67) neurons at 25 dpi. Data are pooled from two independent experiments (n=4-8 mice per group, mean ± SD). (**c**) No difference in new neurons within the DG during recovery. Representative images of recovered hippocampus at 52 dpi, assessed after BrdU labeling during acute infection; BrdU (red), NeuN (green), DAPI (blue). Data from one experiment (n=4 mice, mean ± SD). Scale bar 50 µm. (**d**) ZIKV infection leads to decreased number of neurons at 52 dpi. More neurons were found in *Ifngr1*$^{-/-}$ recovered mice. Representative images of the recovered hippocampus, NeuN (green). Data are pooled from two independent experiments (n=4-5 mice per group, mean ± SD). Scale bar 20 µm. (**e**) WNV infection leads to the acute loss of synaptophysin+ pre-synaptic terminals. Data are pooled from 2 independent experiments (n=4 mice per group, mean ± SD). Scale bar 20 µm. (**f-g**) ZIKV infection leads to acute loss of homer1+ post-synaptic terminals, but preservation of synaptophysin+ pre-synaptic terminals (**f**) Representative immunostaining in the hippocampus at 7 dpi; Synaptophysin (red), DAPI (blue).

Data are pooled from 2 independent experiments (n=4 mice per group, mean ± SD). Scale bar 10 μm. (**g**) Representative immunostaining in the hippocampus at 7 dpi; Homer1 (green), DAPI (blue). Data are pooled from 2 independent experiments (n=4 mice per group, mean ± SD). Scale bar 10 μm. Data was analyzed by two-way ANOVA and corrected for multiple comparisons (**a-g**). *,P<0.05, **, P<0.005, ***, P<0.001.

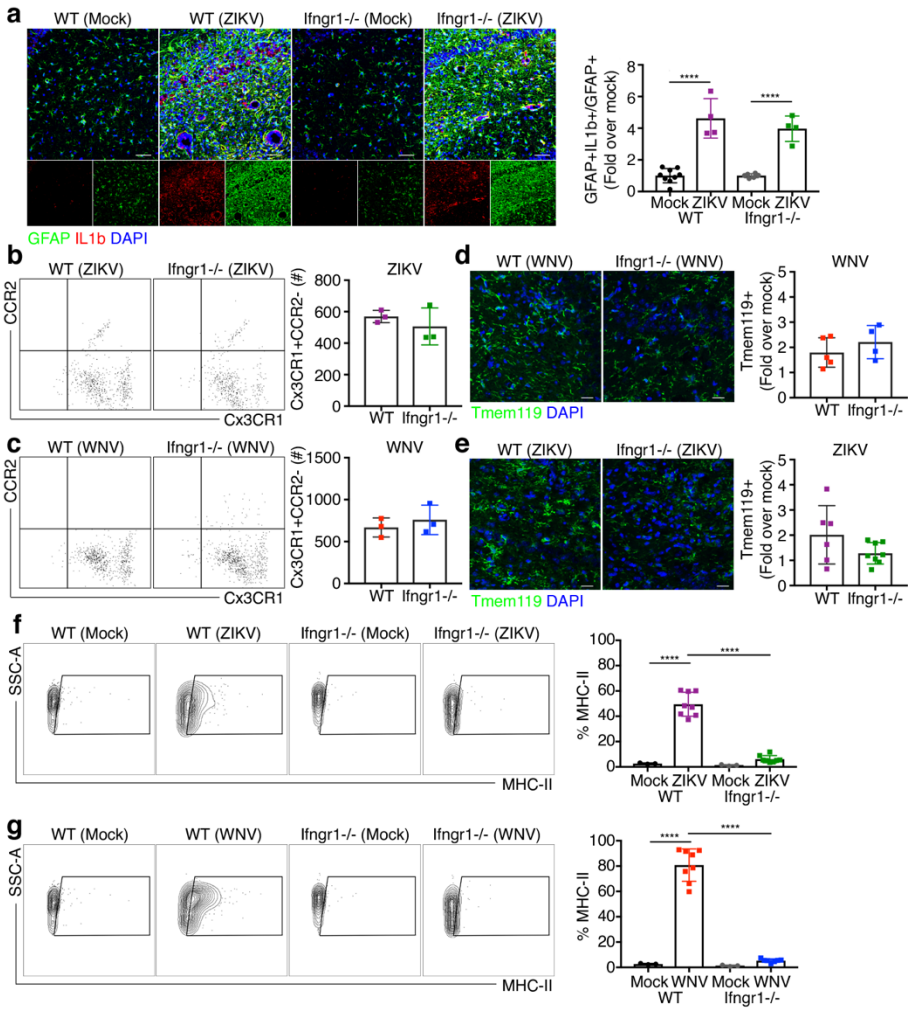

Figure 3.15 Significant differences in numbers of microglia in the hippocampus of WT and *Ifngr1*$^{-/-}$ WNV and ZIKV-recovered mice.

(**a**) Astrocyte expression of IL-1β was similarly elevated in WT and *Ifngr1*$^{-/-}$ mice. Representative immunostaining in the hippocampus; GFAP (green), IL-1β (red), DAPI (blue). Data are pooled from 3 independent experiments (n=4-8 mice per group, mean ± SD). Scale bar 50 µm. (**b-e**) ZIKV- and WNV-recovered animals demonstrate similar numbers of microglia in the hippocampus at 25 dpi. (**b,c**) No differences in the number of $CD45^{mid}CD11b^{+}Cx3CR1^{+}CCR2^{-}$ microglia were observed in cells isolated from the ZIKA- or WNV-recovered hippocampus of reporter mice at 25 dpi. Representative plots of $CD45^{mid}CD11b^{+}$ cells. Data are representative of two independent experiments (n=3 mice per group, mean ± SD). (**d,e**) No differences in the number of Tmem119+ microglia were observed in the hippocampus of WT and *Ifngr1*$^{-/-}$ infected animals at 25 dpi. Representative immunostaining of Tmem119 (green) and DAPI (blue) in the hippocampus. Data are pooled from two independent experiments (n=4-8 mice per group, mean ± SD). Data was analyzed by unpaired t test (**a-d**). (**f,g**) WNV or ZIKV infection induces increased expression of MHC-II in

hippocampal microglia at 25 dpi. Representative plots from flow cytometric analysis of MHC-II expression in $CD45^{mid}CD11b^{+}Cx3CR1^{+}CCR2^{-}$ microglia isolated from the recovered hippocampus of infected WT and *Ifngr1*$^{-/-}$ animals. Data are pooled from two independent experiments (n=8 mice per group, mean ± SD). Data was analyzed by two-way ANOVA and corrected for multiple comparisons (**a,f,g**). *,P<0.05, ***, P<0.001, ****, P<0.0001.

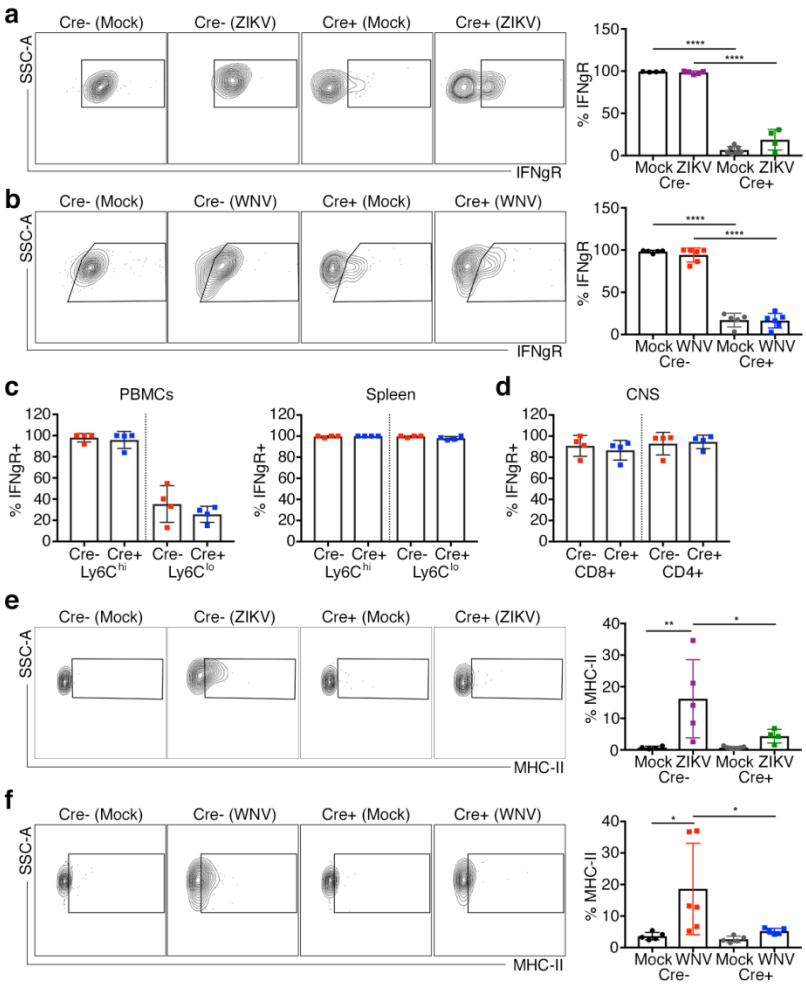

Figure 3.16 Conditional deletion of IFNGR in Cx3CR1^{+} microglia

Specific deletion of IFNGR in microglia was achieved as in Fig. 8a-g. (**a,b**) Flow cytometric analysis of CD45^{mid}CD11b^{+} microglia isolated from the hippocampus of *Cx3CR1^{CreER}Ifngr$^{fl/fl}$* (Cre +) mice and *Cx3CR1^{Cre}-Ifngr$^{fl/fl}$* (Cre-) littermate controls after behavioral testing demonstrated significant deletion of IFNGR in Cre+ mice. Data are pooled from two independent experiments (n=4-7 mice per group, mean ± SD). (**c**) Analysis of peripheral myeloid cells isolated from the blood (PBMCs) and spleen revealed no difference in IFNGR expression between Cre+ and Cre- mice. Data are representative of two independent experiments (n=4 mice per group, mean ± SD). (**d**) Tamoxifen treatment did not alter IFNGR expression in CD45^{hi}CD11b^{-}CD8^{+} or CD45^{hi}CD11b^{-}CD4^{+} T cells isolated from the hippocampus of Cre+ and Cre- mice. Data are representative of two independent experiments (n=4 mice per group, mean ± SD). (**e,f**) Conditional deletion of IFNGR in microglia during recovery led to significant attenuation of MHC-II expression in microglia isolated from the hippocampus of Cre+ but not Cre- mice after behavioral testing. Data are pooled from two independent experiments (n=4-7

mice per group, mean ± SD). Data was analyzed by two-way ANOVA and corrected for multiple comparisons **(a,b,e,f)** or by unpaired t test (**c,d**). *,P<0.05, **, P<0.005, ****, P<0.0001.

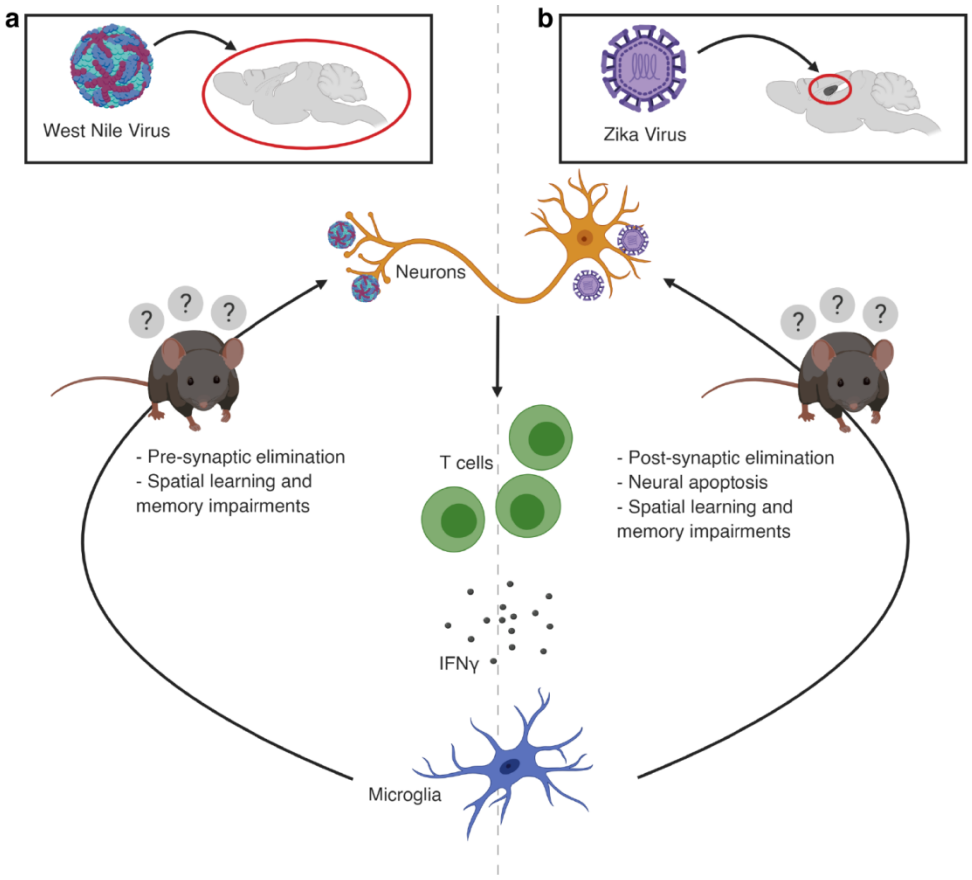

Figure 3.17 T cell-derived IFNγ targets microglia to mediate neurocognitive dysfunction during recovery from WNV and ZIKV infection.

(**a**) WNV infects neurons throughout the CNS. Anti-viral T cells that persist in the CNS after viral recovery produce IFNγ. IFNγ targeting of microglia leads to the elimination of presynaptic termini, most prominently in the CA3 region of the hippocampus, and the development of spatial learning and memory deficits. (**b**) ZIKV preferentially targets neurons in the hippocampus. Like WNV, IFNγ producing T cells persist in the CNS after ZIKV recovery. Targeting microglia, IFNγ induced apoptosis of neurons and the elimination of post-synaptic termini throughout the hippocampus. ZIKV inflicted mice subsequently develop spatial learning and memory deficits.

Chapter 4: Conclusions and future directions

4.1 Astrocytes, neurogenesis and synapse recovery

This work has explored the fundamental processes which prevent cognitive recovery following neuroinvasive disease with West Nile virus. We found that in the case of West Nile Virus, reactive astrocytes prevent recovery of synapses and lead to decreased neurogenesis through IL-1b signaling. Blocking this pathway through genetic deletion of the receptor for IL-1 (*Il1r1-/-*) or pharmacologic treatment with the IL1R1 antagonist anakinra was sufficient to protect animals from WNV-induced spatial learning deficits.

In earlier work we demonstrated that after WNV infection, activated microglia cause synapse elimination in the hippocampus through complement mediated phagocytosis[1], providing a pathological basis for the spatial learning deficits we observed. Synapses are lost during acute infection, but what prevents synaptic repair? In the ventral spinal cord, depletion of region-restricted astrocytes led to differential loss of excitatory and increase of inhibitory synapses. Astrocytes from developmentally distinct regions did not migrate into the depleted area, and thus could not replace the cells that were lost[2]. This raises two important points which may be relevant for understanding the mechanisms underlying synaptic recovery following viral infection.

First, in addition to their developmental role of promoting synaptogenesis astrocytes may also be important for maintaining synaptic connections. *In vivo* imaging studies have demonstrated that synaptic connections are formed and lost in a dynamic way even under normal conditions[3]. Thus, during recovery from infection reactive astrocytes may lose the ability to perform homeostatic maintenance of synapse formation and loss. Indeed, recent work has

demonstrated that reactive astrocytes were unable to promote synapse formation *in vitro*, although resting astrocytes readily performed this function[4].

Second, astrocytic patterning during development may be an important determinant of the functional capabilities and the region-restricted areas in which they divide. Indeed, depletion of astrocytes in a restricted region of the spinal cord led to loss of those astrocytes without infiltration of astrocytes from an adjacent region[2]. Thus, as reactive astrocytes lose their homeostatic functions following WNV infection, it is unlikely that neighboring astrocytes will be able to migrate into the region to fill the functional void.

However, there are several important caveats to this second line of reasoning. First, although patterning has been demonstrated for the spinal cord[2], no studies have explored whether hippocampal astrocytes derive from a developmentally restricted region. Second, *in vivo* imaging studies have shown that during development, differentiated astrocytes locally proliferate and integrate into functional networks[5], and the daughter cells do not appear to migrate tangentially[2]. In the neurogenic zone of the hippocampus, newly generated astrocytes may also contribute to reactive astrogliosis following infection. Indeed, we observed an increase in proliferating astrocytes and a decrease in proliferating neuroblasts. Why these newly generated astrocytes are unable to perform homeostatic functions remains unknown, although it is likely that the inflammatory environment promotes a reactive phenotype. *In vivo* imaging of the astrocyte response to infection could address 1) the dynamics of synapse formation and retraction during recovery and 2) the contribution of local proliferation and/or migration to reactive astrogliosis.

We also observed decreases in the number of proliferating neuroblasts in the subgranular zone of the dentate gyrus and the subventricular zone of the lateral ventricles following WNV

infection[6]. This loss of neural progenitor cells was not due to direct viral targeting, but rather due to cytokine mediated alteration in lineage fate. During development, neurogenesis precedes astrogenesis. The 'gliogenic switch', when neural stem cells switch from making new neurons to making new glia, is mediated in part by JAK-STAT signaling[7]. It is possible that developmental pathways leading to gliogenesis are activated when neural stem cells residing in the dentate gyrus, which typically make new neurons that integrate into the hippocampal circuitry, are exposed to a cytokine milieu following infection. In addition to the effects of reactive astrocytosis on synaptogenesis discussed above, the loss of newborn neurons may also contribute to spatial learning deficits.

Studies in rodents have identified several ways by which adult neurogenesis in the hippocampus contributes to spatial learning and memory. Adult-born new neurons are integrated into the hippocampus during spatial learning[8], and ablation of neural stem cells or young neurons prevents learning[9,10]. Thus, following infection decreases in the proliferating neural precursor pool, may lead to a decrease in the number of new neurons generated and integrated into the hippocampal circuitry. Injecting BrdU, which labels dividing cells, at various days post infection during recovery, in combination with staining for early activation genes could help to identify whether there is indeed a decrease in the number of newborn neurons incorporating into the hippocampal circuit during a hippocampal-based memory paradigm.

Although initially dismissed, the hypothesis that neurogenesis exists in the adult human brain has been widely accepted for many years due to mounting evidence that precursor cells can be found in restricted neurogenic regions. However, two papers published recently have revived the debate. Sorrell et. al analyzed human tissue from birth to 77 years and found a sharp decline in the number of proliferating progenitor cells in the dentate gyrus beginning around 1 year, and

very few cells in any of the later time points. They also found a similar decrease in neural progenitors with age in non-human primates[11]. On the other hand, Boldrini et al analyzed human tissue ranging from 14-79 years of age, using stereologic techniques to quantify and extrapolate the number of newborn neurons in the hippocampus. They identified neural progenitor cells and found a stable population during aging[12]. These studies arrived at different conclusions but raise several important points. First, rodent studies are important and useful for testing mechanistic hypotheses, but have recognized limits in translating findings to humans due to fundamental differences in physiology. Second, human studies utilizing post-mortem tissue are an important step to validate hypotheses generated in rodent studies, but have additional challenges due to an increasing number of variables, including prior exposures and post-mortem interval, which are difficult to fully control. Finally, the ability to determine whether neurogenesis continues during adulthood is limited by the identification and availability of lineage defining markers.

4.2 References

1. Vasek MJ, Garber C, Dorsey D, et al. A complement–microglial axis drives synapse loss during virus-induced memory impairment. *Nature*. 2016;534(7608):538-543. doi:10.1038/nature18283.
2. Tsai HH, Li H, Fuentealba LC, et al. Regional astrocyte allocation regulates CNS synaptogenesis and repair. *Science (80-)*. 2012;337(6092):358-362. doi:10.1126/science.1222381.
3. Trachtenberg JT, Chen BE, Knott GW, et al. Long-term in vivo imaging of experience-dependent synaptic plasticity in adult cortex. *Nature*. 2002;420(6917):788-794. doi:10.1038/nature01273.
4. Liddelow SA, Guttenplan KA, Clarke LE, et al. Neurotoxic reactive astrocytes are induced by activated microglia. *Nature*. 2017;541(7638):481-487. doi:10.1038/nature21029.
5. Ge W-P, Miyawaki A, Gage FH, Jan YN, Jan LY. Local generation of glia is a major astrocyte source in postnatal cortex. *Nature*. 2012;484(7394):376-380. doi:10.1038/nature10959.
6. Garber C, Vasek MJ, Vollmer LL, Sun T, Jiang X, Klein RS. Astrocytes decrease adult neurogenesis during virus-induced memory dysfunction via IL-1. *Nat Immunol*. 2018:1-11. doi:10.1038/s41590-017-0021-y.
7. Bonni A, Sun Y, Nadal-Vicens M, et al. Regulation of gilogenesis in the central nervous system by the jak-stat signaling pathway. *Science (80-)*. 1997;278(October):477-483.

8. Kee N, Teixeira CM, Wang AH, Frankland PW. Preferential incorporation of adult-generated granule cells into spatial memory networks in the dentate gyrus. *Nat Neurosci*. 2007;10(3):355-362. doi:10.1038/nn1847.
9. Deng W, Saxe MD, Gallina IS, Gage FH. Adult-born hippocampal dentate granule cells undergoing maturation modulate learning and memory in the brain. *J Neurosci*. 2009;29(43):13532-13542. doi:10.1523/JNEUROSCI.3362-09.2009.
10. Imayoshi I, Sakamoto M, Ohtsuka T, et al. Roles of continuous neurogenesis in the structural and functional integrity of the adult forebrain. *Nat Neurosci*. 2008;11(10):1153-1161. doi:10.1038/nn.2185.
11. Sorrells SF, Paredes MF, Cebrian-Silla A, et al. Human hippocampal neurogenesis drops sharply in children to undetectable levels in adults. *Nature*. 2018;555(7696):377-381. doi:10.1038/nature25975.
12. Boldrini M, Fulmore CA, Tartt AN, et al. Human Hippocampal Neurogenesis Persists throughout Aging. *Cell Stem Cell*. 2018;22(4):589-599.e5. doi:10.1016/J.STEM.2018.03.015